ORNL-3315
UC-20 – Controlled Thermonuclear Processes
TID-4500 (17th ed., Rev.)

THERMONUCLEAR DIVISION

SEMIANNUAL PROGRESS REPORT

FOR PERIOD ENDING APRIL 30, 1962

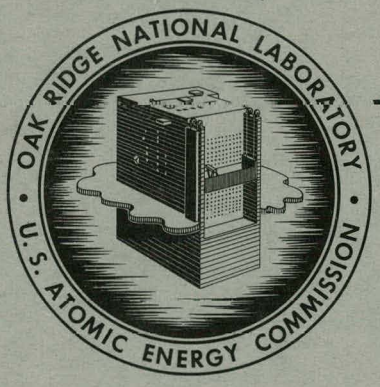

OAK RIDGE NATIONAL LABORATORY
operated by
UNION CARBIDE CORPORATION
for the
U.S. ATOMIC ENERGY COMMISSION

DISCLAIMER

Printed in USA. Price $2.25 Available from the

Office of Technical Services
U. S. Department of Commerce
Washington 25, D. C.

ORNL-3315

Contract No. W-7405-eng-26

THERMONUCLEAR DIVISION

SEMIANNUAL PROGRESS REPORT

For Period Ending April 30, 1962

DATE ISSUED

SEP 12 1962

OAK RIDGE NATIONAL LABORATORY
Oak Ridge, Tennessee
operated by
UNION CARBIDE CORPORATION
for the
U. S. ATOMIC ENERGY COMMISSION

THIS PAGE

WAS INTENTIONALLY

LEFT BLANK

Contents

THIS PAGE

WAS INTENTIONALLY

LEFT BLANK

Introduction

A. H. Snell

Good operating conditions were obtained in DCX-1 during the past half year, and interesting data have contributed to our understanding of the rather complex phenomena that the rotating population of trapped protons breeds within itself. In perusing Sec 1 of this report, the reader should bear in mind that when DCX-1 is run without a dissociative arc (as was true in all of this work) an improvement in vacuum decreases both the rate of feed of the trapped population and the rate of loss. The two counterbalancing effects are both proportional to pressure, so, to first order, the equilibrium population of stored protons remains unchanged. What does happen is that the time scale is stretched, and with mean containment times as long as 40 sec, the development of plasma phenomena can be watched in comfortable fashion indeed.

In tackling the problem of increasing density in DCX-1, we have been forestalled by one of these very plasma phenomena. We had hoped to use positive exponentiation upon protons already trapped as a means toward higher density and had estimated the critical condition to be that for which the product of the input H_2^+ beam current and the containment time is 200 ma-sec. Although this quantity has been approximately reached, there has been no sign of exponentiation, and the reason is that the plasma slowly spreads. Thus we are still in the density range of 10^7 to 10^8 fast protons per cubic centimeter. To obtain higher densities we must either control the spreading or adopt an approach that will yield a greater dissociation efficiency than the 10^{-7} effective in present experiments. Experiments and calculations are being pursued in both of these directions; our choice of three or four courses of action may be the subject of future progress reports.

The phenomena of DCX-1 are still not completely understood. The relationship between the presence of the H_2^+ beam, the clumping, the spatial spread, and the dispersion in energy of the trapped protons has yet to be elucidated in detail. Although the longitudinal spread is sufficient to cause particle loss to the end walls of the liner (which is not serious and which can be rectified), such loss appears mostly to cease when the H_2^+ beam is turned off. The clumping relieves itself in bursts of radio-frequency noise, and the potential of the plasma relative to ground jumps around, but in spite of all of this dynamic behavior, charge exchange accounts for all particle loss up to the containment time of 40 sec.[1]

In Sec 2 we are delighted to be able to present the first observations in DCX-2, fragmentary as they are. The magnetic field checked out in fine style, in magnificent justification of the work of the Engineering Sciences Group and the computational effort. One of the striking first observations is the harmonic richness of the ion cyclotron radiation (Sec 2.7); the hint that the cyclotron radiation may fade as more beam is injected will bear careful watching.

The experiments on electron cyclotron heating in a mirror field continue to present results that are complicated and unpredictable. The measurements of the plasma magnetism have been refined to the point of seeing both diamagnetic and paramagnetic signals, the latter appearing as the probe is advanced axially to the center of the plasma. Furthermore, it has been possible to

[1] In default of conflicting claims, this containment time is claimed as a record for Anderson County, in East Tennessee.

identify two different magnetic signals separately with the short (10 to 20 msec) and the long (200 to 300 msec) components of the decay curve of the magnetic signal. All this seems to imply a distribution of oppositely directed azimuthal currents with separate decay times, and an attempt is made to reconstruct this current distribution from the magnetic probe information. All this is described in Sec 3.1, but in connection with the radio-frequency heating, Fig. 3.4 may be important in a different way. It shows attenuation by a factor of 50 of a beam of room-temperature hydrogen, directed through the hot-electron plasma. Clearly, the interior of the plasma must be largely burned out, and the figure suggests that complete burnout will be possible with the application of a little more power.

Progress in the field of plasma diagnostics has been aided by further development of the "plasma sweeper," the "plasma eater," and the pendulum (Secs 3.4 to 3.6). The-plasma source was used in several experiments, and appears to be a useful technique. The part played by neutral gas in damping the fundamental vibration in ionic sound wave propagation has been clarified (Sec 3.3).

We are starting more work than in the past on the problem of plasma containment, branching out with variants on the simple cusp. One experiment, "Elmo" (Sec 3.2), has given confinement times of the order of seconds for hot-electron plasmas. These striking results are being supplemented by orbit computations (Sec 6.8), but it is difficult to follow a particle for long within the limitations of the IBM 7090 computer.

The carbon arc has been lengthened to 5 m, and the C^{2+} ion temperatures continue to increase with the length so that they are now in the neighborhood of 5,000,000°C. (See Sec 4.1. Note also in Sec 2.4 the operation in DCX-2 of an argon arc 7 m long.) The development of deuterium plasmas in the density range 10^{10} to 10^{12} cm^{-3} for purposes of molecular dissociation in DCX-1 and DCX-2 was successful; two flexible versions are described in Secs 4.2.1 and 4.2.2. The former of these was run through an enclosure at a base pressure of 3×10^{-9} torr without raising the pressure therein and was measured to have a particle density usefully greater than that of the ambient gas. Technological accomplishments of this kind are important to the Sherwood business.

In theory, extensions were found for the minimum criterion for stability mentioned in our last report; the usual indispensable computational support appears in sundry aspects. In fact, the supporting work of the Computational, Magnetics, Engineering Sciences, and Spectroscopy Groups does not appear in the following pages in proportion to its much-appreciated value. Vacuum studies have continued on the nature and performance of titanium films and on the properties of nude ion gages; tests of the polyether diffusion pump oils make them look better and better. Finally, we append two engineering notes: one concludes that a mixture of lithium and beryllium fluorides is promising for use in a tritium-breeding blanket for a fusion reactor, and the other concerns the use of demineralized water in magnet coils.

In conclusion, our present position in the matter of controlled fusion can be discussed in terms of the three not-necessarily-independent requirements of particle energy, particle density, and containment time. In DCX-1 we have achieved energy and containment time but not density, while in the radio-frequency heating we have all three but in electrons rather than positive ions. Meanwhile, DCX-2 is coming up fast, and we should see in a few months how favorable a combination it can yield of the three desiderata for a hot-ion plasma. Perhaps, however, the solution may come in some combination of the radio-frequency heating with injection methods.

Abstracting Summary

1. DCX-1 PLASMA EXPERIMENTS

Engineering modifications to the apparatus resulted in a lowest base pressure of 1.5×10^{-9} torr; operating pressures down to about 2.5×10^{-9} torr, with a pressure increment of less than 1×10^{-10} torr/ma H_2^+; and trapped proton lifetimes as long as 37 sec.

Neutral-particle-detector data indicate that at high pressures the plasma volume is 1 or 2 liters (corresponding to an average fast-proton density of about 10^7 protons per cubic centimeter per milliampere of H_2^+) and that it is relatively independent of the H_2^+ beam current. At lower pressures, the initial volume is again about 1 or 2 liters, but expansion occurs in a few seconds during the buildup interval, and the equilibrium volume becomes quite sensitive to the H_2^+ current. With 8 ma of H_2^+ at 6×10^{-8} torr, the equilibrium volume has expanded to the maximum of 10 liters permitted by the present structural configuration of the plasma chamber. At lower pressures wall collisions contribute to the steady-state proton loss rate. In addition to a slow component whose origin is obviously the charge-exchange loss of trapped energetic protons, the neutral-particle-detector signals also have a fast component which responds very rapidly to the H_2^+ beam and whose origin is not yet known. The decay time constants of the slow component of the signal are in accord with charge-exchange times, and the steady-state loss rates calculated by using only these charge-exchange signals are in excellent agreement with the calculated proton-trapping rates except under conditions of operation where the wall collisions play a role. Even under these conditions it appears that the plasma decays only by charge exchange once the H_2^+ beam is cut off. The specific forces driving the volume expansion are not yet clear, though it appears that they are collective rather than single-particle in origin.

Other data have emphasized the increasing disorder of the plasma with increasing trapped-proton lifetime. Measurements of the energy distributions of escaping charge-exchange neutrals show broad energy spectra, with dependence on both pressure and injected H_2^+ current. As the pressure is lowered, the coherent rf signals from the circulating protons gradually become more discontinuous, the frequency bands wider, and the modulation patterns more noise-like than periodic. Ion-beam probe measurements of the plasma potential show that the lower pressures and larger H_2^+ beam currents produce both the higher potentials (up to 2 kv) and the larger ranges of fluctuation (hundreds of volts).

2. DCX-2

The initial operation of DCX-2 is reported, particularly with regard to the ion cyclotron frequencies and their harmonics as seen when the H_2^+ beam is injected into the trapping volume at a pressure of about 10^{-5} torr.

3. PLASMA PHYSICS

Electron Cyclotron Heating Experiments in Physics Test Facility

The plasma produced by electron cyclotron resonance in a mirror geometry (Physics Test Facility) exhibited a magnetic structure, the study of which is described.

The ΔB (diamagnetic) vs Z curve shows a positive ΔB of 9 gauss in the midplane on the axis and a normal negative ΔB of $4\frac{1}{2}$ gauss,

$5\frac{1}{2}$ in. from the midplane. Construction of plasma shape via calculated equivalent current loops is being attempted. The above experiment is undergoing changes for application of higher power at shorter wavelengths. More and quieter microwave power will permit exploration of density limits vs power and wavelengths and will allow study of the semicorrelated high-energy x-ray bursts. A thermal, neutral feed beam is also being attached so that specific radio-frequency heating zones (remote from walls) may be fed with gas.

Electron Cyclotron Heating Experiments in Elmo

The 13-cm microwave heating system was applied in a preliminary way to the folded-cusp magnetic geometry (Elmo), and significantly favorable containment information was obtained. However, the measure of containment time is made by observation of the decay of microwave noise after interruption of the heating source, and in order to infer favorable containment at this time some rather weak assumptions are required, pending other measurements of temperature and density.

Plasma Diagnostics

Techniques for measuring the ion density, electron temperature, and rate of loss of a plasma are described. An application of these diagnostic techniques to plasmas of up to 10^{13} ions/cm^3 with electron temperatures of approximately 20 ev is also described.

Gas damping of ionic sound waves is analyzed quantitatively.

A conductor in close proximity to the turbulent plasma formed at the intersection of an electron stream and a neutral gas jet reduced the turbulence and increased the density of the plasma (presumably by "tying down" the magnetic flux lines).

The plasma sweeper technique was applied to plasma contained in the simple cusp magnetic geometry. The plasma was stable and quiescent and had a maximum density when an additional folding field was applied.

4. VACUUM ARC RESEARCH

Arc Development of Hydrogen Plasma for H_2^+ Dissociation

At present, dissociation in DCX-1 is effected on the background neutral gas which is primarily hydrogen at about 4×10^8 particles per cubic centimeter. Utilization of an arc to enhance dissociation would be desirable if the arc can satisfy the following characteristics: (1) have an ion species such that charge exchange to the trapped current is negligible, (2) be able to operate in a low-pressure system in order to maintain the low operating pressure of DCX-1, and (3) achieve an ion density of about 50 times background.

The arc developed in this work is a hydrogen-gas arc. A vacuum system was constructed which achieved a base pressure of 2.5×10^{-10} mm Hg in the inner liner region while at liquid-nitrogen temperatures. An arc density of about 10^{10} ions per cubic centimeter can be achieved with a gas flow of 2 cc/min. At this flow, the pressure in the inner liner rises to 3×10^{-9} mm Hg. The ion-to-neutral ratio under these conditions is about 30 to 1.

5. ION PRODUCTION, ACCELERATION, AND INJECTION

Developments in the High-Beam Accelerator

The 600-kv injector was removed from its test stand and installed on DCX-2, where it is operating satisfactorily. A new tube was built in order to continue the study of high-intensity beams and their production. Equipment was developed in order to study the angular and spatial distribution of current in these beams.

100-kev Neutralized Beam Accelerator

Components testing of the accelerator was satisfactorily completed. Failure of the center coil (around the ion source) delayed further testing of the effect of electron injection. Future experimentation with the accelerator will be carried out on a newly constructed vacuum test stand.

Hollow-Cathode Arc Ion Source

Extensive testing of the hollow-cathode arc discharge as an ion source is being initiated. A 300-ma beam of unanalyzed hydrogen has been obtained at a 16-kev accelerating voltage. A new high-voltage shielding arrangement was constructed and should allow the accelerating voltage to be increased to about 35 kev.

Neutral Source Development

A neutral beam source consisting of two coaxially mounted hollow-cathode arc discharges is being constructed. One discharge will serve as an ion source; the accelerated ions will be confined magnetically to move longitudinally through the second or converter arc. Dissociation of molecular ions in the converter arc should be the primary source of neutrals. Optimization of neutral production will be accomplished by variation of the type of converter arc and variation of the dissociation path of the molecular-ion beam in the converter arc. Neutral-beam collimation should be very good because of the confining magnetic field and converter arc geometry.

6. THEORY AND COMPUTATION

Topics discussed are as follows: (1) ion density vs injection current in DCX-2, in which it is shown that refined calculations with charge exchange and ionization cross sections properly averaged over ion and electron energy distributions do not markedly increase previous estimates of upper critical current; (2) secondary plasma phenomena; (3) three new features of a minimum principle for stability; (4) potential distribution calculations for DCX-1; and (5) calculation of electron trajectories in the folded double cusp, "Élmo."

7. MAGNETICS

Auxiliary Curves for Rapid Design of Magnet Coils

Families of normalized curves are presented which allow the rapid calculation of magnet coils. Optimum coil parameters are obtained. In addition the method also gives the field variations when the coil parameters are changed. Examples for both conventional and superconducting coils are shown.

Recent Developmental Work on DC Magnet Coils

The design of a new magnet system is described. This two-coil, vertical-axis system will have variable coil separation and will produce a nominal field of 80 kilogauss. This facility will be used initially to perform carefully planned engineering tests for providing additional coil-design data and to ultimately produce relatively large-volume homogeneous fields for research in superconductivity.

A method for building solenoids from flexible cables was developed which under certain conditions provides magnet coils more quickly and cheaply than possible in the conventional way.

Calculation of Axial Forces in Magnetic Coil Systems

The results of computer studies on the loop-replacement approximate method of calculating axial forces for rotationally symmetrical coil pairs are reported. A systematic application of the resulting computer codes for multicoil systems is presented, with illustrations from Long Solenoid reversed-field studies.

1. DCX-1 Plasma Experiments

J. L. Dunlap
R. S. Edwards
G. R. Haste
L. A. Massengill
H. Postma
J. A. Ray
R. G. Reinhardt
W. J. Schill
R. M. Warner
E. R. Wells

1.1 ENGINEERING MODIFICATIONS

The configuration of the high-vacuum liner in use at the beginning of this report period has been described previously.[1,2] Then, the liner region extended axially to about 40 in. from the median plane, and it was pumped by a combination of titanium evaporated on liquid-nitrogen-cooled surfaces, a 6-in., liquid-nitrogen-trapped diffusion pump, and two small liquid-helium traps. This system had produced base pressures (pressures measured without injecting the H_2^+ beam) in the liner region of about 1×10^{-8} torr (ref 3), operating pressures down to 2×10^{-8} torr with a pressure increment of less than 2×10^{-10} torr per milliampere of H_2^+ beam, and proton lifetimes of about 7 sec.

Operation with this liner configuration suggested a number of modifications which were completed about the middle of this report period. The helium traps, the high-vacuum diffusion pump, and the old liner were removed, and a new liner was installed. As indicated in Fig. 1.1, the midplane section of this liner is very similar to the old; but, as shown in Fig. 1.2, the Z extent is much less. The principal structure of the liner has confining walls at $Z = \pm 6\frac{1}{2}$ in. and was therefore installed without removing the inboard magnetic field coils. Provisions are made for adding other components, such as baffles or "pots" loaded with mesh-supported Zeolite, to extend the high-vacuum region into the inboard coil throats. Twenty-inch-diameter chevron baffles, which can be cooled by water or liquid nitrogen, were fabricated and installed between the intermediate and outer vacuum systems. The use of multiple-unit titanium evaporators increased the number of titanium filaments while decreasing the associated number of vacuum seals. A higher-pressure steam supply and the smaller mass of the new liner permit 400°C bakeouts, whereas with the previous arrangement they were limited to about 225°C.

With the modified liner, a lowest base pressure of 1.5×10^{-9} torr, operating pressures down to about 2.5×10^{-9} torr with a pressure increment of less than 1×10^{-10} torr per milliampere of H_2^+, and proton lifetimes of 37 sec have been obtained. The details of the lifetime measurements and of other experiments performed in the low-pressure range are given in the following sections.

1.2 NEUTRAL-PARTICLE-DETECTOR DATA

Two primary considerations prompted the desire to obtain data from the apparatus at lower operating pressures. The first was to determine whether the neutral-particle-detector (NPD) decay signals measured during the interval after gating off the H_2^+ beam would continue to indicate that charge exchange is the dominant loss process for

---

[1] *Thermonuclear Div. Progr. Rept. Oct. 31, 1961*, ORNL-3239, pp 1–2.

[2] *Thermonuclear Div. Semiann. Progr. Rept. Jan. 31, 1961*, ORNL-3104, p 11, Fig. 1.15.

[3] In this report, ion-gage pressures recorded with the liner at liquid-nitrogen temperature have been multiplied by the temperature correction, a factor of 2. This was not done in the previous report.

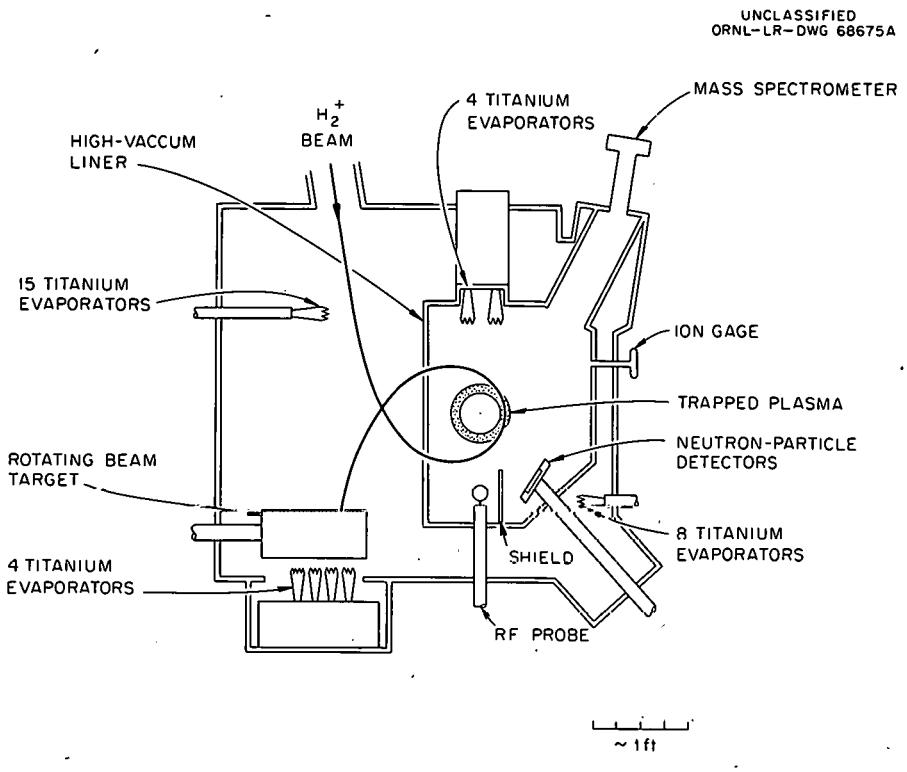

Fig. 1.1. Midplane Section of DCX-1.

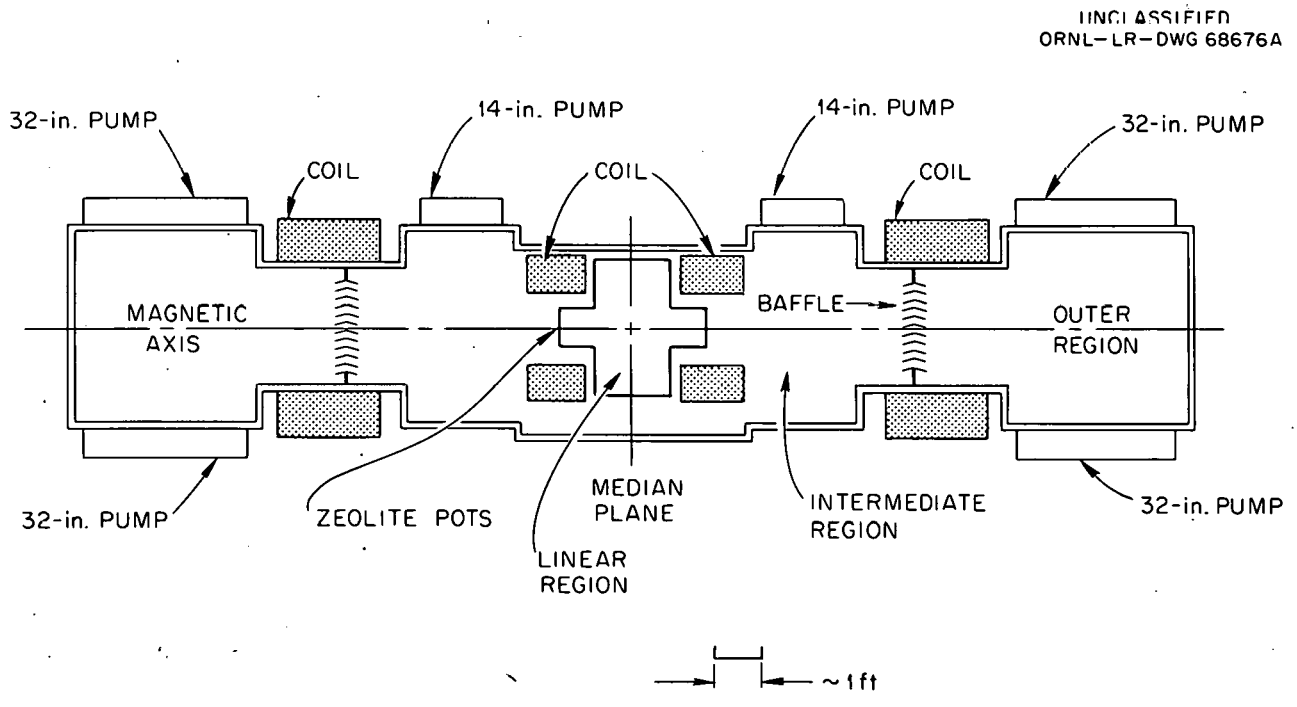

Fig. 1.2. Axial Section of DCX-1.

the trapped energetic protons. The second consideration was that operation at the lowest pressures was thought to be most favorable for observation of the effects of dissociation of the H_2^+ on plasma already trapped. In a simple formulation given earlier,[4] it was shown that an indication of this additional dissociation might be obtained by comparing the NPD signals measured during buildup of the plasma (during the period of plasma accumulation following the injection of the H_2^+ beam) with those measured during decay. If the rate at which protons are trapped by plasma dissociation is greater than the charge-exchange loss rate, then during the buildup interval the number of trapped protons increases with time at a rate that is faster than linear, and the equilibrium density would presumably be limited by scattering, possibly aided by instabilities. When this trapping rate equals the charge-exchange loss rate, a condition associated with a critical product of H_2^+ current and trapped-proton containment time, the number increases at a linear rate to the same equilibrium density. With the trapping rate less than the charge-exchange rate, the number rises exponentially to a lower equilibrium value, but does so with a time constant that is longer than that of the charge-exchange decay of the plasma. The NPD signals are a measure of the charge-exchange reaction rate and therefore a measure of the number of trapped energetic protons; so, studies of the buildup and decay signals could be interpreted in terms of the effects of plasma dissociation.

The initial comparisons of these NPD signals were made by using an array of five of the usual foil-covered Faraday-cup detectors[5] located as shown in Fig. 1.1. This array was centered on the median plane, and, since the detectors were at 1-in. intervals, extended to $Z = 2$ in.

Two experimental difficulties were encountered. One was the existence of a fast component of detector signal, which responded to the H_2^+ beam in the manner indicated in Fig. 1.3. This component was believed to be due to dissociation neutrals from the H_2^+ beam, particularly those from the higher-pressure intermediate-vacuum region. A metal plate was inserted into the liner region so as to completely kill the plasma wrap-up without interfering with the H_2^+ beam trajectory. Then the vertical shield shown in Fig. 1.1 was gradually raised while the H_2^+ beam was gated on and off and the fast signal to the NPD was being observed. This signal disappeared when the shield was in the proper position to intercept the dissociation neutrals. When the metal plate that stopped the proton wrap-up was withdrawn, both a fast and a slow component of NPD signal were again observed, though the fast component was only about a tenth of that obtained without the shield. The origin of this unsuppressed fast component is not yet known. Despite the observations just described, there is also evidence (to be presented later in this section) that it is not a signal from the proton wrap-up. Unless a specific statement is made to the contrary, the NPD data presented in this report pertain only to the slow-time-constant portion of the signal. The second difficulty arose because the NPD array did not extend far enough from the median plane to be sensitive to the full Z extent of the steady-state plasma at low pressures. The implications of this fact will be made more clear.

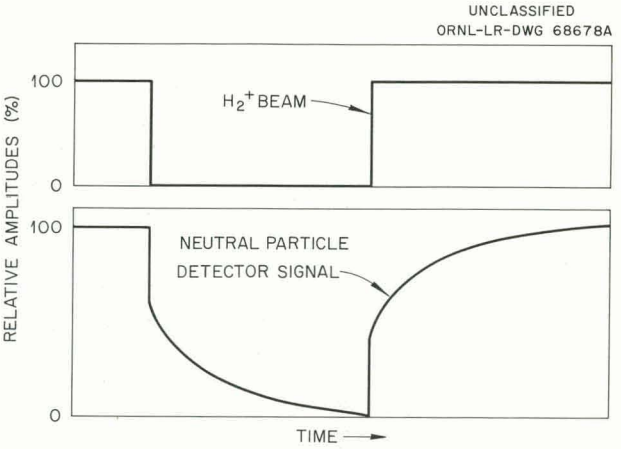

Fig. 1.3. Response of the Neutral-Particle-Detector Signal to Time Variation of the H_2^+ Beam.

Figure 1.4 shows NPD traces typical of the data obtained. In each oscillogram the trace is

[4] *Thermonuclear Div. Progr. Rept. Oct. 31, 1961*, ORNL-3239, pp 8–9.

[5] The operation of these detectors is described in *Thermonuclear Div. Progr. Rept. Oct. 31, 1961*, ORNL-3239, p 2, sec 1.2. Hydrogen-atom beams at normal incidence and having particle energies less than 50 kev do not penetrate the nickel foils. Beams with energies greater than 150 kev are unattenuated in number.

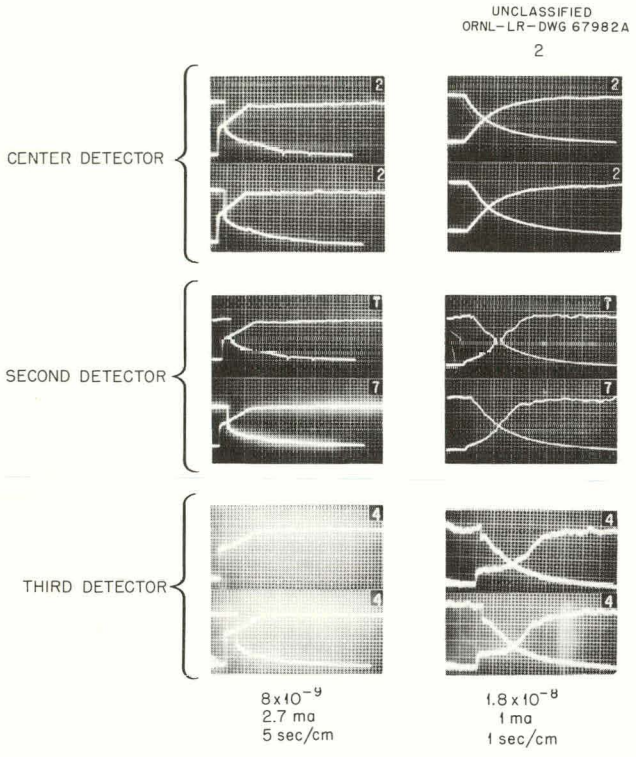

Fig. 1.4. Neutral-Particle-Detector Buildup and Decay Traces. The amplitude sensitivities are different for the different detectors and also for the same detector at different pressures.

started with a steady-state plasma in the apparatus (with the H_2^+ beam being injected). After a centimeter or so, the H_2^+ beam is gated off and the decay signal recorded. The spot is allowed to retrace, and the H_2^+ beam is cut on again to record the buildup signal. As the pressure is lowered into the 10^{-8} and 10^{-9} torr ranges, the decay signals remain exponential with time constants appropriate for charge exchange, but the buildup signals gradually become more nearly linear than exponential. A very approximate calculation based on the formulation previously described suggests a critical $I\tau$ product of about 200 ma-sec for the observation of linear buildups due to the effect of plasma dissociation. That such buildups were actually observed with $I\tau$ products as low as only 3 ma-sec (150-μa H_2^+ beam and 20-sec τ) strongly argues that the effect is not due to this dissociation. A more reasonable explanation is suggested by the delays in the buildup responses of detectors positioned off the median plane as compared with the one on the median plane. These delays indicate that during buildup at low pressures the plasma volume is expanding on a time scale of a few seconds.

It appears that volume expansions of this type can account for most features of the buildup curves. Figure 1.5 is a plot showing the effect of a slowly expanding volume on a buildup signal where it is assumed that the detector responds to the average fast-proton density. The volume is assumed to expand exponentially, according to the expression in the figure, and the buildup signals are shown for several values of the expansion-time constant τ'. Close fits to experimental data have been possible with such curves as these where the expansion-time constants were evaluated from the delay in the buildup responses of detectors off the median plane and the magnitude of the expansion from the full width at half maximum of the detector signal profiles. These profiles are plots of the steady-state amplitudes of the NPD charge-exchange signals as a function of the displacement of the detector off the median plane and are therefore indicative of the spatial extent of the plasma.

As the various vacuum modifications described in Sec 1.1 were completed and the operating base pressure of the apparatus was extended further into the 10^{-9} torr range, the Z extent of the 5-unit NPD became increasingly inadequate. Complete signal profiles could not be obtained below

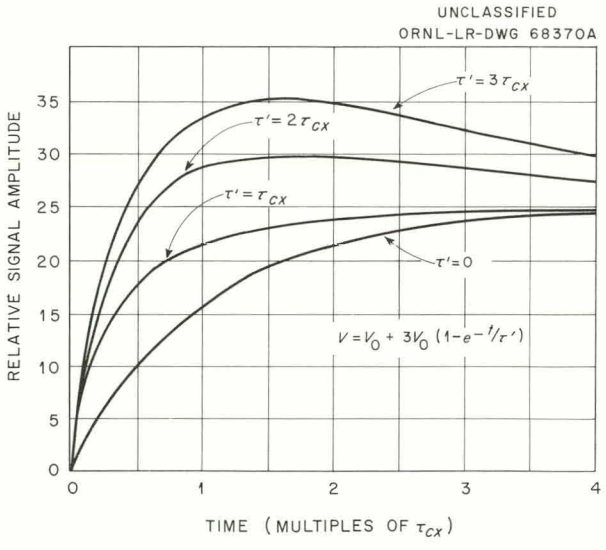

Fig. 1.5. The Effect of an Expanding Volume on Neutral-Particle-Detector Buildup Curves.

a few $\times 10^{-8}$ torr with a 1-ma H_2^+ beam, and even at these pressures it was obvious that there was considerable dependence of plasma volume on injected H_2^+ current. Complete profiles were needed for adequate volume estimates, for an accurate assessment of the total charge-exchange loss rate, and for further experiments comparing buildup and decay signals.

In the most recent work, considerably more data was accumulated by using a set of 12 NPD's at the same angular position as indicated in Fig. 1.1. This detector assembly was also centered on the median plane and the detectors were mounted at 1-in. intervals to extend across the entire axial length of the liner region. As with the previous detectors, both a fast component and a slow, exponentially decaying component of signal were received.

Figure 1.6 shows the reciprocal of the exponential time constant of the slow component as a function of pressure. These particular data are from a central NPD but are also representative of data from the other detectors as well. The curves indicate reasonable agreement with values calculated from the cross section for charge exchange of 300-kev protons, with experimental τ values from 50 to 80% of the calculated values at 2×10^{-9} and 1.5×10^{-7} torr respectively. These data show no τ dependence on injected current for H_2^+ beam values of 1.25, 5.0, and 8.3 ma. Earlier measurements[6] had shown that the measured τ remains 80% of the calculated up to at least 10^{-5} torr. This difference at higher pressures is attributed to about 10-kev energy loss on the part of the circulating protons, a value in reasonable agreement with stopping-power calculations. The progressive deviation from a 45° slope at lower pressures is usual and is attributed to the effects of the base-pressure gases, for which no composition correction has been made to the indicated ion-gage pressure.

That the decaying charge-exchange signal is indeed very nearly exponential at even the lowest operating pressures is indicated in Fig. 1.7, which shows one of the longest containment times yet measured in DCX-1. The time to decay to the $1/e$ point is about 30 sec, and the long straight-line section has a time constant of 40 sec. The experimental decay signal was plotted by an xy recorder, rather than by an oscilloscope, as is usually done, in order to increase the accuracy of the plot. Detectors located off the median plane characteristically show an initially slower rather than faster decay. One suggestion

[6] *Thermonuclear Div. Progr. Rept. Oct. 31, 1961*, ORNL-3239, p 6, Fig. 1.2.

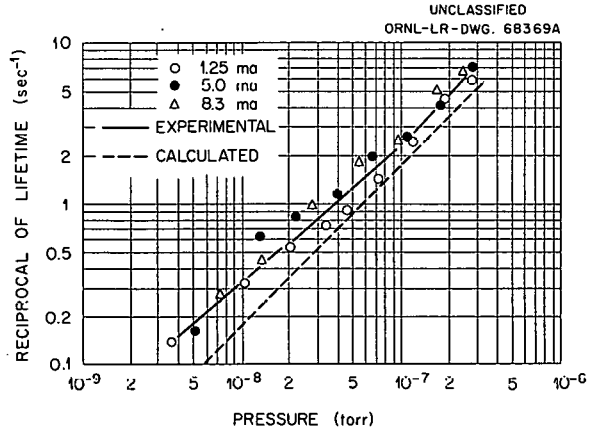

Fig. 1.6. The Reciprocal of the Lifetime as a Function of Pressure for a Helium Leak.

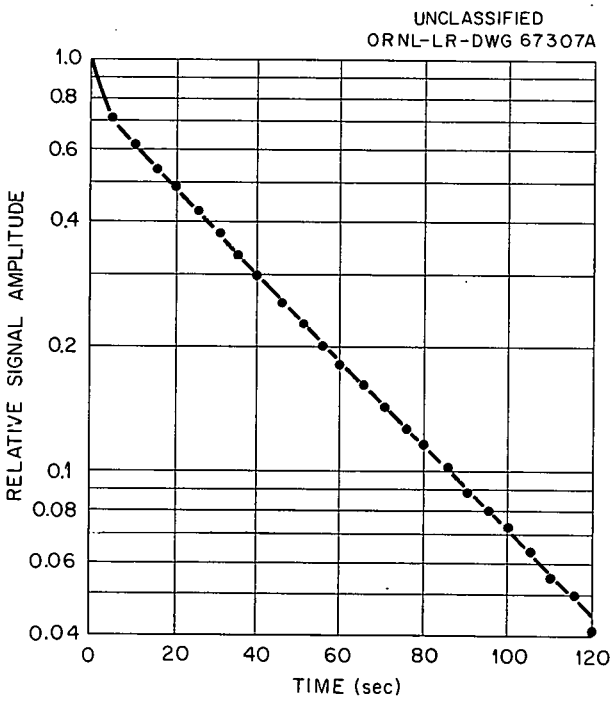

Fig. 1.7. A Semilogarithmic Plot of the Amplitude of the Decay Signal from a Neutral-Particle Detector on the Median Plane. Measured at 3.8×10^{-9} torr with 2.75 ma of H_2^+.

is that this difference is due to a slight feeding of protons outwards from the more densely populated median plane (where the initial trapping occurs) during the initial time interval after gating off the H_2^+ beam.

The point emphasized here is that the shapes of the charge-exchange decay signals and the $1/\tau$-vs-pressure curves show no peculiarities as the measurements are extended to very low pressures. They are simply the curves that have been previously measured at higher base pressures displaced to the lower pressures and to longer τ's. They continue to indicate that after the H_2^+ beam is gated off, the fast-proton density decreases only by virtue of charge-exchange losses.

Such conclusions based on the time constants of the decaying charge-exchange signals apply only to losses after proton trapping has ceased. Evidence pertaining to the loss mechanisms during steady-state operation of the apparatus is supplied by the steady-state amplitudes of the charge-exchange signals. For the purposes of the following arguments these will be taken as the initial amplitudes of the NPD decay signals that have the charge-exchange time constant; that is, the fast component of detector signal will again be ignored.

Figures 1.8 and 1.9 show signal profiles, that is, plots of the NPD steady-state charge-exchange signals as a function of the displacement of the detectors from the median plane. The curves given are representative of measurements made with the 12-unit detector. The median plane indicated on these figures is the geometric median plane. That the profiles peak slightly off this plane indicates that the magnetic median plane of the apparatus does not coincide exactly with the geometric. The profiles obtained with 1.25 ma of H_2^+ have fwhm of $1\frac{1}{4}$ in. at 2.8×10^{-7} torr and $1\frac{3}{4}$ in. at 3.6×10^{-9} torr. Profiles with 8.3 ma of H_2^+ have fwhm of $1\frac{1}{2}$ and 8 in. for pressures of 2.6×10^{-7} and 6.4×10^{-9} torr, respectively. At the lower pressures the profiles

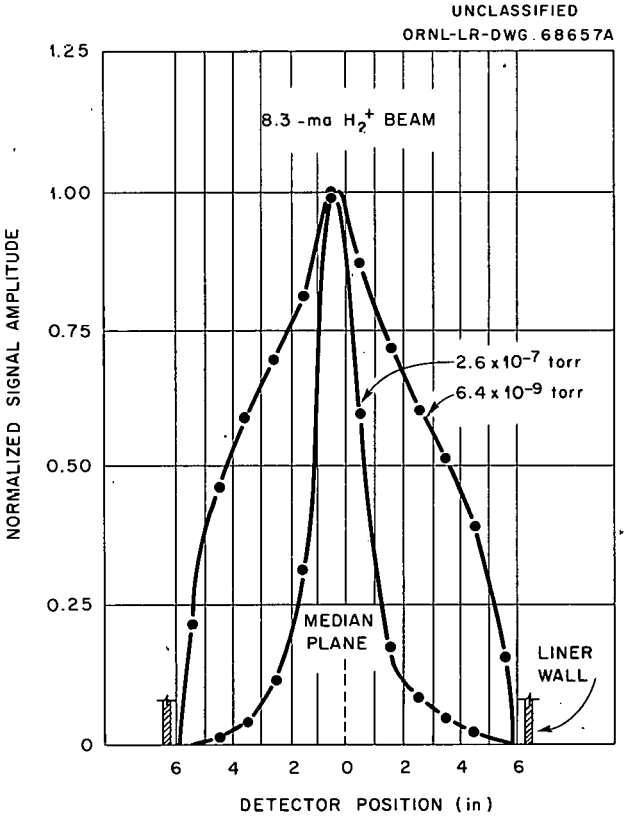

Fig. 1.8. Neutral-Particle-Detector Signal Profiles for 8.3 ma of H_2^+.

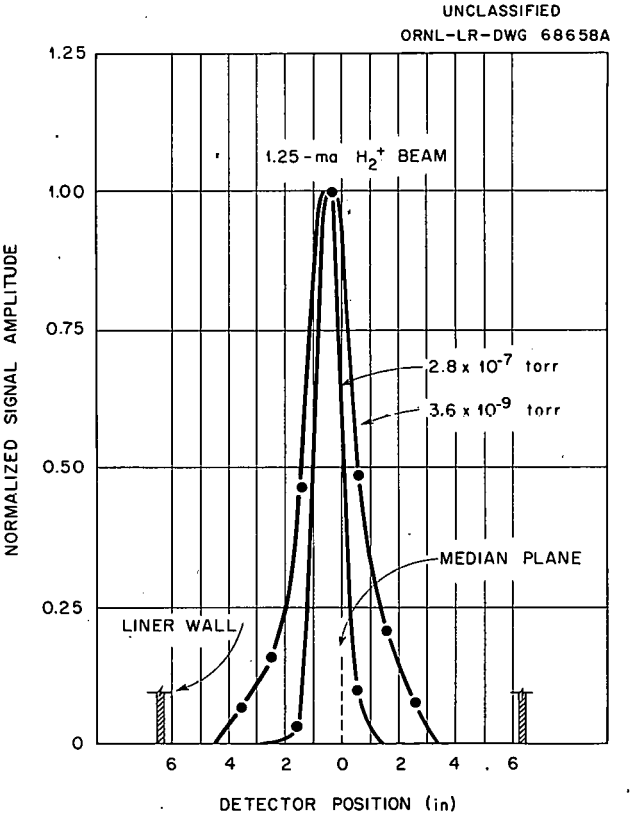

Fig. 1.9. Neutral-Particle-Detector Signal Profiles for 1.25 ma of H_2^+.

are evidently quite sensitive to the H_2^+ current, a point which is emphasized in Fig. 1.10. Also note that the shape of the profile with 8 ma at 6×10^{-9} torr differs from the others in that the signal drops very sharply to zero. As the pressure is raised, the profiles for 8 ma gradually assume the usual bell shape. This transition was complete in a profile measured at 6×10^{-8} torr.

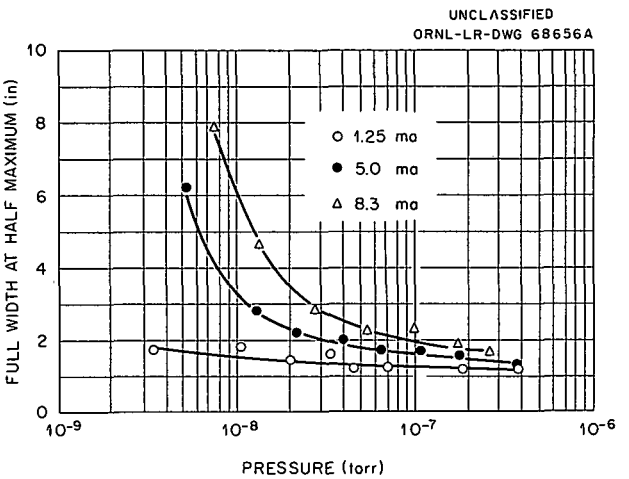

Fig. 1.10. Profile Half-Widths as Functions of Pressure and H_2^+ Current.

These features are interpreted as indicating that with 8 ma at 6×10^{-8} torr the plasma has expanded to fill the 10-liter volume to which it is restricted by the walls, and that at lower pressures wall collisions are contributing to plasma loss during steady-state conditions. The fact that the wall-collision losses occur only during steady-state operation is evidenced by the fact that even with 8 ma at base pressure the slowly decaying component of detector signal still has a time constant appropriate for charge-exchange losses. Also, as will later be argued, this is the only component of detector signal that need be considered in particle-accountability calculations. This 10-liter restriction on the volume is entirely the result of the structural configuration of the chamber. The magnetic-field configuration is such that a volume of 25 liters is absolutely contained, and a simple modification of the chamber would permit the plasma to occupy the entire 25 liters without encountering mechanical obstructions. Profiles such as those shown on this figure indicate that the steady-state plasma volume varies from 1 or 2 liters at high pressures to something more than 10 liters at low pressures with high beam currents.

Studies have also been made in the changes of profiles as a function of time during the buildup interval when operating at low pressures. These show that the initial volume is again 1 or 2 liters, and that this volume expands to the larger steady-state value on a time scale on the order of a few seconds.

Figure 1.11 is a plot of the total steady-state charge-exchange decay signal to the NPD as a function of pressure and H_2^+ beam current. The total signal is the sum of the 12 individual signals and therefore each experimental point represents an integral of a signal profile similar to those shown in Figs. 1.8 and 1.9. Since the charge-exchange losses have θ symmetry, each point represents a fixed fraction of the total charge-exchange loss rate; so, these curves are useful in balancing this loss rate against the proton-trapping rate.

Consider first the curve of 1.25 ma for H_2^+. The shape is again that measured in a number of previous runs at higher base pressures – a high-pressure slope of 45° and a gradual flattening at lower pressures. As in the case of Fig. 1.6, the high-pressure section shows the expected linear dependence on neutral density, and the progressive deviation at lower pressures shows the

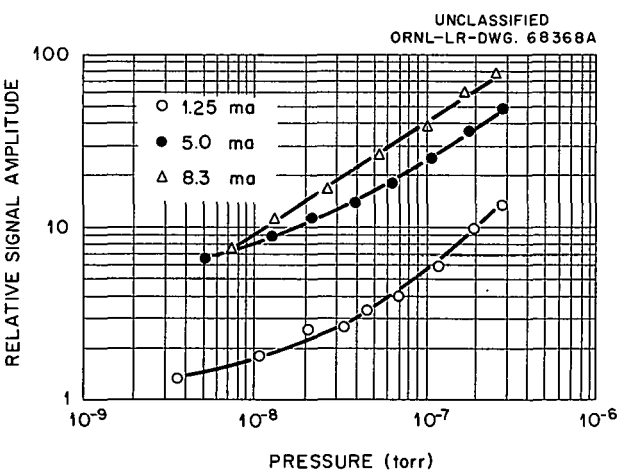

Fig. 1.11. The Total Neutral-Particle-Detector Charge-Exchange-Decay Signal as a Function of Pressure for a Helium Leak.

effect of base-pressure components. The amplitude of the curve at the highest pressure indicates that 1.5×10^{11} protons/sec are lost by charge exchange. This figure is in very good agreement with the calculated trapping rates, which range from about 1 to 1.5×10^{11} protons/sec, depending on the cross section data employed. The 5-ma curve is scaled up by the proper factor of 4 over the 1.25-ma curve. At the higher pressures the 8-ma curve also scales properly. The scaling fails for the lower 3 points, but as was just indicated, these are the pressures at which the signal profiles show that wall collisions are beginning to play a role. The failure of the scaling law is a verification of this fact.

It must be emphasized that the excellent agreement between the calculated proton-trapping rate and the measured loss rate was obtained by using only the charge-exchange portion of the signal to the NPD. A pressure scan of the total amplitude of the unsuppressible fast component of the NPD signal was made with 5 ma of injected H_2^+ and with a helium gas leak. Adding this portion of the signal to the total charge-exchange signal for the 5-ma curve of Fig. 1.11 raises the lowest pressure point by a factor of 4 and the highest pressure point by a factor of 2. The curve between these points is smooth, with a gradual slope. If this curve is then assumed to represent the steady-state loss rate, the agreement is much less accurate in both shape and amplitude with the calculated proton-trapping rate. These considerations suggest that the unsuppressible fast component of signal does not represent a loss of protons from the plasma volume. Investigations of the origin of this signal are planned.

The fast component, in particular the very rapid manner in which it responds to fluctuations of the H_2^+ beam, has so far prevented meaningful measurements of the total NPD charge-exchange signal during buildup intervals at low pressures. Though it is believed that the differences in buildup and decay signals from individual detectors near the median plane are primarily the result of volume expansion, this point should be checked by examining the responses of the total signals.

The neutral-particle-detector data can be summarized as follows: At high pressures, the volume is 1 or 2 liters (corresponding to an average fast-proton density of about 10^7 per cubic centimeter per milliampere of H_2^+) and relatively independent of the H_2^+ beam current. At lower pressures, the initial volume is again about 1 or 2 liters, but expansion occurs during the buildup interval on a time scale of a few seconds, and the equilibrium volume becomes quite sensitive to the H_2^+ current. With 8 ma of H_2^+ at 6×10^{-8} torr, the equilibrium volume has expanded to the maximum of 10 liters permitted by the present mechanical arrangement. With 5 ma at 5×10^{-9} torr, however, the volume limit is not yet reached. In addition to a slow component whose origin is obviously charge-exchange loss of trapped energetic protons, the NPD signal also has a fast component, which responds very rapidly to the H_2^+ beam and whose origin is not yet known. The time constants of the slow component of the signal are in accord with charge-exchange times, and the loss rates calculated by using only these charge-exchange signals are in excellent agreement with the calculated proton-trapping rates, except under conditions of operation where wall collisions play a role.

The specific forces driving the volume expansion are not yet clear, though it appears that they are collective rather than single-particle in origin. Further discussion of this expansion and other low pressure phenomena are given in Sec 1.6.

1.3 MEASUREMENTS OF PLASMA POTENTIAL

The lithium-ion beam probe previously described[7] was used to extend the measurements of plasma potential to the lower operating pressures. Oscilloscope recording of the transmitted ion current as a function of acceleration potential was employed. Figure 1.12 shows typical traces obtained both with and without a trapped plasma. For a steady plasma potential one would expect to measure the upper trace simply shifted to a higher acceleration potential by an amount equivalent to the plasma potential. The fluctuations in the traces actually recorded therefore correspond to fluctuations in the plasma potential. The experimental data were analyzed in terms of the limits between which the potential

[7] *Ibid.*, pp 6–7; also G. R. Haste and C. F. Barnett, *J. Appl. Phys.* 33, 1397 (1962).

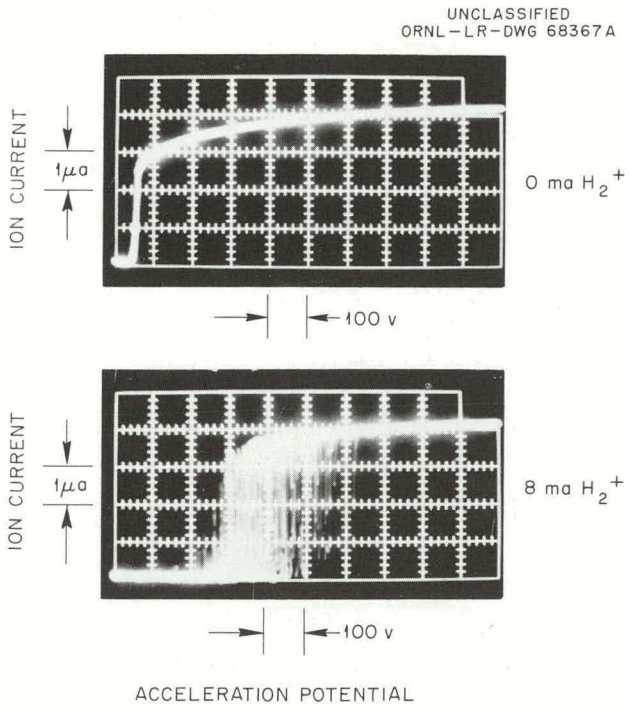

Fig. 1.12. Transmitted Lithium-Ion Current as a Function of Acceleration Potential. Measurements made at 2.8×10^{-8} torr.

fluctuated and the average value of the potential, the latter being a visual assessment of that value of the potential from which fluctuations to a higher value were as probable as fluctuations to a lower value.

Figures 1.13, 1.14, and 1.15 present the results as functions of pressure for different values of H_2^+ currents. The lower pressures and higher beam currents produced both the higher potentials and the larger ranges of fluctuation. The 8-ma data obtained in this set of measurements indicate that the potential at base pressure fluctuated between 200 and 750 v. At about the same pressure and beam but at other times, it has fluctuated as high as 2 kv.

In one measurement with several ma of H_2^+ at pressures high in the 10^{-9} torr range, the fluctuations in potential were observed at an average rate of about 25 per second. The fluctuations, however, were not periodic, and the variation of the rate with pressure and H_2^+ current has not yet been determined.

Computer calculations of the potentials developed by a toroidal charge distribution within

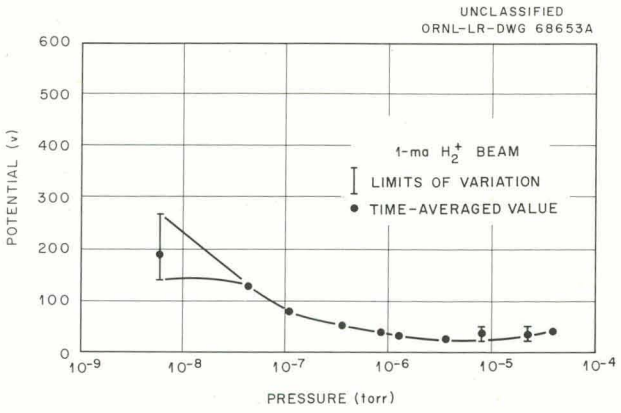

Fig. 1.13. Plasma Potential as a Function of Pressure for a Helium Leak with 1 ma of H_2^+.

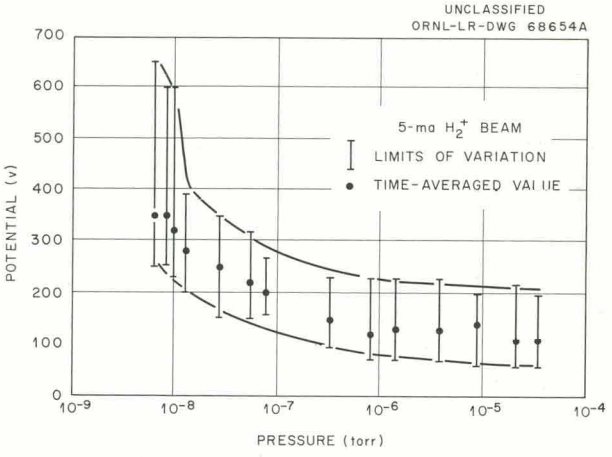

Fig. 1.14. Plasma Potential as a Function of Pressure for a Helium Leak with 5 ma of H_2^+.

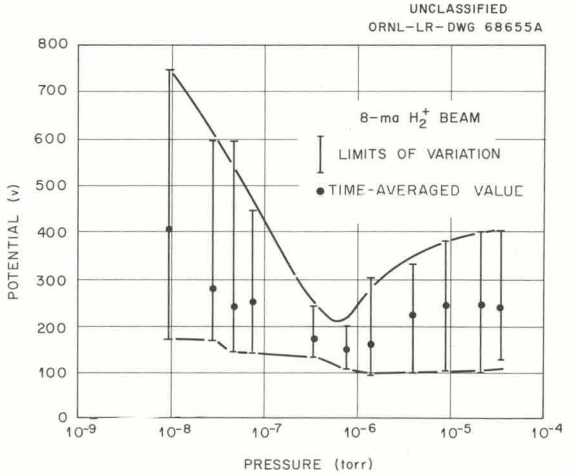

Fig. 1.15. Plasma Potential as a Function of Pressure for a Helium Leak with 8 ma of H_2^+.

conducting walls similar to the DCX-1 geometry are in progress and are described elsewhere in this report.[8]

1.4 MEASUREMENTS OF THE ENERGY DISTRIBUTIONS OF CHARGE-EXCHANGE NEUTRALS

Previous reports[9] have described measurements of the energy distributions of energetic hydrogen-atom neutrals escaping the plasma region as a result of electron capture collisions of the circulating protons with background gas. Other experiments were recently undertaken to confirm the previous results for gas dissociation and to extend the measurements over a wider pressure range and to higher H_2^+ beam currents.

The earlier work had employed a highly collimated spectrometer in which the neutrals were recharged in an argon gas cell and the resulting protons then electrostatically analyzed. The later experiments used a silicon barrier detector[10] mounted in wide-angle geometry (approximately 45° full angle) and operated in conjunction with a 256-channel analyzer. Figure 1.16 shows the position of the detector in DCX-1 and a block diagram of the associated circuits. In data taken thus far, the detector was mounted on the median plane.

With the detector located as shown in Fig. 1.16, comparisons of the counting rate under steady-state conditions with the rate exhibited during the initial interval of plasma decay after cutting off the H_2^+ beam showed that the detector was

[8] This report, sec 6.6.

[9] *Thermonuclear Div. Semiann. Progr. Rept. Jan. 31, 1961*, ORNL-3104, pp 1–8, secs 1.1.1 and 1.1.2.

[10] The first use of these detectors in DCX-1 was described in *Thermonuclear Proj. Semiann. Progr. Rept. July 31, 1960*, ORNL-3011, pp 78–79, sec 7.1.

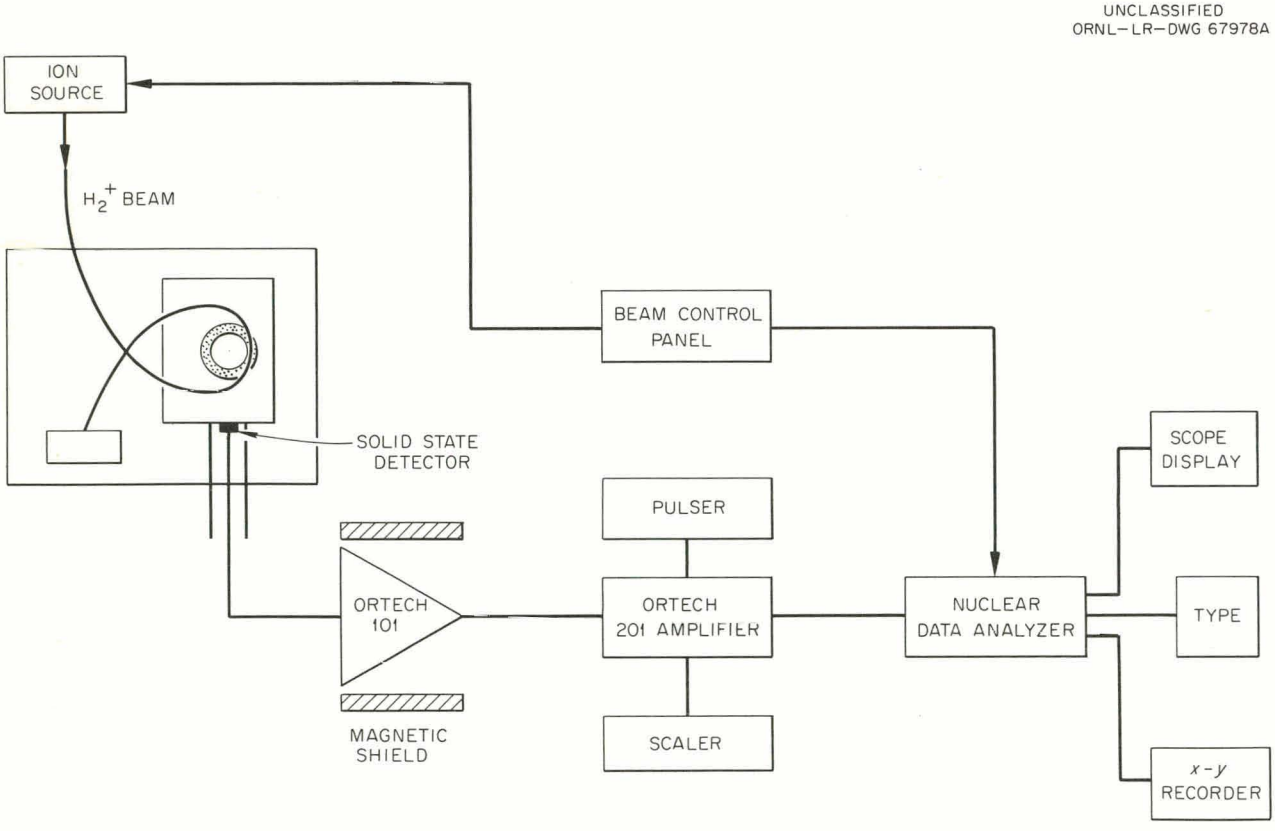

Fig. 1.16. Detector Mounting and Circuit Diagram for Energy Analysis in DCX-1.

responding only to charge-exchange neutrals. It did not register counts from the fast component of the signal that was discussed in Sec 1.2 in connection with the neutral-particle detectors.

Data were accumulated for various conditions of pressure (8×10^{-9} to 1×10^{-4} torr) and H_2^+ currents (0.5 to 4.5 ma). The analyses are not complete, but in general these later measurements appear to confirm the earlier work. The peaks of the proton distributions (derived from the neutral distributions by correcting for the variation of the charge-exchange cross section with energy) remain near 300 kev, and the distributions become broader as the H_2^+ beam current is increased. Figure 1.17 shows plots of typical spectra that illustrate this trend. The variations with pressure are not uniform; the broadest distributions appear near 1×10^{-7} torr, where the fwhm of the proton distributions (not corrected for resolution effects) are about 30 kev for 0.5 ma of H_2^+ and 50 kev for 4.5 ma of H_2^+. These half-widths indicate proton mean collision energies of some tens of kiloelectron volts.

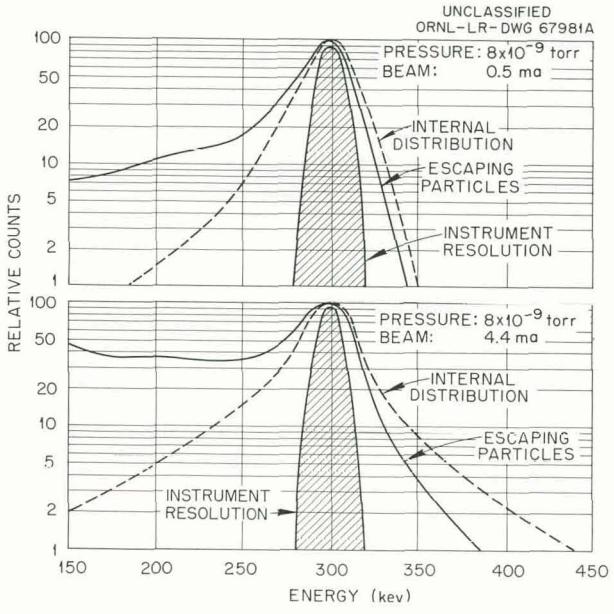

Fig. 1.17. Energy Distributions of Neutrals and Protons in DCX-1. The escaping particles are the charge-exchange neutrals, and the internal distribution is that of the circulating protons.

An IBM 7090 computer code is being prepared[11] to derive the proton distributions and to calculate several quantities characteristic of each spectra.

1.5 MEASUREMENTS OF RADIO-FREQUENCY SIGNALS

A number of the measurements of the coherent proton cyclotron signals reported earlier[12] have been extended to the lower operating pressures. The rf onset times, that is to say, the time intervals required for the coherent signals to appear after cutting on the H_2^+ beam, continue to increase as the pressure is lowered. Figure 1.18 shows the reciprocal of this onset time for the 14-Mc fundamental as a function of pressure. Operation at about 5×10^{-9} torr has resulted in onset times of up to 0.8 sec for this frequency. The peak-to-peak amplitudes of the signals continue to vary nearly proportionally with the injected H_2^+ current.

Studies of the amplitudes of the rf signals as functions of pressure have shown the responses indicated in Fig. 1.19. An explanation for the

[11] By Mozelle Rankin.

[12] *Thermonuclear Div. Progr. Rept. Oct. 31, 1961*, ORNL-3239, pp 4–6, sec 1.3; *Thermonuclear Div. Semiann. Progr. Rept. Jan. 31, 1961*, ORNL-3104, pp 8–10, sec 1.1.3.

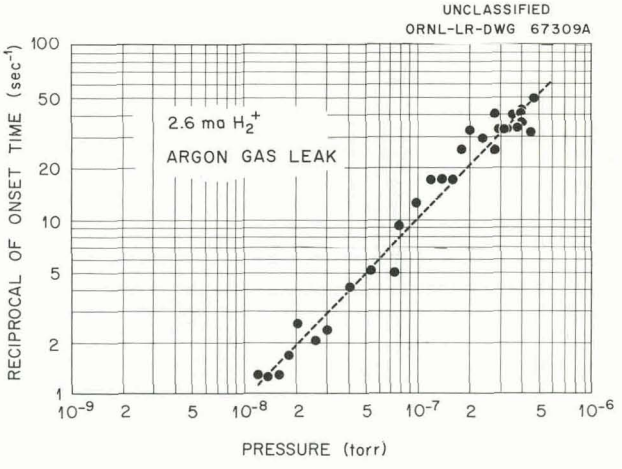

Fig. 1.18. The Reciprocal of the RF Onset Time for the 14-Mc Fundamental as a Function of Pressure.

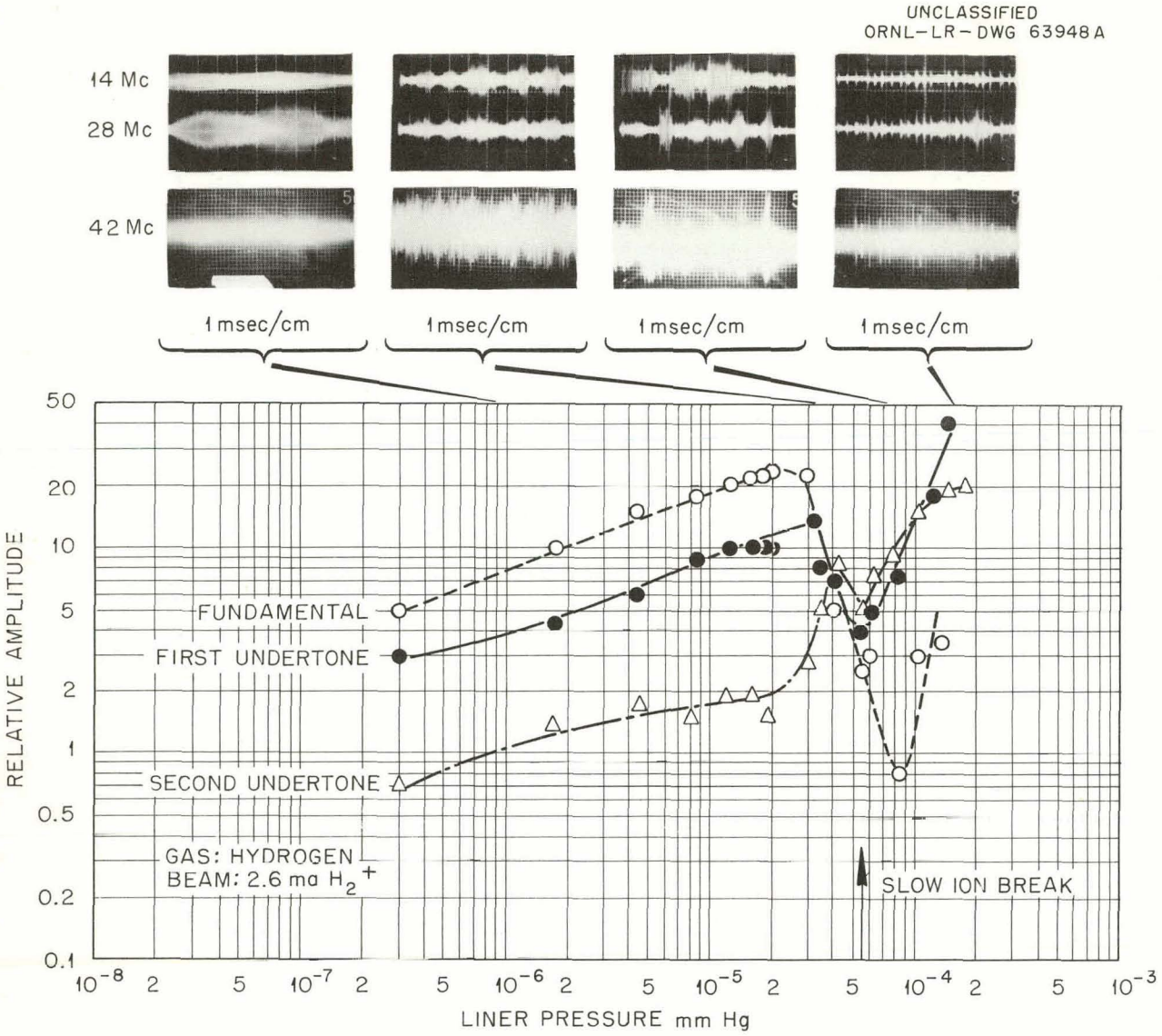

Fig. 1.19. Amplitudes of the RF Signals as Functions of Pressure for a Hydrogen Leak and 2.6 ma of H_2^+.

behavior in the neighborhood of 5×10^{-5} torr is given elsewhere in this report.[13]

There are gradual but significant changes in the character of the signals as functions of pressure. At high pressures (10^{-7} and 10^{-6} torr ranges) the coherent signals are continuous, are strongly modulated at frequencies of the order of 100 kc, and are confined to narrow bands about harmonics of the proton cyclotron frequency. (An fwhm of about 0.5 Mc for the fundamental is typical.) As the pressure is lowered, the signals gradually become more discontinuous and the frequency bands wider. At about 5×10^{-9} torr the rf appears in bursts at irregular intervals of $\frac{1}{2}$ to 1 sec, with durations of about 50 to 100 msec. The modulation patterns appear noisy rather than periodic, and the fundamental band is about 5 Mc wide.

Figures 1.20 and 1.21 show the response of the 14 Mc signal during buildup and decay in-

[13] This report, sec 6.2. Measurements of the slow ion current drifting out the mirrors have also shown breaks near this same pressure.

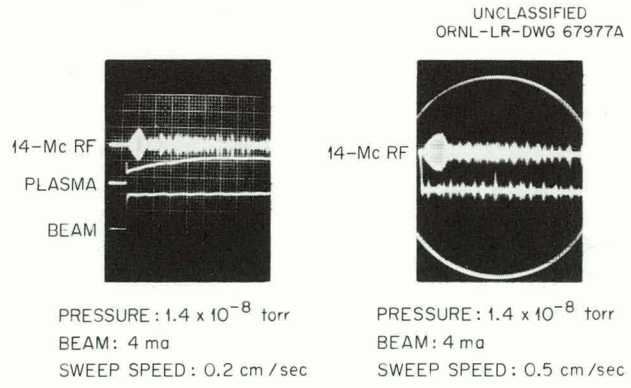

Fig. 1.20. Buildup of the 14-Mc RF and Neutral-Particle-Detector Signals at Low Pressure.

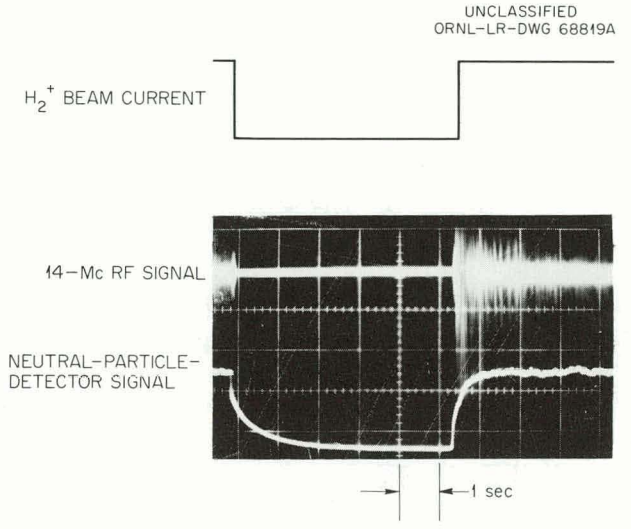

Fig. 1.21. Buildup and Decay of the 14-Mc RF and Neutral-Particle-Detector Signals at 3×10^{-8} torr with 8 ma of H_2^+.

tervals at pressures low in the 10^{-8} range. Note the sporadic nature of the steady-state signals and the rapidity with which the rf decays after the H_2^+ beam is cut off.

It has been found that the electrostatic shielding of the loop antennas customarily used is not completely effective, and about half of the total signal now appears to be electrostatic rather than magnetic in origin.

Evidence for interactions between the H_2^+ beam and the trapped plasma was searched for by comparing the rf signals from two pickup loops placed near the H_2^+ beam, both just outside the liner region (one near the beam entrance and the other near the exit). There was no evidence that noise or modulation was introduced into the H_2^+ beam as a result of its passage through the population of trapped protons.

1.6 MODEL OF THE DCX-1 PLASMA

The characteristics of the plasma at high pressure were explained[14] on the basis of a model that involves relatively stable charge clumps rotating with the circulating ring. These clumps provide steady coherent signals modulated by beat frequencies from clumps at slightly different magnetic-field values. The concentration of radiation about the cyclotron harmonics corresponds to a concentration of the plasma about the median plane, as is indicated by the neutral-particle-detector data. It was shown that the potential wells rotating with the charge clumps could probably account for the observed energy spreads. The question as to why the rf-probe signals were reduced by only a factor of 2 in amplitude when the loop was rotated out of the median plane has apparently been resolved by the discovery that about half the signal is electrostatic rather than magnetic in origin.

The high-pressure data acquired during the present report period confirmed the earlier observations. The low-pressure data emphasized the increasing disorder of the plasma with increasing trapped-proton lifetime. The volume indications from the NPD data and from the band widths of the cyclotron signals indicate an increasing transfer of proton velocity from θ to Z direction. The energy analyses show a broadening of the energy spectra. The noisy, sporadic nature of the rf signals at low pressure indicates that the charge clumping is then a transitory rather than a relatively stable phenomenon. The wide range of fluctuation of plasma potential gives further evidence that the "steady-state" plasma is far from steady.

Of the low-pressure data, the following points presently appear to be most significant: (1) that

[14] *Thermonuclear Div. Progr. Rept. Oct. 31, 1961*, ORNL-3239, pp 7–8, sec 1.5.

the protons are lost only by charge exchange after cutting off the H_2^+ beam even under conditions such that wall collisions are contributing to the steady-state proton loss rate; (2) that rf studies have shown no evidence of interactions between the H_2^+ beam and the plasma; and (3) that the response of the coherent rf signals to the cessation of the H_2^+ beam indicates that the charge clumps disappear in a time very short in comparison with the charge-exchange decay time. These points suggest that the plasma expansion is driven by the charge clumps, and that the role of the H_2^+ beam is to supply well-ordered monoenergetic protons that can easily clump.

Models for explaining the volume expansion are being explored.

2. DCX-2

P. R. Bell
J. S. Culver
S. M. DeCamp
G. G. Kelley
N. H. Lazar
R. J. Mackin, Jr.
J. D. G. Rather
R. F. Stratton
J. C. Thompson
C. W. Wright

2.1 INTRODUCTION

The DCX-2 apparatus (Fig. 2.1) is now nearing the end of its shakedown phase. The design of DCX-2 is most completely described in ref 1. More-detailed discussions of most components are given in the previous progress report[2] and in the earlier work cited there.

DCX-2 is a magnetic mirror experiment in which trapped energetic protons are produced by the dissociation of hydrogen molecular ions. An intense beam of 600-kev molecular ions enters through a magnetically shielded injection channel, or "snout," near one mirror. The ions follow a helical path to the far mirror and return to a target on the snout. The magnetic field is designed to give the helical path a very tight pitch, thus maximizing the path length of the molecular ions. The hydrogen produced as the undissociated ions recombine at the target constitutes the largest gas input to the system. The ion-pumping action of the trapped plasma acts as the primary vacuum pump for the system. Eventually there will accumulate a sufficient density of trapped protons (and an equal number of electrons, produced by ionization) to constitute a target which has a high dissociation efficiency. The initial dissociation is produced by collisions with background gas molecules or with the ions of an auxiliary cold plasma which is introduced into the machine for that purpose. Provision for ion pumping and for possible operation of a highly ionized gas arc as a trapping plasma largely determines the design of the vacuum system.

The following paragraphs describe the performance of the major DCX-2 components and include a discussion of initial experimental results.

2.2 MAGNETIC FIELD

With R. L. Brown and P. A. Thompson

The DCX-2 magnet system is designed to produce a mirror ratio of 3.3, a central axial field homogeneous to better than 0.1% over a length of about 1 m, and a field dip at the injection point of 1.7% averaged over an ion orbit.[1]

The magnet system is in routine operation, and no major difficulties have been encountered. A few internal shorts in the mirror coils have been bypassed without affecting the field appreciably. A paper describing the engineering and fabrication of the coils is now in preparation.[3]

Measurements of the magnetic field along the axis showed that it can be adjusted to show a peak-to-peak variation of 3 gauss out of 12 kilogauss over an axial length of 1.2 m. Simultaneously, a field dip of the desired magnitude can be

[1] P. R. Bell *et al.*, *The DCX-2 Program of Plasma Accumulation by High Energy Injection*, presented at the Conference on Plasma Physics and Controlled Nuclear Fusion Research, Salzburg, Austria, September 4–9, 1961.

[2] P. R. Bell *et al.*, *Thermonuclear Div. Progr. Rept. Oct. 31, 1961*, ORNL-3239, pp 10–15.

[3] J. F. Potts and S. M. DeCamp, *DCX-2 Confining Field Coils – Design, Construction, and Testing* (to be published).

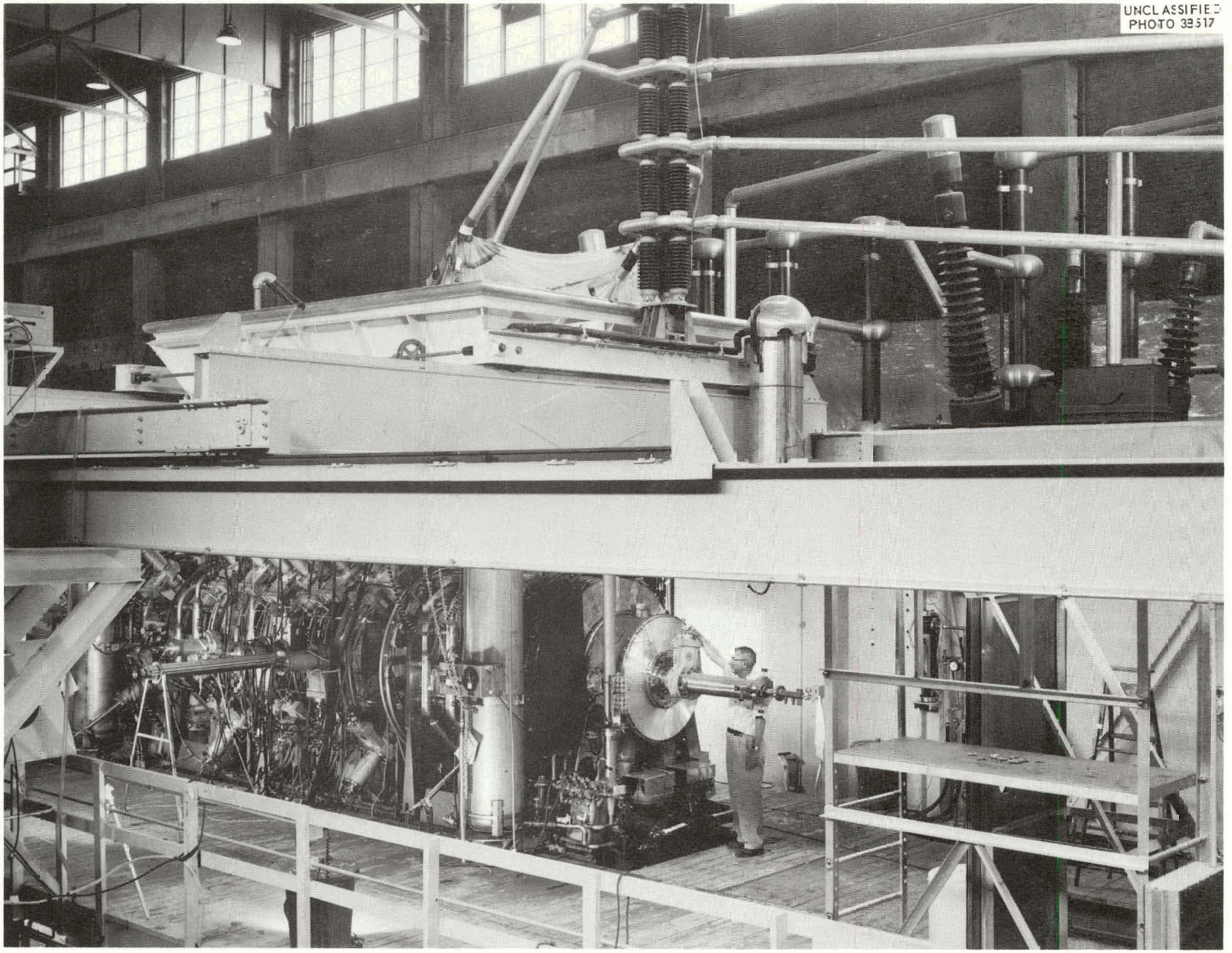

Fig. 2.1. The DCX-2 Apparatus.

produced at the injection point to steer the beam into the fine-pitched helix. It appears that a still greater degree of uniformity can be achieved without appreciable additional effort.

2.3 INJECTOR SYSTEM

With R. C. Davis, R. R. Hall, E. C. Moore, and O. B. Morgan

The arrangement of the injection system may be seen in Fig. 2.2, which also shows the variation in magnetic field transverse to the beam along its path. Coils are used in the pumping manifold for compensation of the deflection produced by this stray field.

A description of the apparatus may be found in previous reports,[1,2] and in Sec 5.1 of this report.

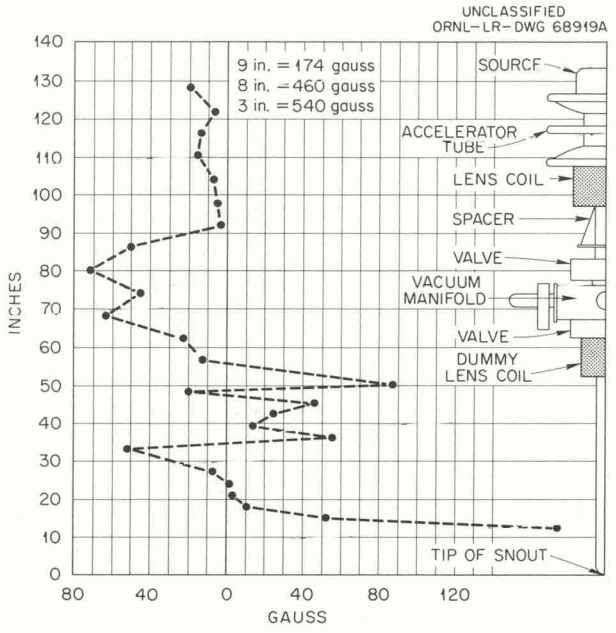

Fig. 2.2. Transverse Magnetic Field Along the Path of the Beam.

2.4 VACUUM SYSTEM

With R. A. Gibbons and T. F. Rayburn

Because of the many access ports and other vacuum joints, the vacuum system has not yet been made entirely leak free. Even so, the plasma-region pressure has been brought down without baking to about 5×10^{-6} mm Hg and the regions containing the diffusion pumps to about 1×10^{-7} mm. By evaporating titanium, the ballast region pressures were made as low as 2×10^{-8} mm.

A high-vacuum argon arc intended for bakeout purposes has been operated in DCX-2. Its length was 7 m, and typical operating parameters were 140 amp, 270 v. Radiated power appears to be roughly uniform along the arc and was as high as 4 kw/m. It is roughly proportional to anode gas flow, increases with arc current, and is much less sensitive to variation of other parameters.

The arc's pumping speed (as an ion pump on the plasma region) is 70 kiloliters/sec for argon and 33 kiloliters/sec for hydrogen. The lowest gage pressure recorded during an arc run was 2.2×10^{-6} mm Hg. The arc has not yet been used for a proper bakeout of the liner because the gas cooling system which controls and limits the liner temperature has not yet been installed.

The problem of the backstreaming of diffusion-pump oil continued for a while.[1] The manufacturer's suggested modification of the upper jet assembly did not appreciably reduce the backstreaming. A satisfactory upper jet assembly was finally designed by one of our group (P. R. Bell), and the problem appears once again to be laid to rest.

2.5 TRAPPING PLASMAS

An experimental lithium arc was operated in DCX-2. This was just a feasibility operation and no data were taken. Other activities leading to the the development of an auxiliary trapping plasma are described elsewhere in this report.[4,5]

2.6 SUMMARY OF INITIAL EXPERIMENTAL RESULTS

The first beam was injected into DCX-2 on January 24. Visual observation of the light indicated excessive beam deflection in the magnetically shielded channel for magnetic fields above 6 kilogauss. The difficulties were traced to insufficient compensation of the component of magnetic field along the channel. This component

[4] W. L. Stirling, this report, sec 4.2.1.

[5] R. A. Gibbons *et al.*, this report, sec 4.2.2.

was large enough to saturate the shielding iron, thereby allowing transverse field to penetrate into the region of the beam. (An applied longitudinal field is relatively more efficient for saturating an iron cylinder than an equal transverse field.) Additional solenoidal compensating coils were built and placed around the duct. Magnetic measurements then showed fields of less than 50 gauss in the channel for axial fields in the confinement region up to ~12 kilogauss.

Under these conditions, but with the pressure in the plasma region of the liner $\sim 1.5 \times 10^{-5}$ mm Hg, a beam was injected into DCX-2 on April 24 and 26, 1962, in order to study the alignment and the effects of beam steering and focus. During the run, a foil-covered neutral-particle detector (FND) and an electrostatic pickup probe were inserted into the DCX-2 near the midplane. The FND uses a 10^{-5}-in.-thick foil as a neutral-to-ion converter, and the ion current is measured in a Faraday cup, with secondary electrons suppressed by the magnetic field. The sensitive area was about 4 cm^2. A dc amplifier with a sensitivity of 10^{-7} amp/v was used to feed the signal to one channel of a 16-channel recorder and to an oscilloscope.

The beam was run continuously so that the current signals represent the equilibrium current of dissociation-produced protons in the machine. If one assumes that the plasma was uniformly distributed over the uniform field region of the apparatus (3 m), the detector saw 4×10^{-5} of the total current. The signal levels varied from 10^{-9} amp up to $\sim 10^{-6}$ amp as beam focus, steering, and output varied.

During the run, it was found that the steering coil in the accelerator pump manifold had insufficient ampere turns to deflect the beam such that the FND signal maximized. The steering field required was opposite in direction to the transverse component of the stray field in the tube and manifold. This was true even with accelerator voltages as low as 400 kv. However, the trapped current at this voltage, assuming uniform plasma distribution, was as high as 25 ma when the total beam current (including all mass species) was 55 ma. At 500 kv, the maximum trapped beam was only about 7 ma with a 60-ma total beam.

At various times, the beam returning to the target was monitored, and typical values were: 7 ma to the snout and 0.75 ma trapped at 500 kv (with improperly adjusted steering current), compared with 7.5 ma trapped and 10 ma returning to the injector, under better conditions.

It had been hoped that the beam entering the tank would be visible, permitting a check of alignment with field on. In fact, however, the illumination produced was completely lost in the background light from the plasma. All that could be distinguished was an increased intensity in the cylinder defined by the molecular ion orbit.

2.7 RADIO-FREQUENCY SPECTRUM PRODUCED BY ION INJECTION

Observations of the radio-frequency spectrum found inside the copper central vacuum liner of DCX-2 are made with two sweeping spectrum analyzers. One analyzer (Panoramic model SPA-3/25) covers the frequency range from 200 cycles to 25 Mc, in sections as wide as 3 Mc, with sweep recurrence frequencies from 1 to 60 per second. The response bandwidth of the analyzer is adjustable from about 50 cycles to about 50 kc. The resultant rise time for response to a line frequency at the widest bandwidth is about 7 msec.

The second analyzer is designed to have a much faster sweep recurrence rate in order to get a more frequent sampling of the spectrum, since we expect a rapid modulation of the ion cyclotron harmonics in DCX-2. This analyzer was made to our specification by Panoramic and has a tentative model number, XPA-5. The frequency range covered is from 10 to 100 Mc in a single range, with sweep rates from 10 to 20 kc so that the spectrum can be sampled every 100 or 50 μsec. The analyzer bandwidth required for such a rapid sampling is quite large, bandwidths of $\frac{1}{2}$, 1, and 2 Mc being supplied. Both analyzers are provided with 50-ohm input circuits.

Shakedown of the analyzers was performed by measuring the spectra emitted by the high-vacuum argon arc used in DCX-2 for baking and radiation cleaning of the central liner. An electrostatic antenna about 10 cm long was inserted radially into the 90-cm-diam central liner of DCX-2 near the central plane, with the base of the probe only a few centimeters inside the wall. A shielded magnetic loop antenna 5 cm in diameter was also supplied about 15 cm from the central plane. These antennas were connected to the analyzers by about 80 ft of coaxial cable.

Operation of the argon vacuum arc excited radiations from H^+ ions produced by ionization of the residual gases of the vacuum in DCX-2. Figure 2.3 shows a small, expanded section of the spectrum around the H^+ ion cyclotron frequency (ICF) fundamental. The magnetic field was about half that of the normal field (about 5800 gauss). The regularly spaced sharp peaks are frequency markers. The upper trace is the spectrum received by the electric probe, the lower by the magnetic probe with its plane perpendicular to the magnetic field. The emission line is here replaced by an absorption line.

UNCLASSIFIED
PHOTO 38488

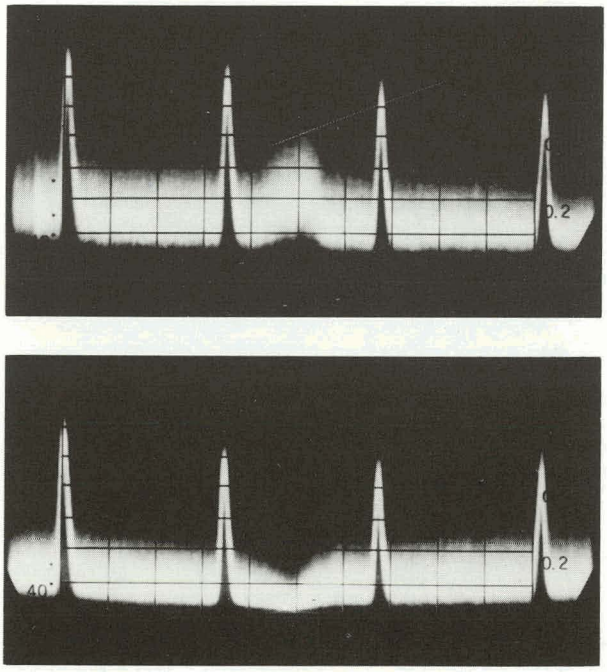

Fig. 2.3. Spectrum Excited by the Argon Vacuum Arc in the Region near the H^+ Resonance Frequency. The left marker is at 8.5 Mc, markers spaced every 0.5 Mc. Upper trace is from the electric probe; the lower trace is from the magnetic probe perpendicular to the magnetic field.

Injection of a 500-kev H_2^+ beam into DCX-2 (runs of April 24 and 26) produced very much stronger signals than did the argon arc. Figure 2.4(*a*), (*b*), and (*c*) are 3-Mc sections of the spectrum taken with the electric probe around the H_2^+,

UNCLASSIFIED
PHOTO 38486

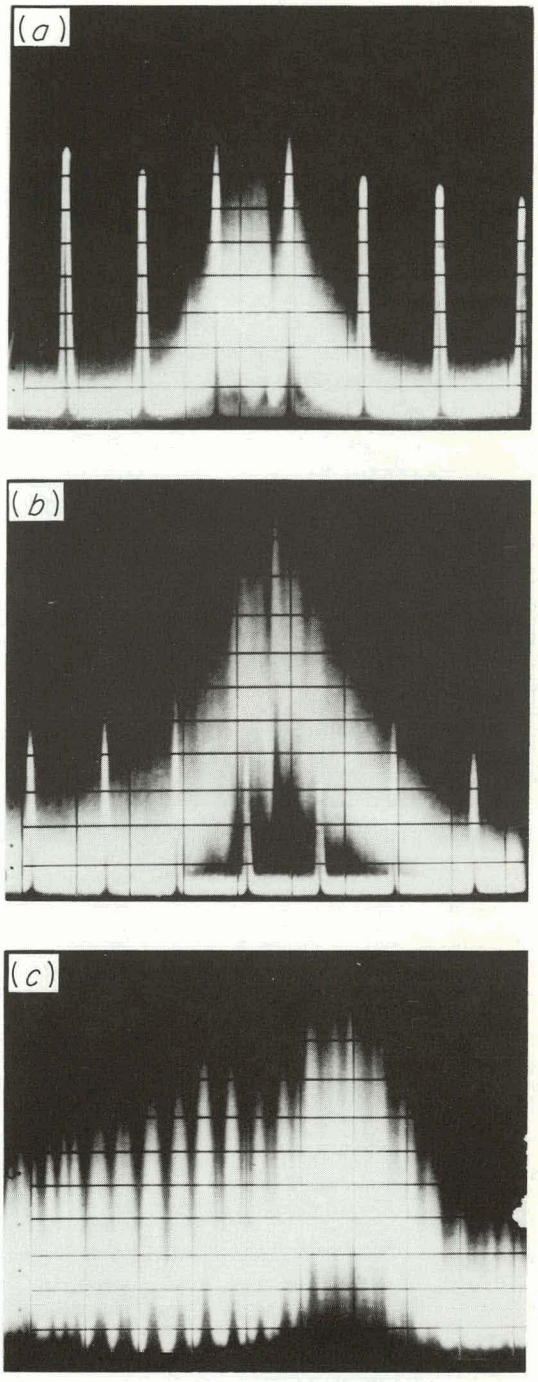

Fig. 2.4. Spectra Produced by 500-kev H_2^+ Injection. (*a*) H_2^+ ion cyclotron resonance line; (*b*) H^+ fundamental resonance and H_2^+ second harmonic; (*c*) H_2^+ third harmonic.

H^+, and third harmonic of H_2^+ ICF's. The peaks are very much broader than those produced by the cold ions excited by the argon arc. Relatively sharp absorption dips can be seen in the emission lines, but the fluted structure seen strongly in the 22-Mc peak and weakly in the others is not understood. A series of sections of spectrum were taken and patched together to make a rough spectrum (Fig. 2.5). The different sections were taken with somewhat different injected currents during adjustment of the DCX-2 parameters and show the effects of increasing broad-band noise with increasing injection so that adjacent sections of the spectrum do not match in amplitude. A series of wide-band spectra are shown in Fig. 2.6. These spectra correspond to different amounts of injected beam as indicated by the foil neutral detector at the center of DCX-2, although the conditions were very poorly controlled. Spectrum (*a*) shows frequencies corresponding to the harmonics of H_3^+ ICF's as well as to the harmonics of H^+. At somewhat larger currents, the even harmonics of the H^+ ICF's become very much stronger, and the broad-band noise also rises greatly, requiring a great decrease in analyzer gain for spectra (*e*), (*f*), and (*g*). When the injected beam was increased further, the even harmonics decreased rapidly without an increase of the broad-band noise, finally becoming almost undetectable.

The significance of this effect is not yet clear, and it could well be an instrumental effect or the effect of a relatively dense cold plasma near the antenna. Further tests, using a monitoring signal generator and shielded magnetic as well as electric antennas, will be performed to check the validity of the effect.

UNCLASSIFIED
PHOTO 38487

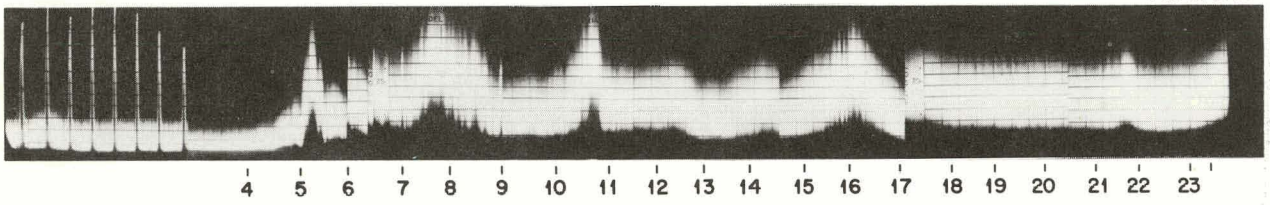

Fig. 2.5. Spectrum of Radio Frequency Produced by H_2^+ Injection into DCX-2. The peaks due to H_2^+, H_3^+, and H^+ can be seen, as well as strong band noise. Markers at 0.5-Mc intervals are shown from 0 to 3 Mc and from 6.5 to 9 Mc only.

UNCLASSIFIED
PHOTO 57837

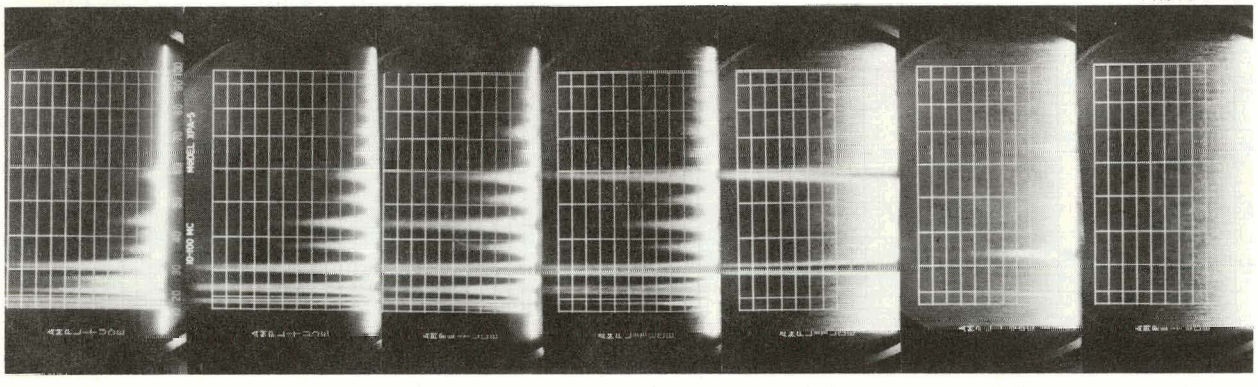

(*a*) (*b*) (*c*) (*d*) (*e*) (*f*) (*g*)

Fig. 2.6. Broad Band Spectra Produced by H_2^+ Injection. The strong lines in (*d*) and (*e*) are the even harmonics of the H^+ ion cyclotron frequency. Note the weakness of the H^+ fundamental in (*d*) and (*e*). The frequency shift in (*f*) and (*g*) is due to a small increase of magnetic field.

3. Plasma Physics

3.1 ELECTRON CYCLOTRON HEATING EXPERIMENTS IN THE PHYSICS TEST FACILITY (PTF)

M. C. Becker
R. A. Dandl
H. O. Eason
A. C. England
R. J. Kerr
W. B. Ard[1]

In previous semiannual reports,[2,3] experiments were described in which both 13- and 3-cm microwave power sources were used to produce a plasma heated at the electron cyclotron frequency in a magnetic mirror geometry.

During the last six months, work with 3-cm heating was concentrated on determining the electron temperature and the plasma configuration. In particular, careful measurements have now been made of the plasma magnetic field as an aid in determining the plasma configuration.

Our usual arrangement for coupling the power to the plasma is seen in Fig. 3.1, in which a copper microwave cavity encloses a mirror magnetic field. The surfaces of constant field intensity and the flux lines are also shown. Microwave power is fed

[1]Consultant from the University of Florida, Gainesville.

[2]*Thermonuclear Div. Semiann. Progr. Rept. Jan. 31, 1961*, ORNL-3104, sec 3.1.

[3]*Thermonuclear Div. Progr. Rept. Oct. 31, 1961*, ORNL-3239, sec 3.1.

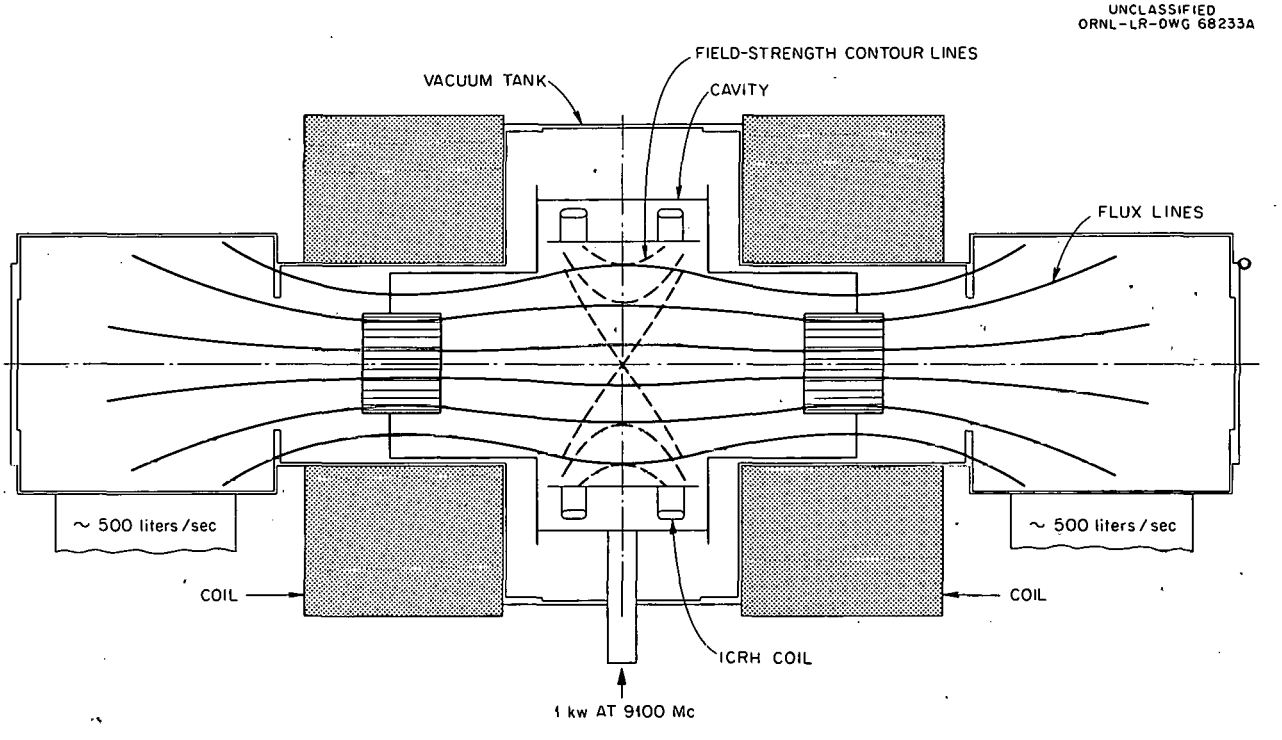

Fig. 3.1. Physics Test Facility Electron-Heating Experiment.

into the cavity and absorbed by the plasma electrons passing through the cyclotron-resonant constant field intensity zones. Variation of the magnetic field permits a choice of resonant zones, and the most favorable plasma conditions are usually correlated with end-zone heating. The plasma is fed with neutral hydrogen gas at a pressure of about 2×10^{-5} torr. Observation of microwave noise decay at 25 kMc (Fig. 3.2) shows that the plasma lifetime is about 200 msec following turnoff of the 9.1-kMc magnetron power source.

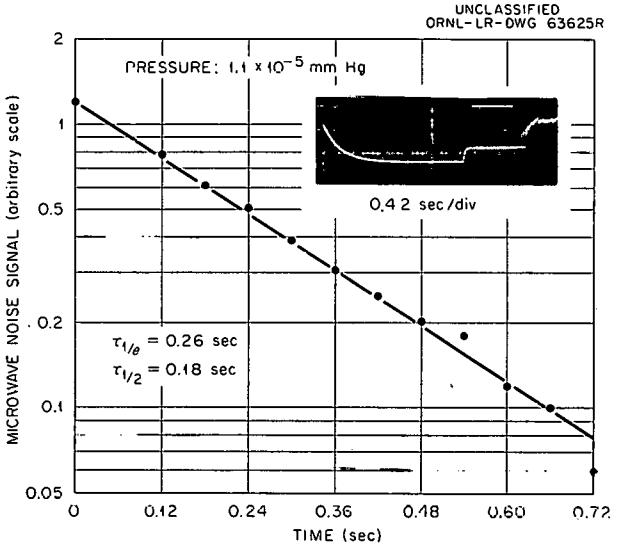

Fig. 3.2. Decay of Microwave Noise.

An electron "temperature" is presumptively estimated from the microwave noise amplitude. This temperature, about 20 kev, agrees with the determination of electron temperature from bremsstrahlung measurements, Fig. 3.3. It will be noted that a higher-energy 140-kev component also appears on this scintillation spectrum, indicating two emitting groups of electrons in the plasma. This "double-humped" energy distribution produces a compound decay for the plasma magnetism, and sometimes also for microwave noise decay. The decay times, 20 msec and 200 msec, agree reasonably with theoretical times for mirror loss, through Coulomb collisions, for electrons of about 20 kev and about 140 kev respectively. The energy density and geometrical configuration of the plasma may be calculated from steady-state measurements of plasma magnetism. Using the previously in-

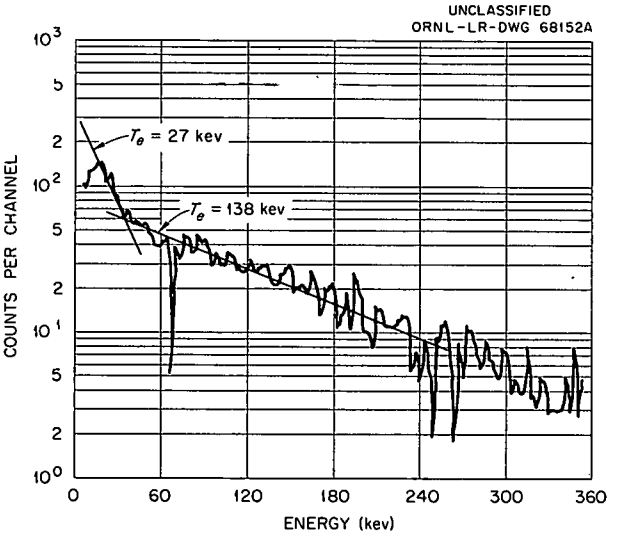

Fig. 3.3. X Rays from Electron Cyclotron Plasma in the PTF.

ferred temperatures, a correlating determination of energy density is possible if electron density is known. Figure 3.4 shows transmission through the plasma of a thermal beam of neutral hydrogen atoms. Using the fact that the product of electron velocity and ionization cross section for ionization by electrons is slowly varying between 1 and 100 kev ($\sigma_i \propto E^{-1/4}$), a maximum density at full microwave power is calculated as about $2 \times 10^{12}/cm^3$, making use of an estimated plasma diameter of 8 in. and correcting for proton-neutral scattering. The resulting energy density is about 2×10^{16} ev/cm^3 or a β of about 10%, assuming that most of the electrons are at the lower temperature. Figure 3.4 also indicates a linear variation of electron density with applied microwave power.

The two distinct electron energy groups are difficult to explain. It is obvious that resonance heating cannot take place much above 500 kev. Therefore, energies even well below this value must be gained in less-efficient stochastic interactions between medium-energy electrons and fluctuating electrostatic fields in the plasma. X-ray bursts from the plasma are added evidence that it is not completely quiescent. These bursts occur at an average frequency of about 50 per second and contain of the order of 10^7 x rays per burst. They are roughly correlated with changes in plasma magnetism and power feed. The short duration of the bursts (0.5 μsec) makes it difficult to resolve their energy spectrum by pulse

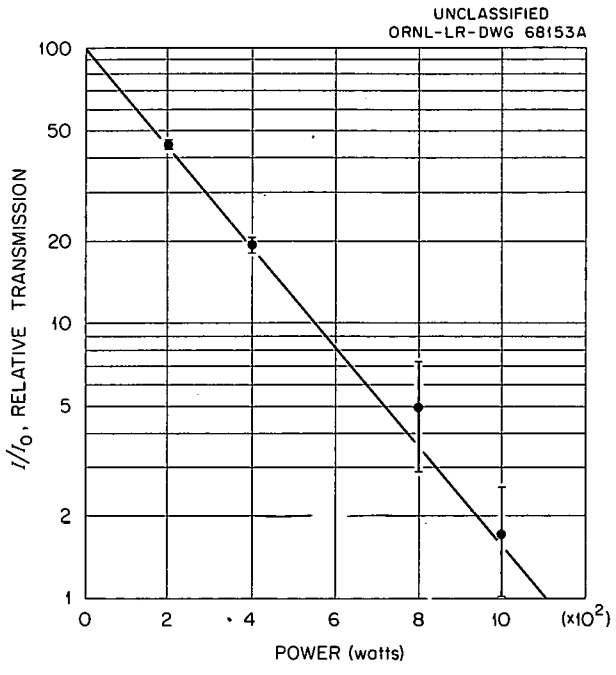

Fig. 3.4. Thermal Neutral Beam Transmission Through Plasma.

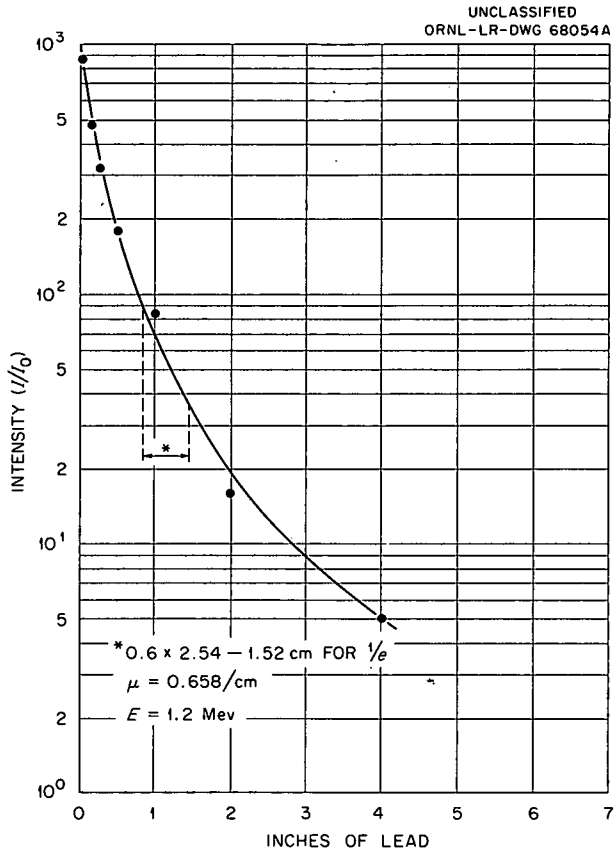

Fig. 3.5. Attenuation of X-Ray Bursts from Electron Cyclotron Plasma in the PTF.

analysis. Therefore, lead absorption was used. The attenuation curve for these x rays is shown in Fig. 3.5. It is seen that a considerable number of x rays have energy in the million-electron-volt range. Disturbances in the high-energy group of electrons give rise to these x-ray pulses by forcing some of them to the copper cavity wall. However, particle losses in this way are at present only a small fraction of end losses. The end losses are due to plasma pumping and will be discussed in a future report. The plasma density has a sharp decline by at least one order of magnitude when background gas pressure goes below 2×10^{-5} torr and plasma pumping ceases. The low-energy electron group ceases to exist, and the plasma is almost transparent to neutral H_2 molecules.

The energy of the positive ions in the plasma (resulting from electron heating) is calculated as 20 v.[4] This is an upper limit on this process and assumes that the ion-electron interaction time is 20 msec. Several methods of concurrent ion heating are under investigation and will be discussed in future reports.

[4]R. F. Post, *Revs. Modern Phys.* 28, 338–62 (1956).

3.1.1 Plasma Magnetic Field Measurements

The magnetic field probe was inserted into the plasma along the axis of symmetry (Z axis) and along a radius in the midplane through tightly fitting tubes to prevent microwave leakage. The sensing device was a Hall element, which was inserted into the vacuum system inside a water-cooled brass well as shown in Fig. 3.6. Uniform temperature of the Hall element was ensured by making the inlet water flow over the inner annular tube of the brass well. Heat deposited on the probe by the plasma and microwave radiation was carried off by water flow through the outer annular tube so that heated water did not come in contact with the tube holding the Hall element.

The magnetic-field measuring circuit is shown on Fig. 3.7. The bucking ladder attenuator was used to bias out the effect of the containing field of up to 6500 gauss. Measurements were made by noting

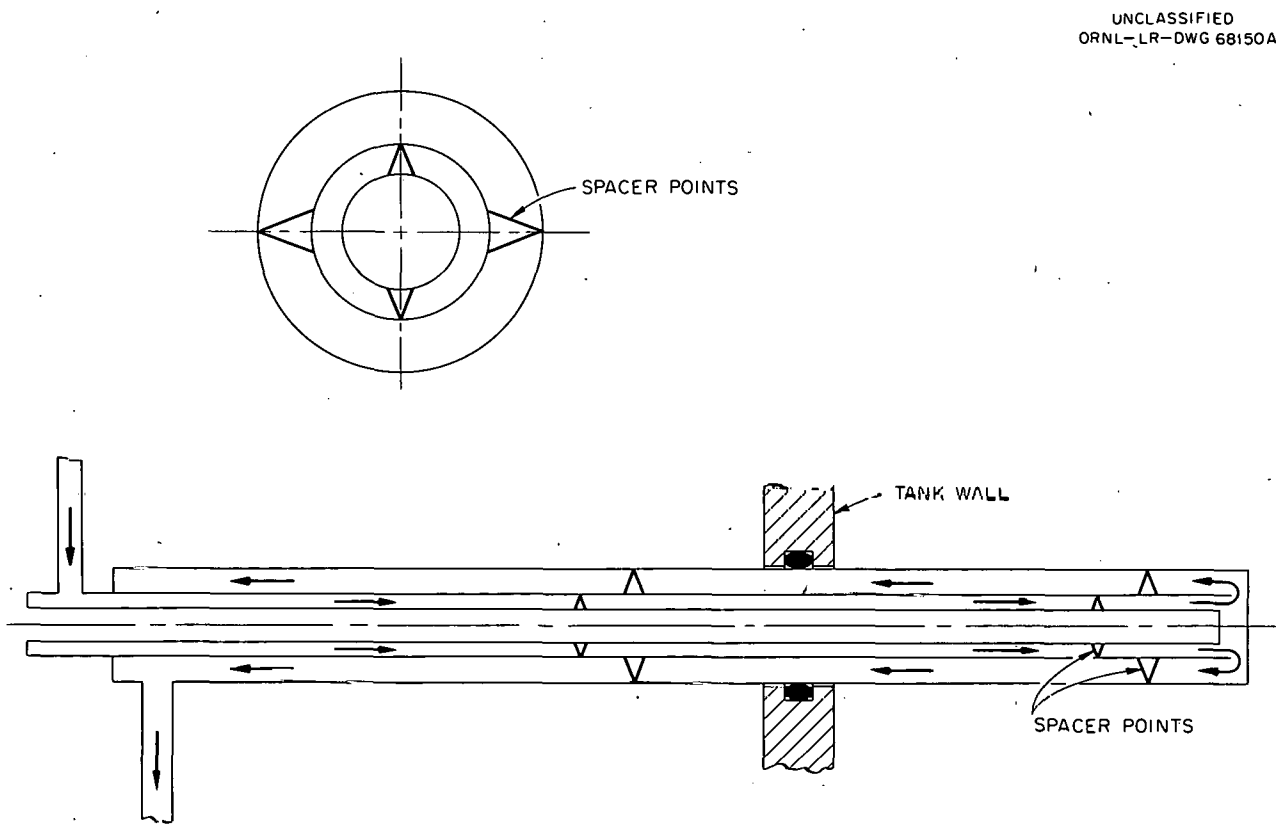

Fig. 3.6. Water-Cooled Well for Hall Probe.

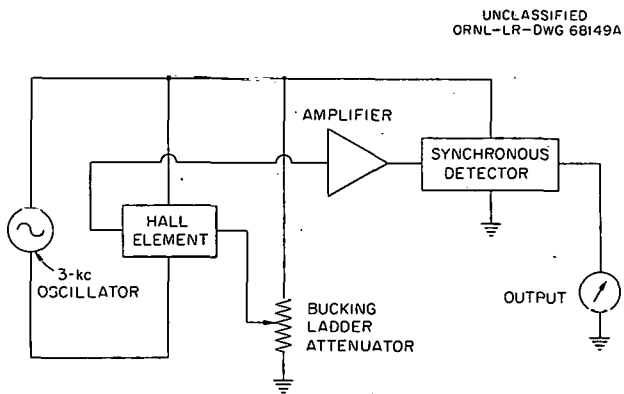

Fig. 3.7. Hall-Probe Circuit.

the change in the output when the microwave power was turned off. A minimum magnetic induction of a few tenths of a gauss due to the plasma was observable above the noise under these conditions.

Inserting the probe radially into the plasma seriously affected the noise temperature as measured by a microwave radiometer. The stability of the plasma as observed visually was also affected. Measurements could not be made with the probe radially outside the cavity due to the unfavorable signal-to-noise level.

On the other hand, the probe could be inserted axially into the cavity past the midplane without grossly perturbing the plasma. This condition was ascertained by observing the noise temperature and the radial-field-gradient monitor. Figure 3.8 shows the measured axial magnetic field as a function of the distance from the midplane of the machine. It is observed that the field changes sign at about $3\frac{1}{2}$ in. from the midplane, indicating the existence of at least two oppositely directed net-current distributions about the axis. The measurements were not carried out beyond 12 in. from the midplane because of the unfavorable signal-to-noise ratio; so, the field was traced further with a gradient probe. The gradient-probe measurements could not be satisfactorily fitted to the measured field, but it was observed that the field decreased toward zero and was well behaved.

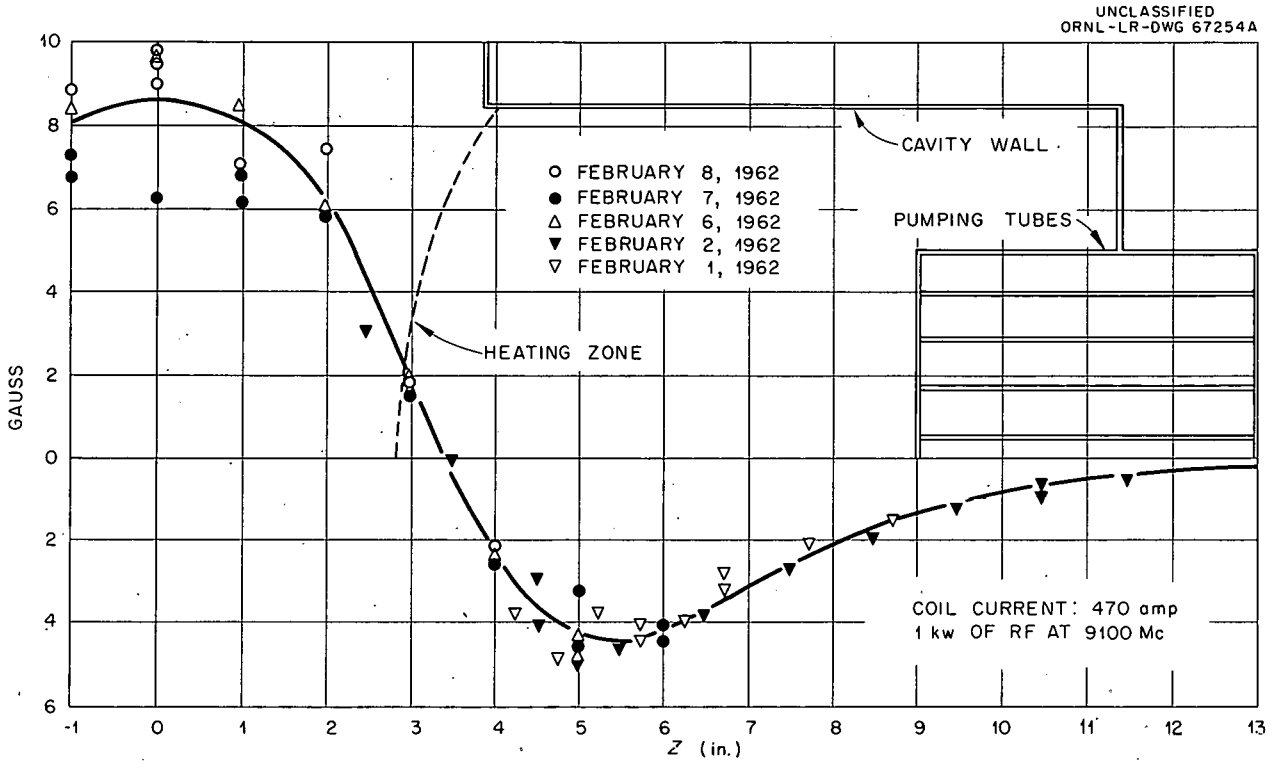

Fig. 3.8. Plasma Magnetic Field.

Further observations indicated that the field decay with power turnoff had two components. Figure 3.9 shows the decay as a function of time for three axial positions. The fast component had a typical decay time of 10 to 20 msec, and the slow component had a decay time of 200 to 300 msec. It was also observed that the two components were of opposite sign near $Z = 3$ in.

Figure 3.10 again shows the measured field as a function of distance, now with the separation of relative magnitudes of the slow and fast components. The slow component attains its maximum absolute value 5 to 6 in. from the midplane, while the fast component has its largest relative magnitude about 2 in. from the midplane. The fast component is largely in a direction aiding the steady magnetic field, while the slow component largely opposes the main field.

If it is assumed that the decay times of the two components are indicative of a self collision time, and if it is also assumed that the density is the same for both groups of particles, then the difference between decay times implies a factor of an order of magnitude in the difference between the mean energies for the two groups, the longer decay time corresponding to the more energetic particles. Under the assumption that the two groups of particles were of the same energy (but necessarily

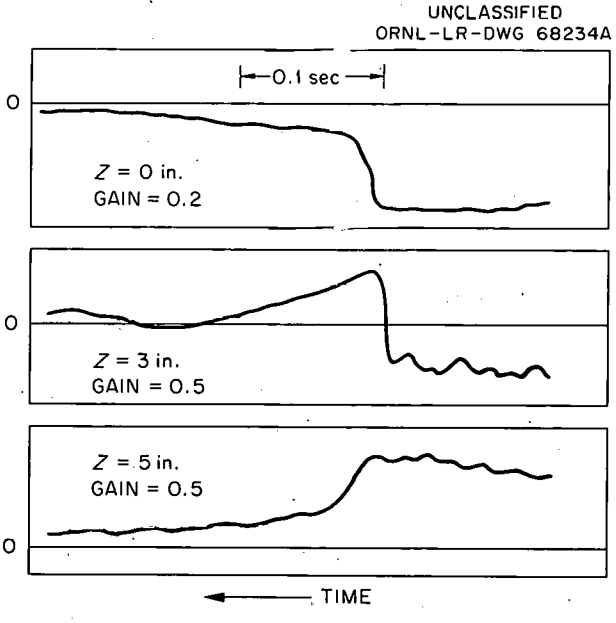

Fig. 3.9. Decay of the Plasma Magnetic Field.

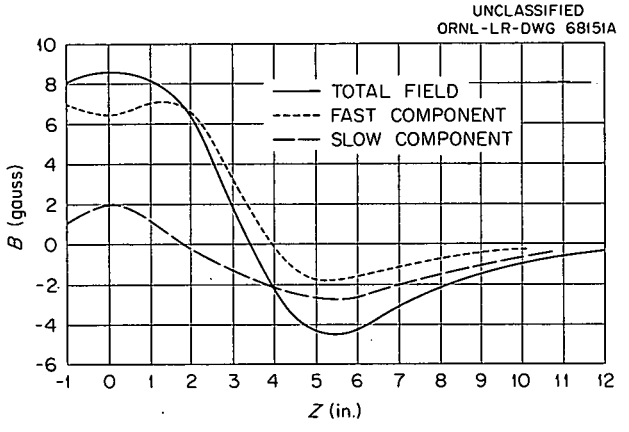

Fig. 3.10. Plasma Magnetic Field.

spatially separated), the decay time difference implies a density difference of more than an order of magnitude. As mentioned above, information obtained from x-ray spectral analysis and microwave noise decay times implied that the former assumption was more reasonable, this assumption being that there were two groups of particles with a mean energy difference of an order of magnitude.

With the aid of W. F. Gauster and C. E. Parker of this division, a program was instituted to calculate probable current distributions that could give rise to the measured field, using existing IBM 7090 computer codes. The calculation of the current distributions from fields cannot in this case produce a unique answer, but the attempt was made in order to give some indication of the most likely current distributions.

Three assumptions were made in the analysis: (1) The currents were assumed to have azimuthal symmetry, that is, they encircled the Z axis at a constant radius. (2) The currents were symmetrical about the midplane. (3) The currents were confined to the volume inside the cavity walls. Unfortunately, at present the analysis is not complete. Presented here is the best solution obtained to date. The main difficulty is that the computer cannot handle a large number of current distributions. The determinant of the matrix of the coefficients of the expressions

$$\sum_{i=1}^{n} a_{ij} I_i = B_j \qquad j = 1, \ldots, m$$

(where m is the number of field points used in the fit and n is the number of current distributions) becomes very small for a large number of current distributions.

So far, solutions have been obtained for only a maximum of nine separate rectangular (constant current density) distributions on each side of the midplane. This small number of current distributions represents a fairly crude approximation to the actual plasma configuration. Some conclusions can be drawn, however. The total positive or negative current is in the range of 100 to 500 amp, while the total net current appears to be near zero. Figure 3.11 indicates the current distribution giving the best fit to date. The negative sign shown with some of the currents in Fig. 3.11 was chosen according to the convention that this current would produce a normal diamagnetic field depression inside the plasma if it were a surface current. The numbers shown here are in amperes per square inch. Each number must be multiplied by the number of square inches in the rectangle in which it is found to give the total current.

A few other conclusions can be drawn from this preliminary result. It is clear that most of the plasma is within 4 in. of the midplane. Also, there is almost an equal amount of current going in both directions about the axis.

This fit was made with 50 matching points by a least-squares method. The points $Z = 0$ in. to $Z = 49$ in. were used in steps of 1 in. It was necessary to fit points at least to $Z = 20$ in. to get well-behaved solutions beyond the point $Z = 12$ in. That is to say, if the field was not specified at

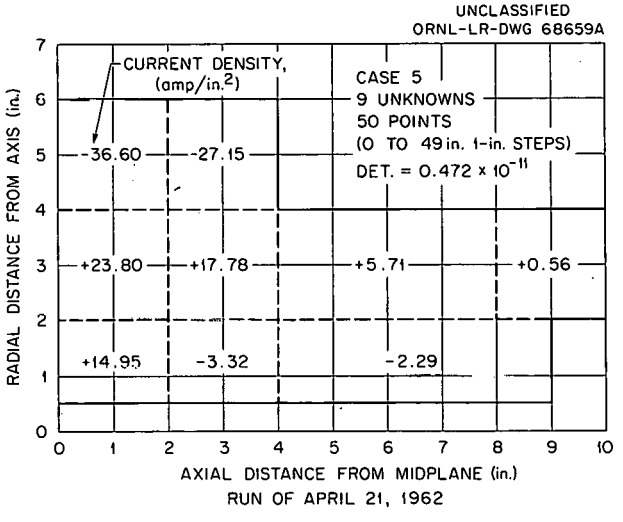

Fig. 3.11. Plasma Currents in PTF.

least 20 in. from the midplane, large excursions in the calculated field occurred. Unfortunately, the field beyond $Z = 12$ in. was too small to be measured, but it was known to be well-behaved from gradient-probe measurements. Specifying an arbitrary but well-behaved fit beyond 12 in. was all that was necessary for success.

As mentioned above, this program to calculate the current distributions is not yet complete. By the exercise of care, we feel that we can perhaps double the present number of current loops and still obtain solutions.

From these measurements, it can be tentatively inferred that the negative surface current near $r = 5$ in. in Fig. 3.11 is probably largely responsible for the slow component of the field and hence represents the high-energy group of electrons. These are probably the electrons responsible for the bursts of x rays which are produced when small groups of electrons strike the cavity walls. The nearly periodic behavior of the bursts may be due to the periodic noise observed in the magnetron power source that was used in these experiments. It would also appear that this high-temperature group of electrons is very important to the maintenance of the plasma. As mentioned above, insertion of the magnetic probe radially into the plasma in the midplane results in the serious degeneration of the plasma.

The current distribution observed inside the plasma in Fig. 3.11 is probably peculiar only because the "grid" of the calculation is so coarse. By increasing the number of current loops, more information as to the surface and volume currents should become available.

Additions to the apparatus are under construction in order to improve the operation and behavior of the electron cyclotron plasma (ECP). For example, a Klystron power source is being installed which will supply 5 kw of 10.8-kMc microwave power. This power source will have much less noise modulation than the magnetron source used at present and will enable regimes of operation at higher power to be investigated.

3.1.2 Spectroscopic Observation of the Physics Test Facility (PTF)

W. F. Peed

A low-resolution spectroscopic survey has been made of the PTF, using a JAco 82000 spectrometer in conjunction with a Visicorder recorder which permitted scanning speeds of 250 and 500 A/min. The PTF was operated with D_2 feed gas, with the addition of H_2, He, CO, or CH_4 as an impurity for spectroscopic observation.

In general it can be stated that all spectroscopic observations are consistent with a low-energy electron distribution such as might be expected in a secondary plasma region outside the primary heating zone. With D_2 feed, seven members of the Balmer series were observed. With the addition of helium, only He I spectral lines were observed. The He II line at 4686 A (51 ev above the ground state), usually observed as a bright line in gas arcs, was not seen. With CO or CH_4 as an impurity O I and O II lines were observed as well as C II. The C III line group at 4650 A was present but quite weak (32- or 26-ev excitation energy required from metastable triplet states).

Although a low-resolution instrument was used, it appears that the ion energy from spectral-line profiles is less than 20 ev, based on observed widths of lines of He I and O II. The decay time of light in the deuterium atomic spectrum was observed as being a few milliseconds, which is characteristic of the Visicorder unit. The rapid decay time of the visible light, which is not consistent with x-ray decay times that are observed, lends additional support to the belief that the plasma observed was of a secondary nature.

3.2 ELECTRON CYCLOTRON HEATING EXPERIMENTS IN ELMO

M. C. Becker, R. A. Dandl, H. O. Eason, A. C. England, R. J. Kerr, W. B. Ard[5]

Preliminary experiments have been performed on the Elmo facility since its completion in March. In addition, some orbit calculations have been performed on the IBM 7090 computer for particles in selected zones in the machine.[6]

The preliminary experiments in the Elmo apparatus have proved quite encouraging. Figure 3.12 shows a schematic diagram of the apparatus, indicating the cusp lines. The surfaces of constant

[5]Consultant from the University of Florida, Gainesville.

[6]This report, sec 6.8.

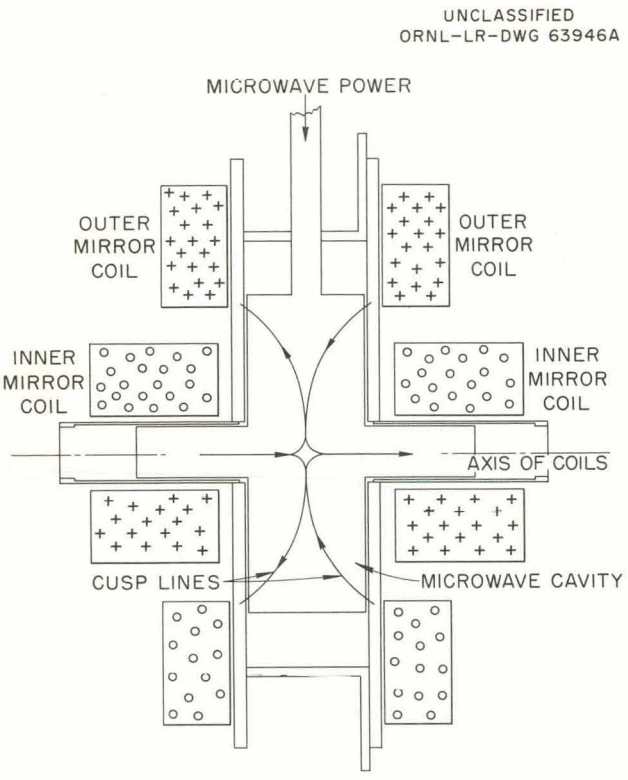

Fig. 3.12. Schematic Diagram of Elmo.

magnetic field are roughly pillbox shaped, and the surface selected for resonance by the microwave power source can be completely free of the walls. Current operation involves the use of 1 kw of 13-cm microwave power. As in the Physics Test Facility (PTF), the electron cyclotron plasma (ECP) exhibits two modes of operation, but their behavior is distinctly different from the ECP in a mirror.

Figure 3.13 shows the plasma in the "glow" condition. The "horns" on the plasma indicate the position of the folded cusp lines, while the general shape follows a surface of constant magnetic field quite closely. In this mode, contrary to experience in the PTF, there is very little microwave noise radiation.

Figure 3.14 shows the plasma in the "no glow" mode. A faint visible light appears to come only from the adiabatic zones of the magnetic field, implying that particle containment is quite good for these zones. In this mode, the microwave noise radiation at the K band is quite large again, contrary to experience with the PTF. Figure 3.15 shows the K-band noise "temperature" (compared with a 1-ev source) and the decay time of the microwave noise as a function of pressure. The

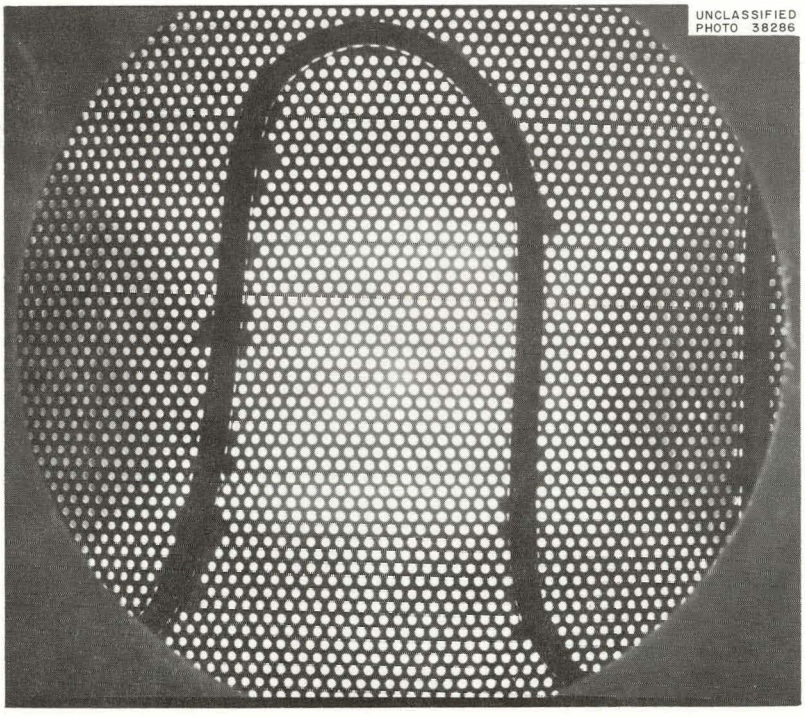

Fig. 3.13. Plasma in the "Glow" Condition.

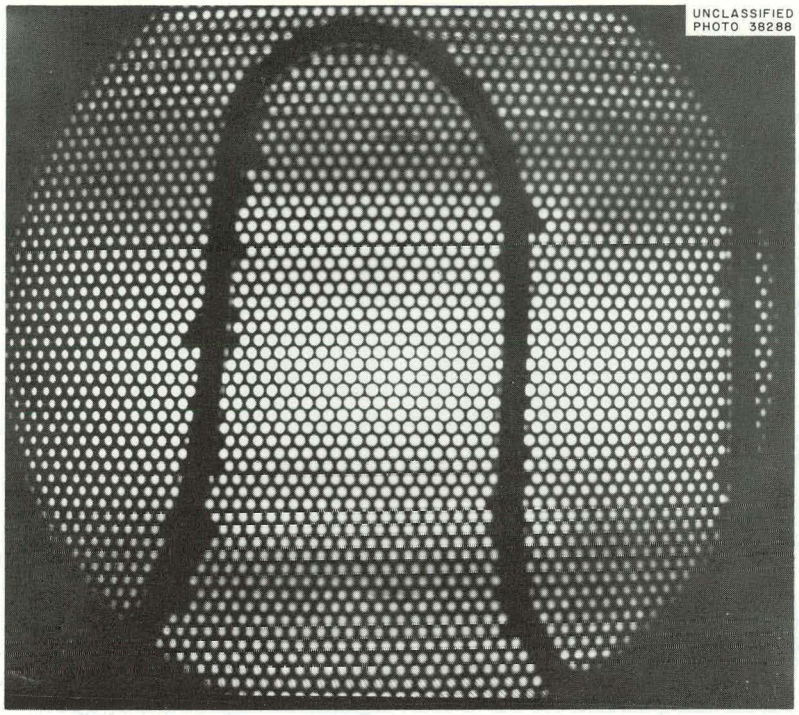

Fig. 3.14. Plasma in the "No Glow" Condition.

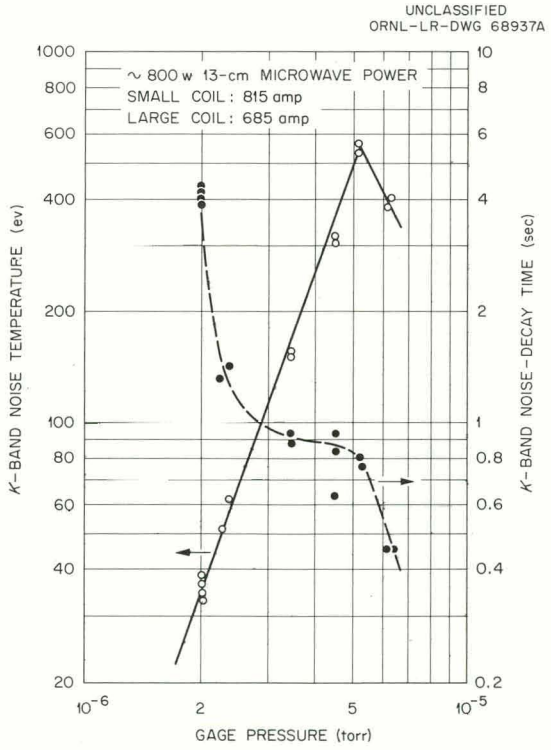

Fig. 3.15. Noise Temperature and Noise-Decay Time as a Function of Pressure.

existence of a noise temperature of several hundred electron volts and a containment time of about 1 sec implies that the magnetic configuration of Elmo may be an effective and useful containment configuration.

3.3 GAS DAMPING OF IONIC SOUND WAVES

I. Alexeff R. V. Neidigh

3.3.1 Introduction

In previous reports, we described extensive experiments made with ionic sound waves.[7] The question arises: If the waves are so easy to produce and observe, why have they not been studied in the past? The answer is that ionic sound waves are very easily damped by un-ionized gas in the system.

[7] I. Alexeff and R. V. Neidigh, *Thermonuclear Div. Semiann. Progr. Rept. Jan. 31, 1961*, ORNL-3104, pp 31–45; I. Alexeff and R. V. Neigigh, *Thermonuclear Div. Progr. Rept. Oct. 31, 1961*, ORNL-3239, pp 27–34; I. Alexeff and R. V. Neidigh, *Bull. Am. Phys. Soc.* 6, 309 (1961); I. Alexeff and R. V. Neidigh, *Phys. Rev. Letters* 7, 223 (1961).

3.3.2 Theory

Gas damping of ionic sound waves in a plasma occurs because collisions between the plasma ions and the gas atoms rob the ions of their coherent ionic sound-wave motion. The effects of gas damping in plasmas are easily discussed quantitatively.

In discussing gas damping, some assumptions are needed to define the system. The following assumptions define a plasma similar to that in an ordinary gaseous discharge tube: (1) Ions and gas atoms are assumed to have the same mass. (2) A second assumption is that the coherent velocity of the ions due to the ionic sound wave motion is small compared with the thermal, random velocity of the ions.

According to the above assumptions, the average frequency of collision of an ion with a gas atom is independent of the ionic sound-wave motion. The ion-gas atom rate of collision is given by the equation,[8]

$$\nu_c = \sqrt{2}\sigma n_g (1.13)\sqrt{\frac{2kT}{m}}. \qquad (1)$$

Here, ν_c is the average number of collisions per second made by one ion with gas atoms, σ is the collision cross section in square centimeters between an ion and a gas atom, n_g is the number of gas atoms per cubic centimeter in the plasma, k is Boltzmann's constant in ergs per °K, m is the mass of an ion or an atom in grams, and T is the temperature of the ions and the gas atoms in °K. In this equation, the temperature of the ions is assumed to be equal to the temperature of the gas atoms. However, if the ion temperature is much higher than the gas temperature, Eq. (1) is modified by removing the factor $\sqrt{2}$, and using the ion temperature for T.

Every time an ion collides with a gas atom, the ion is assumed to lose all the energy which it could return to the ionic sound wave. This assumption is not strictly correct, for the ion may lose only part of its energy. However, the assumption is not too unrealistic. (Because the fraction of energy lost per collision is large, the assumption is made in order to simplify the calculation.)

A large energy loss occurs in ion–gas-atom collisions because two kinds of energy-loss effects are present. The first effect is due merely to the ion's losing kinetic energy and slowing down. The second effect is due to the angular deflection of the ion, for only the momentum parallel to the ionic sound wave motion belongs to the sound wave. Thus, scattering an ion elastically through a right angle would not reduce the ion's kinetic energy but would deprive the ionic sound wave of all the wave energy that the ion had possessed.

An example of the two kinds of energy loss can be computed for hard-sphere scattering. For a moving sphere incident on a stationary sphere of equal mass, the average fraction of the total kinetic energy lost is $\frac{1}{2}$. However, the average fraction of the kinetic energy lost from the motion in the initial direction is $\frac{2}{3}$, which is large.

Under the above assumptions, the rate at which an ionic sound wave loses energy is calculated. Half the total energy of a sound wave is stored in the kinetic energy of the moving mass, on the average. This fact is easily shown by elementary analysis of sound-wave wave motion. Thus, the average sound wave energy stored in the motion of one ion in a cubic centimeter of oscillating plasma is

$$E_i = \frac{E}{2N}. \qquad (2)$$

In this equation, E_i is the ion energy in ergs, E is the energy of the ionic sound wave in ergs/cm^3, and n is the number of ions/cm^3. The rate at which an ion loses energy to the gas atoms is the average energy the ion possesses times the rate at which it collides with the gas atoms:

$$-\frac{dE_i}{dt} = \frac{E}{2n}\nu_c. \qquad (3)$$

Here, $-dE_i/dt$ is the energy loss rate per ion in ergs/sec. The rate at which the plasma volume loses energy is the rate of loss for one ion times the number of ions in the volume,

$$-\frac{dE}{dt} = -n\frac{dE_i}{dt} = \frac{E}{2}\nu_c. \qquad (4)$$

Here, $-dE/dt$ is the energy loss rate for all the ions in the plasma volume in ergs per cubic centimeter per second.

---

[8] Georg Joos, *Theoretical Physics*, 2d ed., p 559, Eq. (11′), and p 585, Eq. (64), Blackie and Son, Ltd., 1950.

One next evaluates the damping for an ionic sound wave. Consider, for example, a resonant system formed by a standing ionic sound wave in some apparatus. The Q, or quality factor of the system, can be defined as 2π times the energy stored per cycle of the undamped wave divided by the energy dissipated per cycle. The value of Q for a standing ionic sound wave, assuming uniform plasma and background gas density, is:

$$Q = \frac{2\pi E}{-(dE/dt)(1/\nu)} = \frac{4\pi\nu}{\nu_c} . \qquad (5)$$

Here, ν is the frequency of the undamped ionic sound wave in cycles per second. As Q becomes smaller, the damping of the wave increases until (for $Q = \frac{1}{2}$) the system is critically damped. For critical damping, the system does not show oscillatory behavior.

For a particular standing ionic sound wave mode to appear in a system, the Q of the mode must be greater than $\frac{1}{2}$. As Eq. (5) shows, the higher-frequency modes have higher values of Q. Thus in a system containing much un-ionized gas, the lower-frequency standing-wave modes are damped out. High-frequency modes might be excited, but they have frequencies very close to each other. Thus, standing ionic sound waves in a system containing much gas would probably produce a spectrum which appears to be a structureless continuum.

3.3.3 Results

The effect of gas damping on the oscillations of a magnetically supported plasma column is evaluated to verify that the oscillations are permitted.

The Q of the plasma oscillation is given by Eqs. (5) and (1).

$$Q = \frac{4\pi\nu}{\nu_c} .$$

For a typical case, argon in the 23-cm-long plasma column, the observed fundamental frequency of oscillation ν is 2×10^4 cps. The rate of collision of an argon ion with argon atoms ν_c is obtained from Eq. (1):

$$\nu_c = \sqrt{2}\sigma n_g (1.13)\sqrt{\frac{2kT}{m}} .$$

The argon ion–argon atom scattering cross section σ is obtained from the argon atomic radius[9] (1.54×10^{-8} cm), assuming that the ion has the same radius. In this case, the total cross section for collision is $4\pi r^2$, where r is the atomic radius in centimeters. The scattering cross section is about 3.0×10^{-15} cm^2. The number of argon atoms per cubic centimeter, n_g, is computed from the operating pressure of 5×10^{-4} torr. The gas damping depends on the ion temperature. As the ion temperature was not measured, assumptions are made which define an upper and lower limit to the gas damping.

As an upper limit for Q, the ion temperature is assumed to equal room temperature, $\frac{1}{40}$ ev. In this case, the Q of the fundamental mode of oscillation is 78. As a lower limit, the ion temperature is assumed to equal the average electron temperature in the plasma, 17 ev. In this case the Q is 4.3. The true value of Q lies between these two limiting values, $4.3 < Q < 78$. As Q is probably much higher than the limiting value of $\frac{1}{2}$, the lowest mode of ionic sound wave oscillation in the magnetically supported plasma column is permitted.

In the case of ionic sound oscillations in discharge tubes, the effects of gas damping are very serious. A discharge tube must operate at a higher gas pressure than a magnetically supported plasma column because plasma losses to the walls of the tube are greater. The effects of gas damping are easily calculated for the spherical discharge tubes which were studied.[10] As an example, the damping of the fundamental mode in an argon-filled discharge tube 10 cm in diameter is evaluated. Typical operating parameters are a gas pressure of 10^{-2} torr, an electron temperature of 3 ev, and a fundamental frequency of about 3.3×10^4 cps. The quality factor Q of the oscillating system is computed from Eqs. (5) and (1).

For an upper limit for Q, the ion temperature is assumed to equal room temperature, $\frac{1}{40}$ ev. The argon gas atom temperature is also assumed to be $\frac{1}{40}$ ev. The argon ion–argon atom collision cross section is again assumed to be 3.0×10^{-15} cm^2. Under these assumptions, the rate of collision between an ion and gas atoms is 8.4×10^4 collisions

---

[9] *Handbook of Chemistry and Physics*, 34th ed., p 2877, Chemical Rubber Publishing Co., Cleveland, Ohio, 1952.

[10] I. Alexeff and R. V. Neidigh, *Thermonuclear Div. Progr. Rept. Oct. 31, 1961*, ORNL-3239, pp 30–34.

per second, and the Q of the fundamental mode of oscillation is 5.

The value of 5 computed above for Q is sufficiently close to the limiting value of $\frac{1}{2}$ to cause strong damping of the fundamental mode of oscillation in the argon-filled sphere. If the ion temperature is higher than the assumed value of $\frac{1}{40}$ ev, the gas damping is even more severe. Increasing the value of Q by decreasing the background gas density was not possible, because at lower pressures the glow discharge was not maintained.

The effect of gas damping on the oscillating discharge was studied by increasing the gas pressure. As the pressure was increased, the lowest possible modes of oscillation were progressively damped away. This observation is consistent with Eq. (5) which states that the higher the frequency of a given mode, the higher the Q of that mode. However, any given mode can be damped away if the ion-atom collision rate is increased sufficiently.

3.3.4 Conclusions

The effect of gas damping of the ionic sound oscillations can be quite serious. If the gas density in the magnetically supported plasma column were increased a hundredfold, damping of the fundamental mode of oscillation would be severe. In the spherical discharge tubes, the gas pressure required to maintain a discharge is so high that gas damping often prevents the fundamental mode of oscillation from appearing.

3.4 A WAY TO MEASURE PLASMA DENSITY – THE "PLASMA SWEEPER"

I. Alexeff R. V. Neidigh

Further developments of the plasma sweeper[11] suggest that it is a good quantitative research tool. The results of this work were reported[12] at the Rochester Conference and will be published in the proceedings of the meeting. A detailed discussion of the more recent work follows.

3.4.1 Introduction

The plasma sweeper provides a simple method of measuring ion density in a magnetically supported plasma column.[13,14] This method supplements conventional methods, which often do not work. For example, measurements with a Langmuir probe may fail because the required electron current saturation often is obscured, and microwave methods require complex equipment and have limited application.

Measurements of plasma densities up to 10^{13} ions/cm^3 have been made with the plasma sweeper. The plasma column was produced by a reflex discharge in a magnetic field of 3000 gauss. The column was roughly 24 cm long and 0.6 cm in diameter. The sweeper measurements of plasma density have been checked in several ways and appear to be accurate to within, at worst, a factor of two.

The plasma sweeper also appears to give the steady-state rate at which plasma streams to the ends of the plasma column. Under certain conditions, the ion temperature in the plasma column can also be measured. Both the plasma streaming rate and the ion temperature measurements have been made experimentally, and both kinds of measurements appear to work.

3.4.2 Description of Apparatus

Measurements are made with a plasma sweeper by turning off the source of the plasma and then "sweeping out" the plasma along lines of magnetic flux and collecting it. The schematic of a plasma sweeper is shown in Fig. 3.16. Normally in this apparatus, a reflex discharge, the anticathode is electrically floating. However, for a plasma sweeper, the anticathode is connected to ground through a resistor and a battery. The voltage of the battery is so chosen that the anticathode electrode draws no net current. Effectively, the end of the plasma column is still electrically floating. In practice, the correct battery voltage is a few volts more negative than the cathode potential.

---

[11] *Thermonuclear Div. Progr. Rept. Oct. 31, 1961*, ORNL-3239, secs 3.3.1–3.3.3.

[12] Third Annual Symposium on the Engineering Aspects of Magnetohydrodynamics, University of Rochester, Rochester, N.Y., March 28–30, 1962.

[13] *Thermonuclear Div. Progr. Rept. Oct. 31, 1961*, ORNL-3239, secs 3.2.5, 3.3.1–3.3.3, and 4.4.

[14] I. Alexeff and R. V. Neidigh, Paper D6, *14th Annual Gaseous Electronics Conference, Schenectady, N.Y., Oct. 11–13, 1961.*

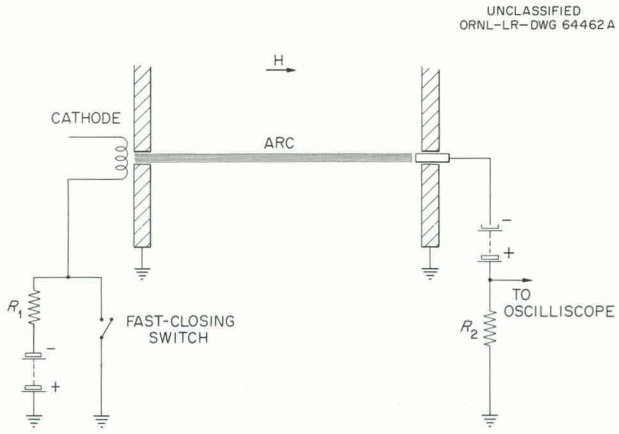

Fig. 3.16. Schematic Diagram of Plasma Sweeper. Typical operating parameters: length of plasma column, or "arc", 24 cm; cross-sectional area of plasma column, 0.3 cm^2; cathode voltage, 100 v; cathode current, 0.3 amp; magnetic field, 3000 gauss; gas pressure in system, 5.5×10^{-4} torr; gas used, argon; ion density, 1×10^{12} ions/cm^3.

Measurements are made by shorting the cathode to ground. The switch used was a mercury-wetted contact relay (Durakool Catalog No. BF-74) with a making time of 2 μsec. Grounding the cathode has two effects: The electron stream from the cathode ceases, so no new plasma is made, and a voltage is applied to the ends of the plasma column. This voltage "sweeps out" charge from the plasma column. The resulting current to the anticathode as a function of time is recorded as a voltage drop across the low resistance R_2 in the anticathode circuit.

After the cathode is shorted to ground, the plasma in the column escapes. The rate of plasma loss is governed by the slowly moving ions because, at these plasma densities, the plasma must remain electrically neutral. Two assumptions are that electron-ion recombination is not appreciable in the plasma and that the magnetic field prevents the escape of plasma from the sides of the column. The total charge in the plasma column is obtained from the area under the current-vs-time curve; the steady-state plasma flow rate is obtained from the current at zero time; and the ion temperature may be found from the shape of the current-vs-time curve. An example of such a curve is shown in Fig. 3.17.

3.4.3 Measurement of Ion Density

An average value for the plasma ion density is obtained by dividing the total ion charge in the column of plasma by the volume occupied by the column and by the charge of one ion. In using the plasma sweeper, the volume is assumed to correspond to the luminous region of the plasma column. The total ionic charge in the column, however, appears to be *twice* the total charge which flows to the anticathode electrode.

The conclusion that the total ionic charge in the plasma column is twice the charge measured is derived from the following model. During the escape of the plasma, a thin sheath forms over the negative anticathode electrode. This sheath is present only if the Debye cut-off length, L_D, is smaller than the length of the plasma column. The numerical value for L_D is:[15]

$$L_D = \left[\frac{kT_e}{4\pi n_e e^2} \right]^{1/2},$$

where L_D is in cm, k is Boltzmann's constant in ergs per °K, T_e is the electron temperature in °K, n_e is the number of electrons per cm^3, and e is the electron charge in e.s.u.

The sheath prevents the sweeping electric field from penetrating into the column. Under this condition, ions escape symmetrically from both ends of the column. Electrons, however, are reflected by the anticathode sheath and escape only from the cathode end. Under the above conditions, only half the ionic charge in the plasma column passes through the measuring apparatus.

The following predictions concerning the plasma column decay are derived from the above model. First, the rate of plasma loss must be independent of the sweeping voltage, as the sweeping electric field does not penetrate the plasma column. Second, the fraction of the ion charge collected is $\frac{1}{2}$ and is independent of the sweeping field.

The conclusion that the plasma sweeper measures only half the ionic charge in the plasma column is supported by the following five pieces of experimental evidence. The first three pieces of evidence are indirect and support the model of the plasma column decay. The last two pieces of

[15] Lyman Spitzer, Jr., *Physics of Fully Ionized Gases*, p 17, Interscience, New York, 1956.

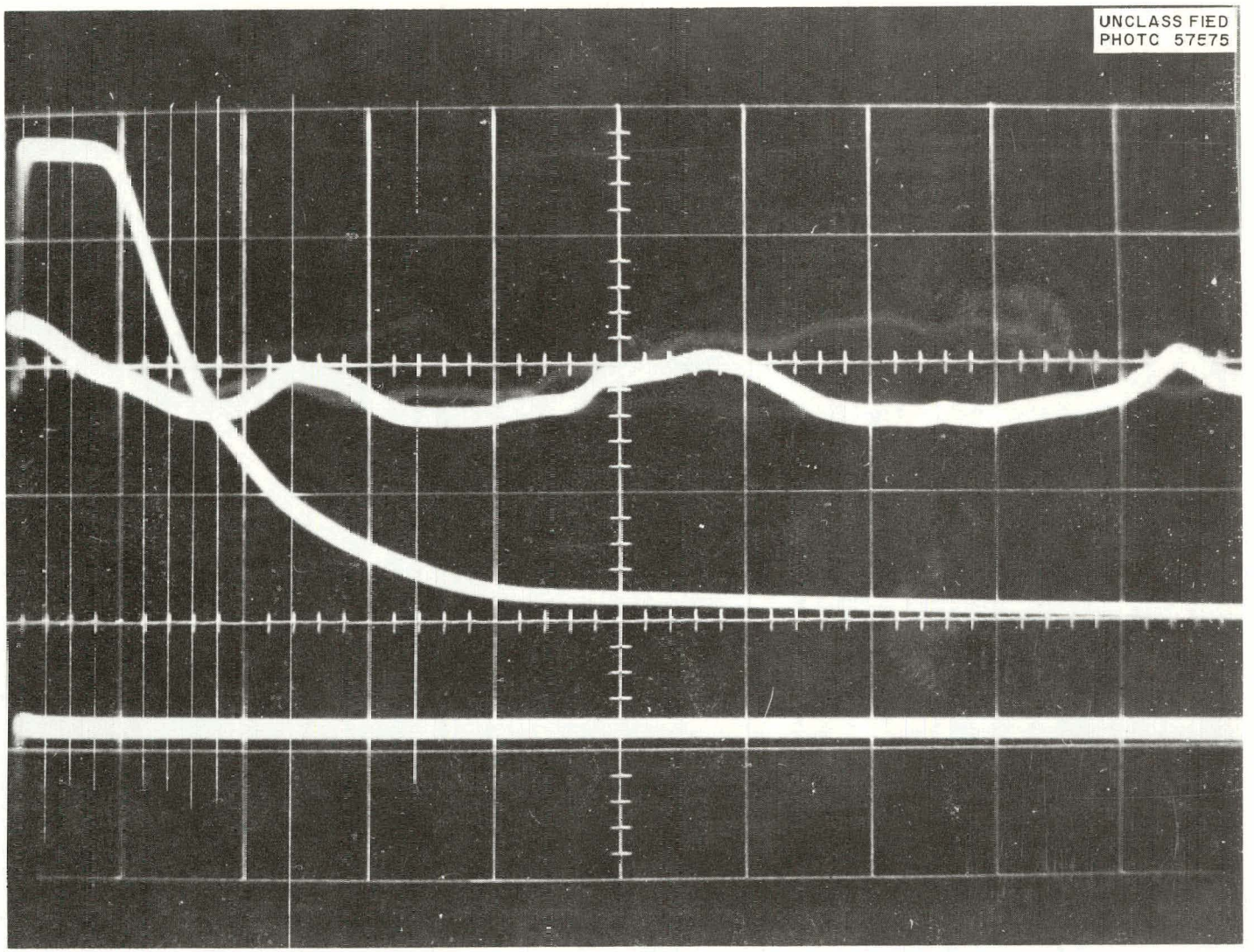

Fig. 3.17. Curve of Experimental Current vs Time Obtained with Plasma Sweeper. The curve beginning the highest is the one of interest. Vertical scale, 10 ma per large division; horizontal scale, 50 μsec per large division; experimental points taken from this curve are shown in Fig. 3.22.

evidence are direct and compare the plasma-sweeper charge-density measurements with charge-density measurements made by using other techniques.

1. Photomultiplier Studies. – Photomultiplier studies suggest that ion-electron recombination in the plasma column is not a serious plasma loss mechanism. The light from the plasma column ceases a few microseconds after the incident electron stream is turned off, although the plasma streams out of the column for a much longer time. As recombination does not remove ions from the column, the ions must all escape from one or both ends of the column.

2. Time-Delay Studies. – A variable time delay was inserted between the stopping of the exciting electron stream and the applying of the sweeping voltage. These studies indicate that the sweeping voltage does not affect the plasma loss rate. Apparently, ions with and without the sweeping voltage are lost in the same way – by drifting equally out of both ends of the plasma column. As the sweeper does measure a net current, the plasma electrons must not reach the negative anticathode electrode. Since the sweeping voltage does not change the plasma loss rate, this voltage must appear over only a short length of the plasma column, that is, across a sheath at the negative anticathode electrode.

A set of curves showing current to the anticathode vs time is shown in Fig. 3.18. For each curve, the electron stream was stopped, a time delay took place, and the sweeping voltage was applied. As the curves having different time delays superimpose, the rate of plasma loss from the column is not affected by the sweeping voltage.

3. Variable Sweeping Potential Studies. – Varying the sweeping potential over a wide range of voltages apparently had no effect on the total amount of charge collected. Thus, if electrons are being reflected at a sheath at the negative anticathode electrode, the percentage reflected is independent of voltage. The simplest assumption for explaining why the percentage reflected is independent of voltage is that in all cases it is the limiting value of 100%.

Experimental evidence showing that the amount of charge collected is independent of sweeping voltage is shown in Figs. 3.19 and 3.20. In Fig. 3.19, the sweeping voltage is less than the initial cathode voltage; in Fig. 3.20, it is greater.

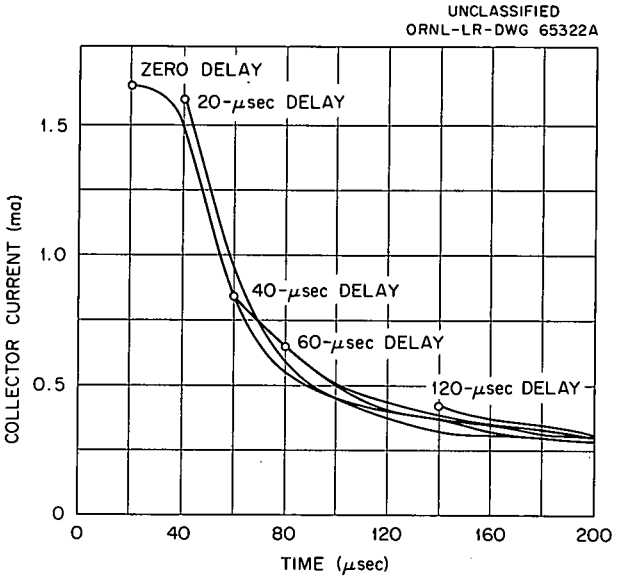

Fig. 3.18. Plasma Sweeper Current with a Delayed Sweeping Voltage. The first 20 μsec of each curve was partly obscured by a switching transient and is not shown. Each curve represents the average of three runs.

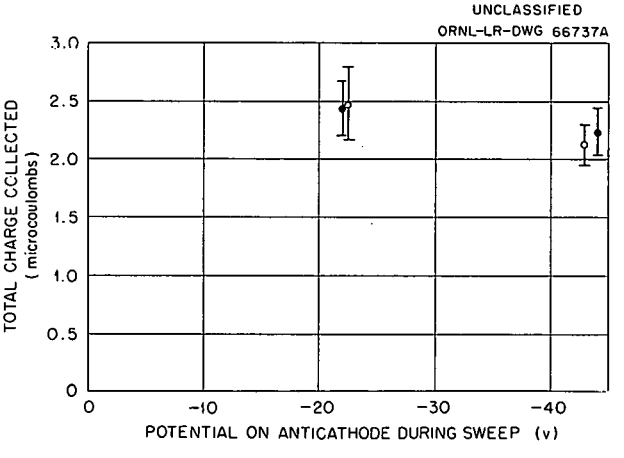

Fig. 3.19. Charge Collected for a Sweeping Voltage Less Than Cathode Potential.

The experimental arrangement used to obtain the data for Fig. 3.19 is as follows: For all runs, the cathode and anticathode voltage were initially the same, –45 v. However, in two sets of runs, when the cathode voltage was switched to zero, the anticathode voltage was switched to about –22.5 v.

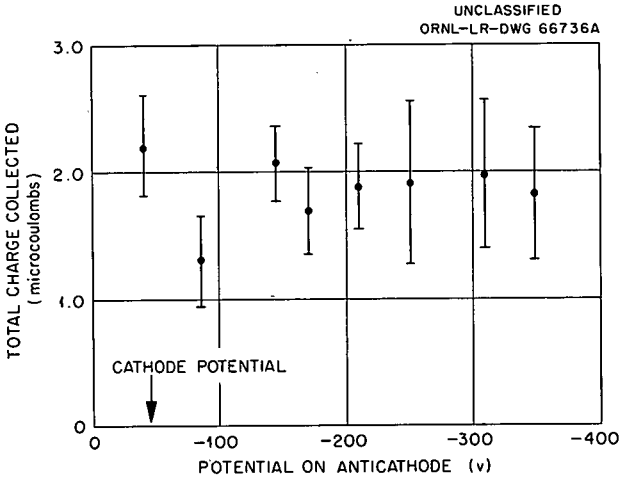

Fig. 3.20. Charge Collected for a Sweeping Voltage Greater Than Cathode Potential.

The error bars represent the root-mean-square scatter for five charge collections. The data show no significant difference in the amounts of charge collected at −22.5 v and at −45 v.

The experimental arrangement for obtaining the data of Fig. 3.20 is as follows: In these runs, the anticathode was always kept at a given voltage, and no switching techniques were used. Having the anticathode initially more negative than the cathode is admittedly not desirable for forming a quiescent plasma. Having both ends of the plasma column initially at the same potential is better. However, two reasons for using the present arrangement are as follows: First, the negative potential on the anticathode may not penetrate into the plasma column, being shielded out by the previously mentioned anticathode sheath; second, the experimenters did not have on hand the apparatus required to switch the anticathode from cathode potential to several hundred volts negative. In any case, the experiment was tried to see what would occur.

The data of Fig. 3.20 indicate that for sweeping potentials ranging from cathode potential, −45 v, to roughly eight times higher, −350 v, the quantity of charge collected is a constant. The large error bars are due to the use of an especially noisy, turbulent plasma column. As before, the error bars represent the root-mean-square scatter in five charge collections.

4. Direct Measurement of Neutral Plasma Flow. – The rate of flow of plasma from the end of the plasma column was measured directly. For these measurements, the electron stream was turned off, but no sweeping voltage was applied to the plasma column. Presumably, in this case the plasma escapes symmetrically from the column, half reaching the anticathode end. By measuring all the plasma that escapes to the anticathode and then doubling the amount, one presumably obtains the amount of plasma initially in the plasma column. The ion-density measurements made with the neutral plasma flow agree to within roughly 10% with measurements by the plasma sweeper. The 90% agreement occurs only if the plasma sweeper collects half the ion charge in the plasma column.

Measurement of the rate of flow of neutral plasma was made with a "plasma eater."[16] This device absorbs or "eats" the plasma entering it and appears to yield a current equal to the number of ions entering the device per second.

5. Measurements of Ion Density by Plasma Electron Pressure. – Measurements of the plasma electron pressure can give the ion density. In a plasma having the electrons hotter than the ions, pressure is given by: $P = n_e k T_e$. Here P is in dynes/cm^2, n_e is the electron density in electrons/cm^3, k is Boltzmann's constant in ergs/°K, and T_e is the electron temperature in °K. By measuring P and T_e, one can obtain n_e. However, n_e is equal to n_i, the ion density, in the predominantly electrically neutral plasma.

Experimental measurements of the plasma electron force exerted by the plasma column on the anticathode electrode have been made with the apparatus shown in Fig. 3.21, and preliminary results have been reported.[14,17] Recent, more precise experiments indicate that the ion density given by the plasma electron pressure and the plasma sweeper agree if the plasma sweeper collects half the ions in the plasma column.

Thus, the five experimental tests of the plasma sweeper all suggest that under our operating conditions the device collects half the ion charge in the plasma column. The average ion density in the plasma column is found by dividing the total ion charge in the column by the volume of the column and by the charge of one ion.

---

[16] I. Alexeff and R. V. Neidigh, *The Plasma Eater, a Device to Measure the Rate of Flow of a Plasma*, ORNL-3246 (Feb. 5, 1962).

[17] *Thermonuclear Div. Progr. Rept. Oct. 31, 1961*, ORNL-3239, sec 3.2.5.

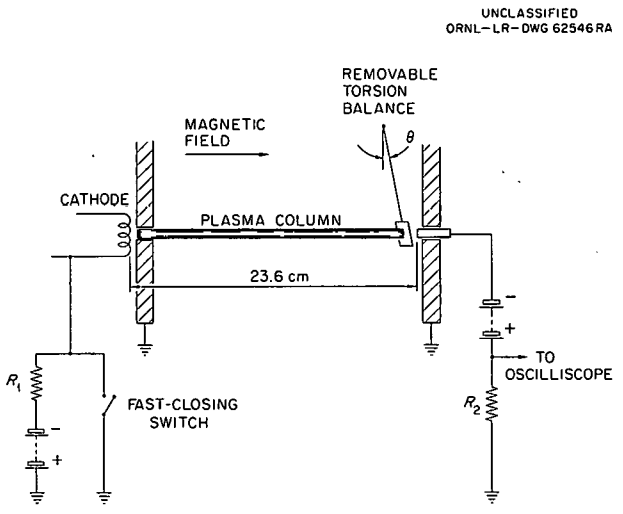

Fig. 3.21. Apparatus Used for Plasma Electron Pressure Measurements.

3.4.4 Measurement of the Steady-State Flow of Plasma

The rate of flow of neutral plasma to the electrically floating anticathode is found by measuring the rate at which positive ions reach the anticathode. The steady-state positive ion flow is apparently equal to the peak current of the plasma sweeper, found immediately after the electron stream is stopped. Two pieces of experimental evidence support this hypothesis.

1. Time Delay Studies and Variable Sweeping Potential Studies. – The experimental data in Sec 3.4.3 indicate that the current through the plasma sweeper corresponds to the rate of ion flow to the anticathode. This rate of ion flow is independent of the sweeping voltage. Therefore, the rate of ion flow just after the electron stream is turned off should be the same as the rate of ion flow just before the electron stream is turned off.

2. Direct Measurement of Neutral Plasma Flow. – The rate at which neutral plasma flowed to the anticathode was measured directly with a plasma eater. Both the steady-state flow rate and the flow rate for a decaying plasma column were measured. When these measurements were compared with those made by the plasma sweeper in a similar plasma column, agreement was good. The plasma sweeper gave results 11% higher than the steady-state plasma-eater results, and about 30% higher than the transient plasma-eater results.[17] Thus the plasma sweeper voltage in these runs may have helped push the plasma out somewhat. As a first approximation, however, the plasma sweeper does seem to yield the steady-state rate at which neutral plasma flows to the anticathode.

3.4.5 Measurement of Ion Temperature

Finding the ion temperature in a plasma column by means of a plasma sweeper may be possible, but only under certain restrictive conditions. Under these conditions, the shape of the current-vs-time curve has been predicted. In the equation of this curve, the ion temperature is a free parameter. By fitting the curve to the experimental data, a value for the ion temperature is obtained. This particular technique for measuring plasma ion temperature has been used by Backus and Huston.[18] In some cases in our work, the experimental data fit the theoretical curve, and a reasonable ion temperature is obtained.[19] However, no independent check of the ion temperature has been made.

The basic assumptions are as follows: A plasma column of uniform cross section and uniform ion density along its length is assumed. Initially, the ions are assumed to have a Maxwellian velocity distribution. Another assumption is that during the decay of the plasma column, each ion preserves the velocity that it had before the electron beam was stopped.

The last assumption, that an ion preserves its velocity, implicity contains two conclusions. First, the interaction of an ion with the rest of the plasma is small during the decay; second, the sweeping voltage applied to the plasma column does not influence the ion drift appreciably. Another way of stating the second conclusion is that the sweeping voltage appears only across short sheaths at the column ends.

With the above assumptions, the collected current as a function of time is computed. The resulting equation is best exhibited in reduced form:

$$i_{+_{\text{reduced}}} = 1 - \exp\left[-\frac{1}{(t_{\text{reduced}})^2}\right].$$

[18] J. Backus and N. E. Huston, *J. Appl. Phys.* 31, 400 (1960).

[19] *Thermonuclear Div. Progr. Rept. Oct. 31, 1961*, ORNL-3239, sec 3.3.2.

Here,

$$i_{+_{\text{reduced}}} = i_{+}\left[\frac{2(\pi)^{1/2}}{eAN_0}\left(\frac{m}{2kT}\right)^{1/2}\right]$$

and

$$t_{\text{reduced}} = t\left[\frac{1}{L}\left(\frac{2kT}{m}\right)^{1/2}\right],$$

where i_+ is the measured collector current in amperes, t is the time in seconds, e is the ion charge in coulombs, A is the plasma column cross section in cm^2, N_0 is the number of ions per cm^3 in the column at $t = 0$, m is the ion mass in grams, k is Boltzmann's constant in ergs/°K, T is the ion temtemperature in °K, and L is the length of the plasma column in cm. The reduced equation shows two characteristic features: a flat initial portion, and a subsequent decay of t^{-2}. The flat portion indicates approximately constant current for a time in which an ion of average energy travels the length of the plasma column.

The theoretical curve of collector current vs time is shown in Fig. 3.22. Experimental points for one particular run are shown, and they appear to fit the theoretical curve quite well. The agreement of the experimental data with theory implies two conclusions: First, the plasma column in this run corresponded to the basic assumptions. Second, the ion temperature was 12 ev. The ion temperature of 12 ev was not checked by an independent method, but it appears to be reasonable for the apparatus.

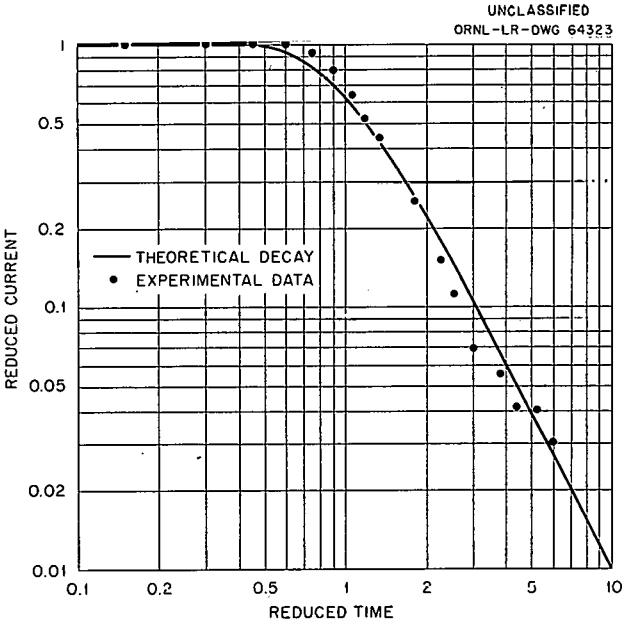

Fig. 3.22. Plasma Sweeper Current vs Time: Theoretical Curve and Experimental Points. The theoretical curve is valid only under the assumptions shown in Sec 3.4.5. The experimental points are taken from Fig. 3.17.

3.4.6 Conclusions

The plasma sweeper appears to be useful in measuring the average plasma density in a magnetically supported plasma column. The steady-state rate of plasma flow to the end of the column can be found. The ion temperature, under certain conditions, may also be obtained. Since the plasma sweeper is apparently a new device, more extensive tests are desirable. However, finding the average ion density with a plasma sweeper appears to be simple and fairly accurate.

3.4.7 Acknowledgment

The authors greatly appreciate the suggestion of Dr. Hartland Snyder to use the time-delay technique described in Sec 3.4.3 of this paper.

3.5 THE "PLASMA EATER": A DEVICE TO MEASURE THE RATE OF FLOW OF A PLASMA

I. Alexeff R. V. Neidigh

The plasma eater is a device which measures the rate of flow of a neutralized plasma. It absorbs or "eats" the plasma entering it and yields a current equal to the charge of the electrons entering the device per second. An experimental model of the device was successfully used with a Mode I arc,[20] a reflex discharge, to measure steady-state plasma flow rate, ion density, and plasma decay time.

The device is composed of closely spaced metal plates, as shown in Fig. 3.23. Alternate plates

[20] R. V. Neidigh, *The ORNL Thermonuclear Program*, ORNL-2457 (Jan. 15, 1958), pp 55–59, 164–65; R. V. Neidigh, *The Effect of a Pressure Gradient on a Magnetically Collimated Arc*, ORNL-2288 (May 27, 1957).

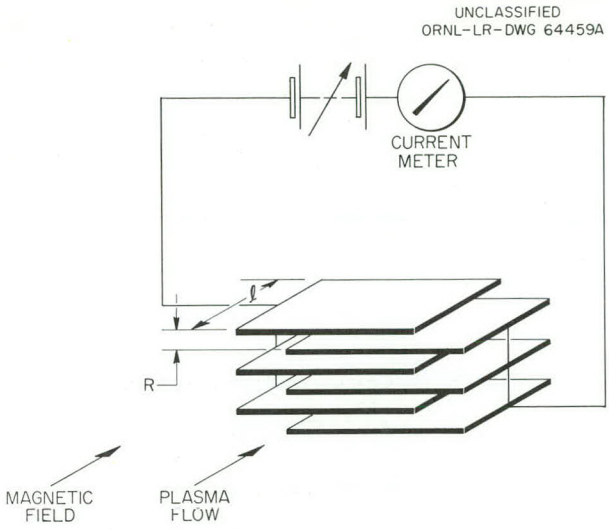

Fig. 3.23. Schematic Diagram of "Plasma Eater."

are connected to a source of voltage. Plasma is directed between the plates. If conditions are correct, the ions and the electrons can be pulled to alternate plates across a restraining magnetic field. Because the plasma is absorbed or eaten by the device, it was named the "plasma eater." A photograph of the plasma eater in operation is shown in Fig. 3.24. A more detailed report of the device has been given elsewhere.[21]

[21] I. Alexeff and R. V. Neidigh, *The Plasma Eater: A Device to Measure the Rate of Flow of a Plasma*, ORNL-3246 (Feb. 5, 1962).

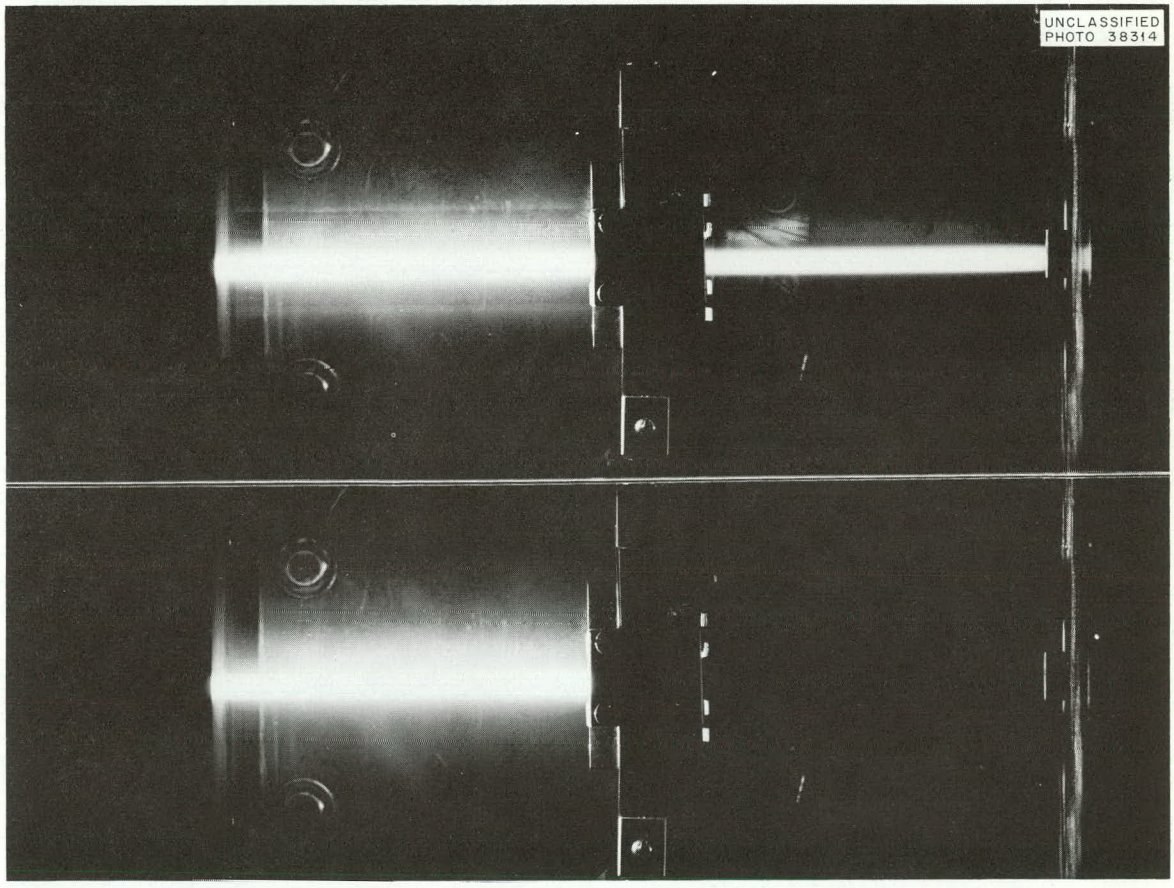

Fig. 3.24. "Plasma Eater" in Reflex Arc. Top – voltage off and plasma streams through the device; bottom – voltage on and plasma is "eaten." This photograph suggests that a plasma eater might be useful in producing short bursts of plasma for experimental purposes.

3.6 MEASUREMENT OF PLASMA ELECTRON PRESSURE

I. Alexeff R. V. Neidigh

Measurements of the plasma electron pressure were made more accurately and over a larger pressure range than in the previous report.[22] In a magnetically supported plasma column, the mechanical force parallel to the magnetic field exerted on an electrically floating balance was measured over the range of 2 to 40 dynes. This measured force agrees with the force computed from the experimentally measured plasma electron density and the electron temperature. The large range of agreement between this measured force and the computed force implies that, in this apparatus at least, the plasma pressure is due to the electrons, and it can be measured directly. A more sensitive and quantitative version of the previous apparatus was used, as shown in Fig. 3.21. Experimental and computed results are shown in Fig. 3.25. A detailed report of this experiment is being published.[23]

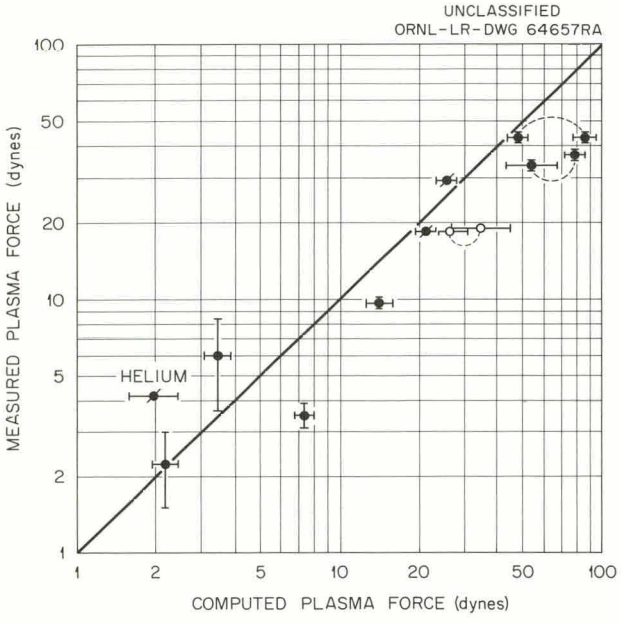

Fig. 3.25. Experimental vs Computed Plasma Force. Unlabeled points are for argon.

3.7 MODE II PLASMA GENERATION BETWEEN MAGNETIC MIRRORS

I. Alexeff R. V. Neidigh
E. D. Shipley

Experiments are being made in an apparatus like that shown in Fig. 3.26, in which plasma is generated between magnetic mirrors by use of the Mode II arc, operating from the throat of one mirror coil with hot cathode and gas feed located as in the figure. Measurements are being made of the density and decay time of plasma located between magnetic boundaries designated as 2 and 3; for this purpose the annular "ion collector plate" is used as a plasma sweeper. Preliminary results, particularly with deuterium, suggest a surprisingly favorable combination of density and containment time. This result is being checked in several ways against possible reasons for misinterpretation; the experiments will be described more fully in our next semiannual progress report.

---

[22] I. Alexeff and R. V. Neidigh, *Thermonuclear Div. Progr. Rept. Oct. 31, 1961*, ORNL-3239, p 34.

[23] I. Alexeff and R. V. Neidigh, "Experimental Observation of Plasma Electron Pressure," to appear in *Physical Review* in the issue of July 1, 1962.

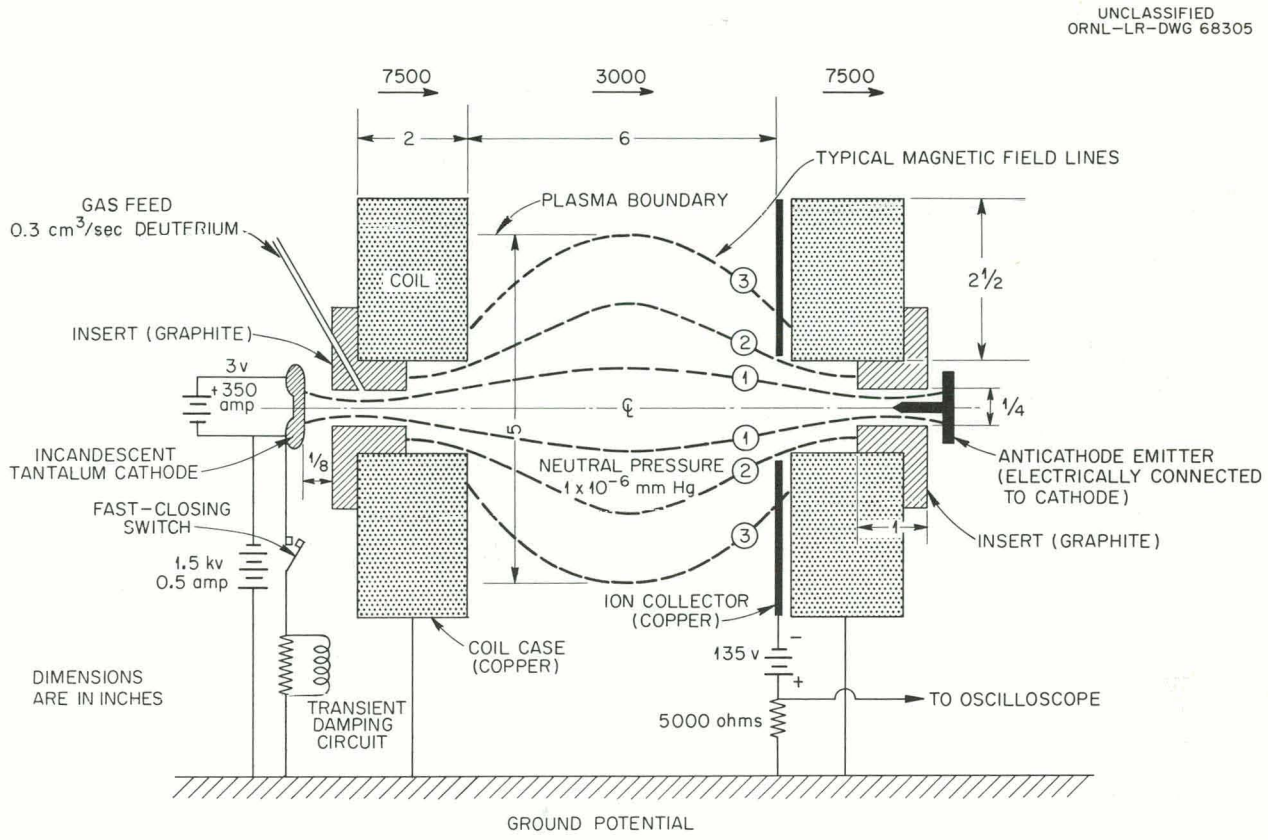

Fig. 3.26. Schematic Diagram of the Apparatus. Values indicated for the various parameters were typical but not necessarily the only ones used in the experiment.

3.8 EXPERIMENTAL STUDY OF A PLASMA ASSOCIATED WITH AN ELECTRON BEAM

I. Alexeff R. V. Neidigh

Experiments concerning the magnetic confinement of a cold plasma have been reported.[24] A steady-state plasma in a magnetic field has been generated by an electron stream along magnetic field lines which passed through a neutral gas jet. Plasma turbulence was observed by a technique which removes the plasma ions without greatly disturbing their density distribution. In general, the amplitude of the turbulence increased with the magnetic field strength and decreased with increasing ion mass. Transport of plasma across the magnetic field increased as the turbulence increased. Mirror and cusp magnetic field configurations were compared with uniform magnetic fields. The mirror configuration produced the most turbulence, the uniform field less, and the cusp produced very little.

Techniques for reducing the turbulence on the plasma formed at the juncture of the electron beam and the directed gas jet (in the vacuum environment) were investigated. Generally speaking, tubes of magnetic flux can move across a conducting material only very slowly. It was thought that the turbulence of the plasma would be reduced if a conducting mass (copper was used) were placed close to the plasma and arranged so that the magnetic flux tubes which were distributed by the turbulent plasma passed through the copper. The effect was positive. With the copper in place, a plasma which had been turbulent at magnetic

[24] I. Alexeff, R. V. Neidigh, and E. D. Shipley, *Bull. Am. Phys. Soc.* **7**, 152 (1962); "Experiments Concerning the Magnetic Confinement of a Cold Plasma," *J. Nuclear Energy, Pt C: Plasma Physics, Accelerators, Thermonuclear Research* (to be published).

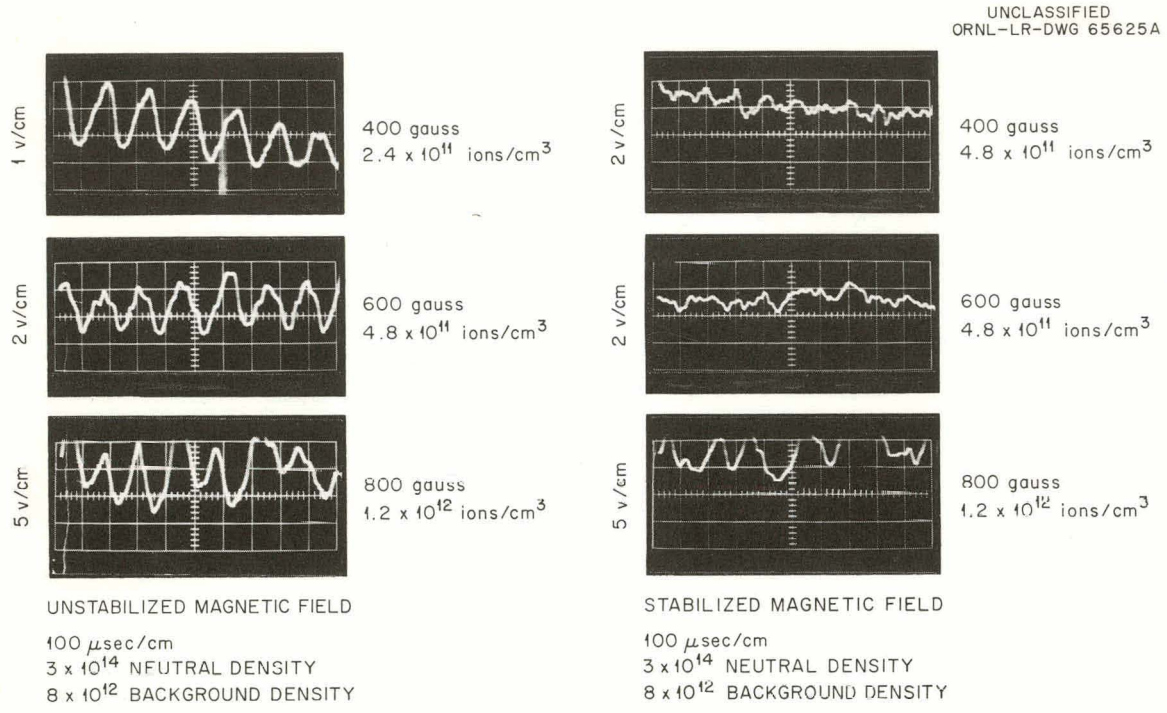

Fig. 3.27. Steady-State Signal to the Plasma Sweeper. The magnetic field was stabilized by a copper ring placed close to the plasma.

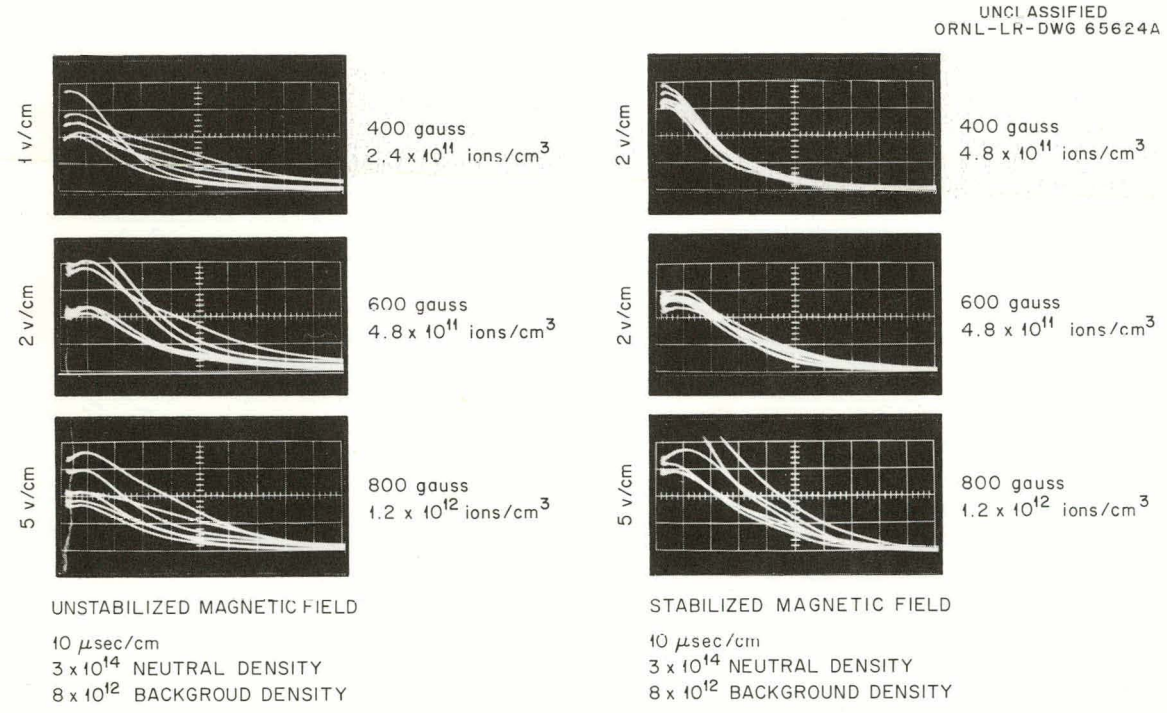

Fig. 3.28. The Time-Analyzed Ion-Collection Current After the Electron Stream was Removed. The magnetic field was stabilized by a copper ring placed close to the plasma.

field strengths greater than 400 gauss did not become turbulent until the field strength was 800 gauss. The steady-state signal to the plasma sweeper is shown in Fig. 3.27, and the signal from the decaying plasma is shown in Fig. 3.28.

Carbon was substituted for copper to see whether its lower conductivity would be apparent, and to be sure that the effects observed with the copper were not just electrostatic effects. The results for carbon and copper stabilizers are compared in Fig. 3.29. Notice that the manner of reducing the turbulence was such that the low-density regions of the plasma were filled. The plasma also escaped faster; that is, both the average plasma temperature and the average density appeared to be raised slightly.

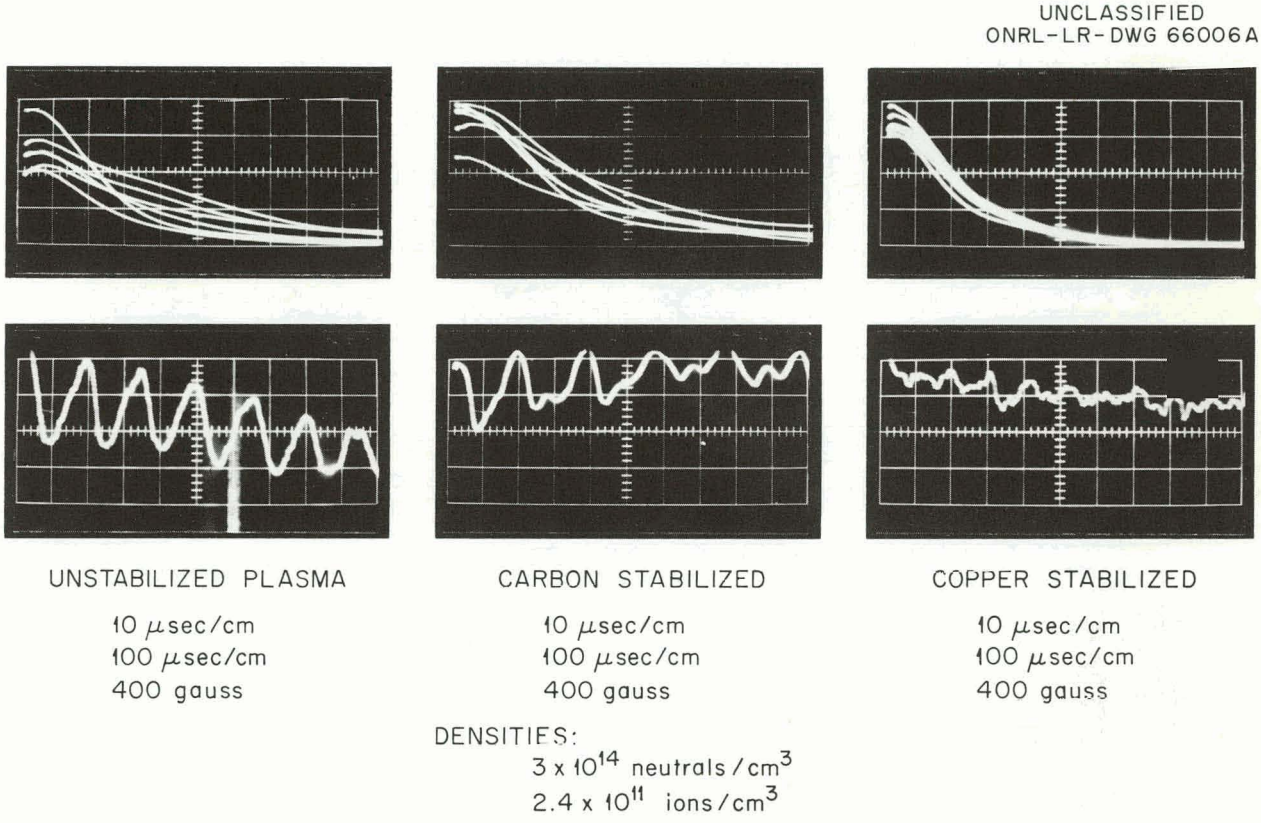

Fig. 3.29. The Unstabilized Plasma Is Compared with the Plasma Having a Carbon or a Copper Stabilizing Ring.

3.9 BEAM-PLASMA INTERACTIONS

O. C. Yonts A. M. Veach[25]
E. D. Shipley

The study of the interaction of an ion beam with its environment continued during this report period.

When argon is replaced by helium as a background gas in the calutron, the sharp break in the slow ion current to the side wall[26] does not occur – in fact the ion current decreases slightly with increased background pressure.

A number of Faraday cups were placed around the beam, and they gave the same type of break with gases other than helium, regardless of location. Although amplitudes are different, the breaks occur at the same pressure.

A series of observations were also made by using a calcium-ion beam. Calcium is superior

[25] Isotopes Division.

[26] O. C. Yonts *et al.*, *Thermonuclear Div. Progr. Rept. Oct. 31, 1961*, ORNL-3239, p 45.

to argon in that control of the background pressure is much better, because of the gettering action. Focus of the calcium beam is sharp, and as a result perturbations in the beam are easier to observe. When the background gas is varied, the general shape of the slow ion curves is unchanged. Thus the mutual influence (strong interaction) between beam and plasma can be experimentally studied in a bilateral way – on the one hand by measuring drain current from a secondary plasma to a Faraday cup and on the other by measuring the motion of the primary beam itself.

4. Vacuum Arc Research

4.1 THE CARBON ARC

4.1.1 Studies on High-Temperature Ions in the Luce Carbon Arc: Possible Implications to Fuel Feed in a Thermonuclear Reaction

J. R. McNally, Jr. M. R. Skidmore
J. E. Francis P. M. Jenkins
D. A. Griffin

Introduction. – Earlier Doppler broadening studies[1,2] of the C III triplet at λ 4650 A demonstrated that unusually high ion temperatures (up to 900,000°K at 48 in. from the anode) were observed in a Luce arc.[3] This steady-state arc is a long, high-current (about 150 amp), magnetically-confined, low-pressure, carbon arc having[1] an electron "temperature" of about 30,000 to 60,000°K and an electron density of about 10^{14} cm^{-3}. The original interest in the arc stemmed from its potentiality[3,4] as a localized, highly ionized target for efficient conversion of energetic H_2^+ ions into H^+ ions which could be trapped in a magnetic mirror device known as DCX-1. Its use in the ORNL Thermonuclear Direct Current Experiment, DCX-1, has been temporarily abandoned because of the discovery of presently serious loss properties associated with the arc in this application. The arc itself, however, remains an interesting plasma because of the relatively high ion temperatures – an ion temperature of 1.4×10^6 °K was reported in the last semiannual report[5] from data taken in the new 120-in. solenoid. This report discusses recent experiments leading to still higher ion temperatures.

A linear relation was found to exist between the line half-widths, $\Delta\lambda_{1/2}$, and the distance of the point of observation from the anode.[2] Since the ion temperature is proportioned to $(\Delta\lambda_{1/2})^2$, the ion temperature increased quadratically with this distance. Line profiles were essentially Gaussian, whether observed along or perpendicular to the arc, indicating that a "three dimensional" or true temperature could be assigned to the ions in this arc; thus, the *mean* ion energy is given by the conversion factor 7730°K/ev *if* the axial temperature is found to be the same as the transverse temperature. This conversion factor is to be distinguished from that for a two-dimensional or "kinetic temperature," for which 11,600°K = 1 ev.

Higher Steady-State Temperatures in Longer Carbon Arcs. – Doppler studies have been continued in the 120-in.-long solenoid having observation ports 8 in. apart and a magnetic field (usually 8200 gauss) uniform to within ±5% on axis.[6] Results indicated a continued rapid increase of ion temperature with distance from the anode. Figure 4.1 shows a spectrogram of the 4650 C^{2+} triplet taken 80 in. from the anode, using a JAco 3.4-m spectrograph at a grating angle of 55°. The

---

[1] J. R. McNally, Jr., *Optical Spectrometric Measurements of High Temperatures*, P. J. Dickerman, ed., University of Chicago Press, 1961.

[2] P. M. Griffin, J. R. McNally, Jr., and G. K. Werner, *Proceedings of Third Symposium on Temperature, Its Measurement and Control in Science and Industry, Columbus, Ohio, March 1961* (to be published); P. M. Griffin, G. K. Werner, M. R. Skidmore, and J. R. McNally, Jr., *Thermonuclear Project Semiann. Rept. Jan. 31, 1960*, ORNL-2926, pp 34–38.

[3] J. S. Luce, *Proc. U. N. Intern. Conf. Peaceful Uses Atomic Energy, 2nd, Geneva, 1958* 31, 305 (1959).

[4] C. F. Barnett *et al.*, *Proc. U. N. Intern. Conf. Peaceful Uses Atomic Energy, 2nd, Geneva, 1958* 31, 298 (1959).

[5] M. R. Skidmore and J. R. McNally, Jr., *Thermonuclear Div. Progr. Rept. Oct. 31, 1961*, ORNL-3239, pp 47–49.

[6] W. F. Gauster and J. N. Luton, Jr., *Thermonuclear Project Semiann. Rept. July 31, 1959*, ORNL-2802, pp 111–13.

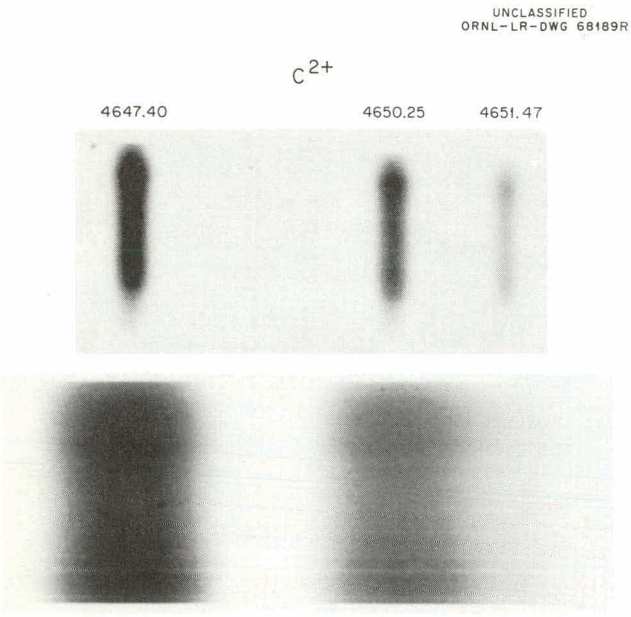

Fig. 4.1. Relative Line Broadening of λ 4650 C^{++} Triplet Group Near Anode and 80 in. from Anode (Broad Lines) in an 88-in.-Long Carbon Arc.

4650.25- and 4651.47-A lines show no intensity minimum between them, and the 4647.40-A line width is comparable to the interval between it and the 4650-A line.

The Doppler "slant" spectrum line effect due to azimuthal rotation of ions about the axis in a radial, negative potential well is still pronounced in the regions near the anode but is not apparent in the cathode region because of the large Doppler broadening. It is believed, however, that both the axial potential gradient as well as the localized radial potential gradients and time variations of these may increase the ion energy through randomization processes and may be somewhat analogous to charge motion in tornadoes.[7]

Scanning of the triplet at 5 A/min (using a JAco-8200, 50-cm spectrometer having an instrumental width less than 0.3 A) gave adequate data for line profile studies of the 4647-A line and evaluation of ion temperatures.[8] A π transmitting polarizer was used to reduce Zeeman structure contributions to the line broadening to less than 3%. A magnetic field strength of about 8000 gauss gave steady operation of the arc between a 2-in.-diameter carbon anode and a $\frac{1}{2}$-in.-OD, $\frac{3}{8}$-in.-ID carbon cathode at an arc current of about 140 amp and voltage of about 150 v. The usual bright filamentary structure or streamer character of the arc is observed along the whole length of arc and apparently originates in cathode hot spots (usually about 4 to 8 filaments may be observed). These streamers may be related to the early work of Cummings and Tonks,[9] which was done at 4 amp in fields less than 100 gauss, but at high neutral gas densities of mercury vapor.

The temperature evaluations and data handling for numerous cases were done on the Oracle, using a Linear Regressions and Correlation Code.[10] This code gives a linear least-squares fit to the curve of log I vs $(\Delta\lambda)^2$, as shown in Fig. 4.2, the slope of which determines the best value of the half-width of the line. The spectrum line profiles were in all cases Gaussian (down to about 5% of the peak intensity for T about 1.4×10^6 °K at a neutral background pressure of 1×10^{-5} torr, but only about 15% for $T > 2.5 \times 10^6$ °K where overlap with 4650 began), as indicated by

[7] B. Vonnegut, "Electrical Theory of Tornadoes," *J. Geophys. Res.* 65, 203 (1960).

[8] See, for example, A. N. Zaidel, G. M. Malyshev, and E. Ya. Shreider, *Soviet Phys. – Tech. Phys.* 6, 93 (1961).

[9] C. S. Cummings and L. Tonks, *Phys. Rev.* 59, 514 (1941).

[10] Oracle Code CPOOD, A. H. Culkowski and N. M. Dismuke, Mathematics Panel, Oak Ridge National Laboratory.

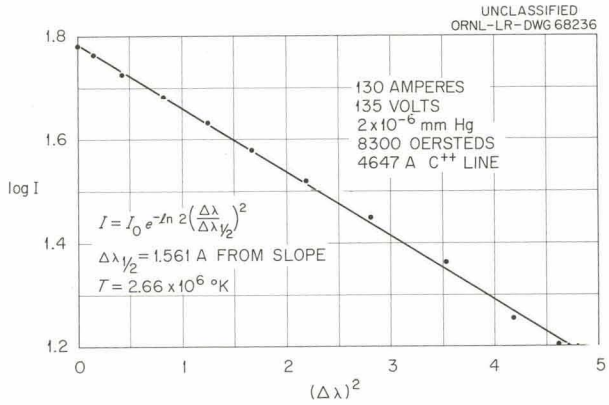

Fig. 4.2. Evaluation of Best-Fitting Gaussian (Straight Line) to Data Points Obtained from 100-in. Carbon Arc.

the linearity of the curve. The line slope corresponded to half-widths generally in excess of 1.5 A ($T_{C^{2+}} = 2.5 \times 10^6$ °K) at the lowest operating pressures ($\sim 2 \times 10^{-6}$ torr). This improvement in base pressure by a factor of about 5 over the previously reported data[5] resulted in approximately doubling the ion temperature.

In an 88-in.-long arc and at a distance of 80 in. from the anode, $T_{C^{2+}}$ was determined to be 2.7×10^6 °K from a series of measurements, using half-widths only, in which $T_{C^{+}}$ from λ 2512 A was evaluated as 3.0×10^6 °K, and $T_{C^{3+}}$ from λ 2529 A was 3.3×10^6 °K. Detailed line profile studies of λ 2512 A and λ 2529 A were not made because of their low intensity; also, no corrections were made for fine structure or Zeeman σ components. The average C^{2+} temperature was also found to be 2.6×10^6 °K at an observation point 96 in. from the anode in a 100-in.-long arc, using the Oracle computational method.

It is concluded that the ion temperature in these long arcs continues to increase rapidly with distance from the anode, although the quadratic increase predicted 2.5×10^6 °K for the 80-in. case and 3.6×10^6 °K for the 96-in. case. The difference between predicted and observed results for the 96-in. case may be associated with the fact that different arc lengths, electrode properties, magnetic field geometries, or closeness of observation to the cathode may have affected the results.

Very High Steady-State Temperatures in Very Long Carbon Arcs. – More recent Doppler studies have been made of a 194-in. arc, obtained by adding the old solenoid facility[11] to the 120-in. solenoid.[6] Preliminary observations, made transverse to the arc axis, gave carbon ion temperatures up to 5×10^6 °K at a point 178 in. from the anode. Instrumental half-width was 0.16 A, and a Glan prism was used to isolate the π polarization. The quadratic increase of the ion temperature with anode distance is illustrated in Fig. 4.3, the extrapolated portion at small half-widths (lower dashed line) agreeing approximately with the slope of the earlier studies.[2] The slope of the curve from the first point on is definitely less than that previously observed for the shorter arc and different magnetic geometry. The maximum temperature in this particular series of measurements, as shown in the figure, is 4.1×10^6 °K.

Overlap of λ 4647 A with λ 4650 introduces a 7% overestimate of the half-width at $\Delta\lambda_{1/2} = 2.0$ A (Fig. 4.4), which is partially compensated for by a 6.3% underestimate of the dispersion due to shift of the λ 4650-A line peak toward the λ 4651-A component of the triplet. The C^{2+} singlet transition at λ 2296 A gave transverse ion temperatures for the π component also ranging

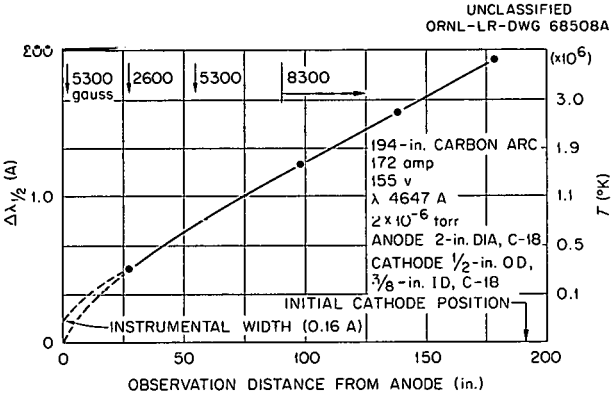

Fig. 4.3. Observed Line Half-Widths, in Angstroms, and Ion Temperatures for Four Observation Ports (Transverse Views) in 194-in.-Long Carbon Arc. Magnetic field at various points indicated at top of figure.

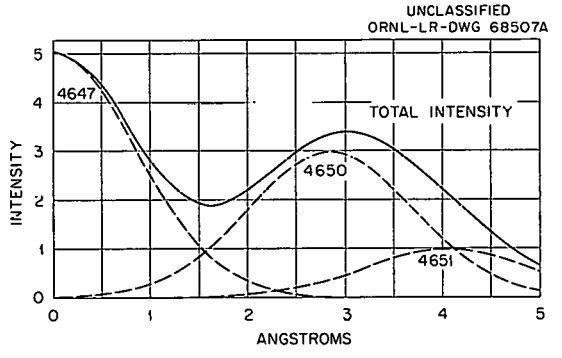

Fig. 4.4. Theoretical Line Shape for Doppler Broadened C^{++} Triplet to Evaluate Errors in Half-Width Determination at High Temperatures. Doppler profile, 4650 group at $\Delta\lambda_{1/2} = 2.0$ A, $T = 4.3 \times 10^6$ °K, and $\bar{E}$ equal to 560 ev.

[11] J. F. Potts, *et al.*, *Thermonuclear Project Semiann. Rept. Jan. 31, 1959*, ORNL-2693, pp 41–44.

from 4 to 5 × 10^6 °K, and the line profile was Gaussian down to at least 10% of the peak intensity.

Axial observations of λ 4647 A near the cathode, using a Stellite mirror to view the arc nearly axially (about 6° off axis and in the direction of the cathode end of the system), gave line half-widths of 0.9 to 1.0 A (approximately 10^6 °K), whereas the transverse views gave 2.1 A (4.8 × 10^6 °K). The line profile for the axial view was, in addition, non-Gaussian, indicating high-energy tails greater in intensity than to be expected for a half-width of 1 A. The tail toward longer wavelength was somewhat more intense, indicating a net, small ion-drift motion toward the cathode. Thus, most of the ions seen axially are relatively cooler than those seen transversely but do have a high-energy tail present. This is evidence that a true temperature does not exist in this region of the carbon arc and is also in keeping with the longer mean free path expected for the scattering of energetic ions along flux lines to other portions of the arc. The mean free path for 90° multiple small-angle scattering of doubly charged carbon ions at $T = 5 \times 10^6$ °K is approximately 40 m, whereas for 1 × 10^6 °K it is still approximately 1.7 m. Randomization in this very long arc apparently occurs in two directions (r, ϕ), but, because of the long scattering mean free path, scattering into the z direction results in loss of ions to other points along the arc or to the electrodes. Thus, it is probably more meaningful to describe the temperature roughly as a "kinetic" or two-dimensional temperature near the cathode in this long arc; that is to say,

$$\bar{E} = 5 \times 10^6/11{,}600 = 430 \text{ ev}$$

(see Sec 4.1.1).

Cooperative phenomena may reduce gross loss of energetic ions in the axial direction, or the existence of negative potential wells both axially and radially (see ref 12) might account for some "holding" of ions in localized regions. The consumption of 27.9 g of anode material over a 9 hr 21 min total run time for one anode indicates a carbon ion current of about $7 \times Z_{eff}$ amp (28 amp if $Z_{eff} = 4$, or about 20% positive ion current). This assumes negligible neutral material loss from the anode, and no return flux. The anode burns away primarily along flux lines from the cathode face, frequently leaving a carbon peak ($\frac{1}{2}$ to $\frac{3}{4}$ in. high) at the arc center. In view of the large Larmor radii for these energetic ions and the requirement for quasi-electrical neutrality, this suggests that the majority of the electron current is associated with energetic electron streams originating from the annular face of the cathode. It is intended to make time studies of these energetic streams to ascertain what influence they may have on ion heating processes.

Tentative Conclusions About Steady-State Stability and Possible Fuel Feed in a Thermonuclear Reaction. – It is believed that the apparent stability of these long, magnetically confined arcs may be associated with the dynamic character of the system and may have an important relation to stability in fusion systems. It seems that strong interactions or instabilities, if any, occur mainly along flux lines and may be tolerated if appropriate potential gradient, ion and electron feed, and electron damping are present. Diffusion across field lines, according to normal diffusion theory of electrons in a magnetic field of 8000 gauss, is presumably small (i.e., $1/(\omega^2\tau^2) \cong 10^{-6}$). Fuel feed and ion heating in a thermonuclear device may possibly be related to these or analogous axial and radial heating mechanisms for the ions of a dense plasma. The only significant difference between a steady-state thermonuclear reaction[1] and tornado-like systems[7] may be mainly in the nuclear rather than molecular energy feed mechanisms which sustain the respective system.

4.1.2 Acknowledgments

We wish to acknowledge the significant contributions of H. H. Terry and B. B. Coulter, research mechanics in the Y-12 Research Services Department.

4.2 THE DEUTERIUM ARC

4.2.1 Development of Hydrogen Plasma for H_2^+ Dissociation

C. W. Blue
H. C. Hoy
R. L. Knight
O. D. Matlock
V. J. Meece
W. L. Stirling

Introduction. – A low-density plasma has been developed which is to be used for molecular ion dissociation in DCX.

[12] R. V. Neidigh, *Thermonuclear Project Semiann. Rept. July 31, 1959*, ORNL-2802, pp 31–36.

At present, the primary H_2^+ beam is dissociated on the neutral background gas remaining in the system during operation. According to Dunlap's calculations,[13] the background gas is effective only over a 5-cm path segment of the input beam in producing plasma in the wrapped-up ring. Operation at 2 to 5 × 10^{-9} torr (uncorrected gage pressure) is easily achieved with a primary 600-kev H_2^+ beam from 2 to 8 ma. The low operating pressure is desirable, of course, in order to minimize charge-exchange losses of the wrapped-up plasma, but it results also in a reduction of the dissociation efficiency to about 10^{-7}.

The purpose of this experiment was to develop an arc or plasma that might increase the dissociation efficiency but not the charge exchange. In order to be useful, the arc or plasma must satisfy three conditions during operation: (1) It should possess an ion species such that charge exchange between the trapped ions and the arc is negligible. (2) It should provide an ion density sufficiently high to make the dissociation probability higher by about a factor of 10 or more than that achieved by dissociation on the neutral background gas existing in the vacuum system. Thus the ion density should be at least 50 times the neutral density over a dissociation path length, equal to the arc diameter, of 1 cm. (3) It should be capable of stable operation at an inner-liner neutral density of no more than 4 × 10^8 particles cm^{-3}. This value of neutral density requires that the ion density be about 2 × 10^{10} cm^{-3}.

Description of the Plasma. – Work on the 100-kev neutralized-beam accelerator indicated that an arc such as that associated with the electron gun[14] might be able to produce a plasma that would meet the three requirements listed above. Figure 4.5 shows an assembly drawing of the electron gun. The arc exists between the hollow anode (gas fed) and the resistance-heated cathode filament. When used as a source for the dissociative plasma, the only applied voltage is that necessary to sustain the arc; neither electrons nor ions are extracted. The entire assembly is placed in either magnetic mirror coil, and the secondary plasma of the arc is allowed to drift downfield through the low-pressure region between the mirrors to a target in the high-pressure region on the other end (see Fig. 4.6). It has been shown that the arc can be operated without adversely affecting the low pressure of the inner-liner region. It is believed that a plasma column created in this manner does not have the driving mechanisms necessary to sustain an arc in which the cathode is at one end of the low-pressure region and the anode on the other. Consequently, the drifting plasma should be more quiescent than the ordinary or conventional arc, and the radially outward flow of ions into the low-pressure region may thereby be reduced.

The arc is struck between the externally heated tantalum filament and the 0.190-in.-ID, hollow carbon anode. The cathode-to-anode separation is between 0.050 and 0.070 in. A magnetic field is necessary for proper operation. The arc has been run in fields from 1.5 to 15 kilogauss; the higher the field, the more efficiently the arc operates.

Vacuum System. – The design of the vacuum system was copied in so far as possible from the one existing in DCX-1. It was modified only in such a way as proved beneficial to obtain the lowest possible pressure in the inner liner.

The system falls naturally into three regions, as shown in Fig. 4.6:

1. Outer Region. – This region contains the arc electrodes and target as shown and is pumped by two 20-in. diffusion pumps. A base pressure of 1 × 10^{-7} torr is easily obtained.

2. Intermediate Region. – This region is pumped by three 20-in. diffusion pumps and by titanium pumping. It is separated from the outer vacuum region by 4-in.-long baffles at each end, with an inner diameter of 0.4 in., through which the plasma passes. Two baffles 2 in. long and with an inner diameter of $\frac{5}{8}$ in. are provided to allow transmission of the plasma between the intermediate and inner regions. In addition, there exists a pump-out path, containing a Zeolite baffle, between the inner and intermediate regions. A target collector used for density measurements is positioned as shown in the diagram. A base pressure of 5 × 10^{-8} torr is easily achieved in the intermediate region.

3. Inner Region. – Figure 4.7 shows the construction of this region. It is pumped by titanium; it is also connected by a slide valve to the intermediate region through a Zeolite baffle.

---

[13] J. L. Dunlap, private communication.

[14] *Thermonuclear Project Semiann. Rept. July 31, 1960*, ORNL-3044, p 10.

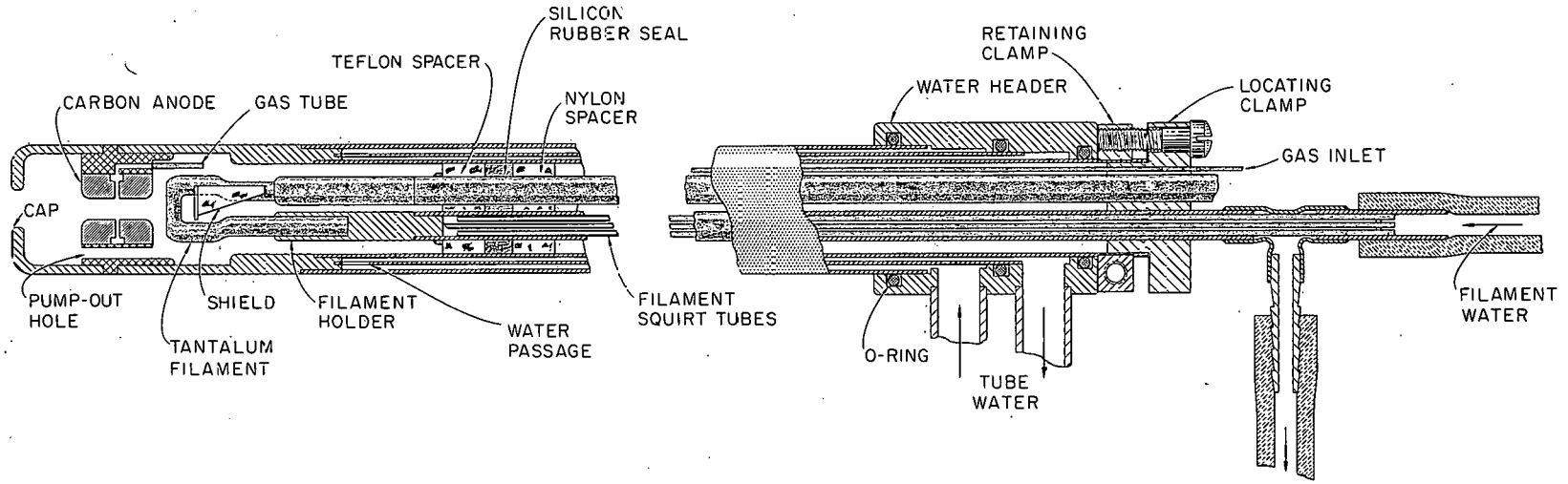

Fig. 4.5. Electron Gun.

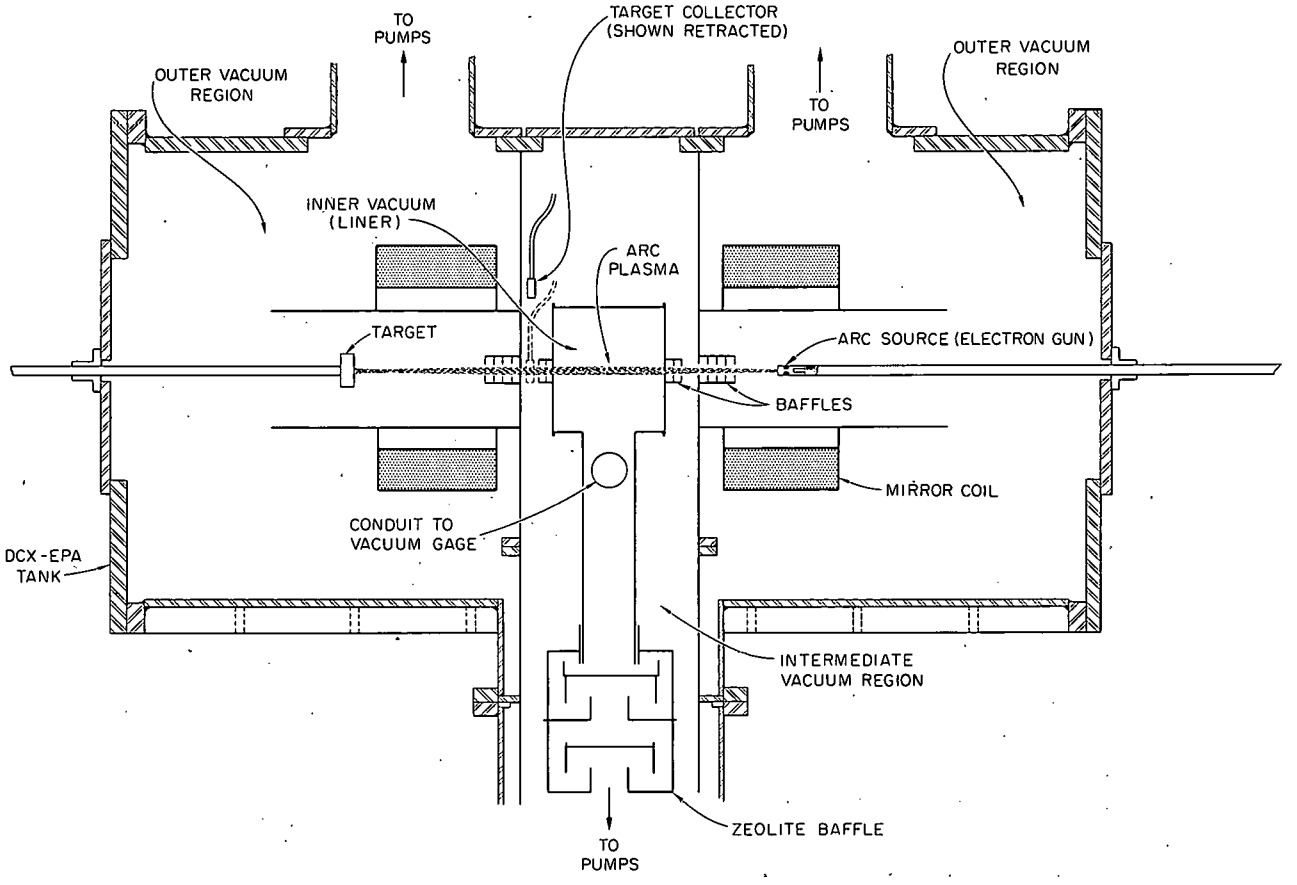

Fig. 4.6. Low-Density-Arc Experiment.

The Zeolite baffle of Fig. 4.7 is an improved version of that shown in Fig. 4.6. With the new arrangement, the baffle is of cartridge construction which can be loaded and preheated in a vacuum furnace. Transfer to the inner liner can be accomplished in 10 to 15 min, thereby minimizing the adsorption of water vapor during transfer and thus bakeout time before operation.

The inner vacuum liner consists of a copper cylinder 12-in. long and with a 14-in. inner diameter. Baffles $1\frac{3}{8}$ in. long, $1\frac{5}{8}$ in. in inner diameter, and with three $\frac{1}{16}$-in.-thick copper baffle disks having $\frac{9}{16}$-in. holes are located on either end to allow passage for the drifting plasma. Two 3-in. quartz windows facilitate observation of the liner interior. The copper cylinder is connected to the Zeolite trap by a 6-in.-diam copper tube. A 4-in.-diam copper tube connects the 6-in. one to an adequately shielded ion gage tube, Veeco RG-75. The surface area covered by the evaporated titanium is about 5000 cm^2.

The entire inner vacuum liner is bakable to 400°C. During operation, the inner liner is cooled to liquid-nitrogen temperature. A base pressure of 2.5×10^{-10} torr has been achieved in this region.

Experimental Results. – The plasma sweeper method[15] was used for measuring the density of the arc. Figure 4.8 shows schematically how this works. A current meter, not shown, was inserted between the 50-ohm resistor and ground. For a given gas feed into the arc, the arc voltage and

[15] This report, sec 3.4.

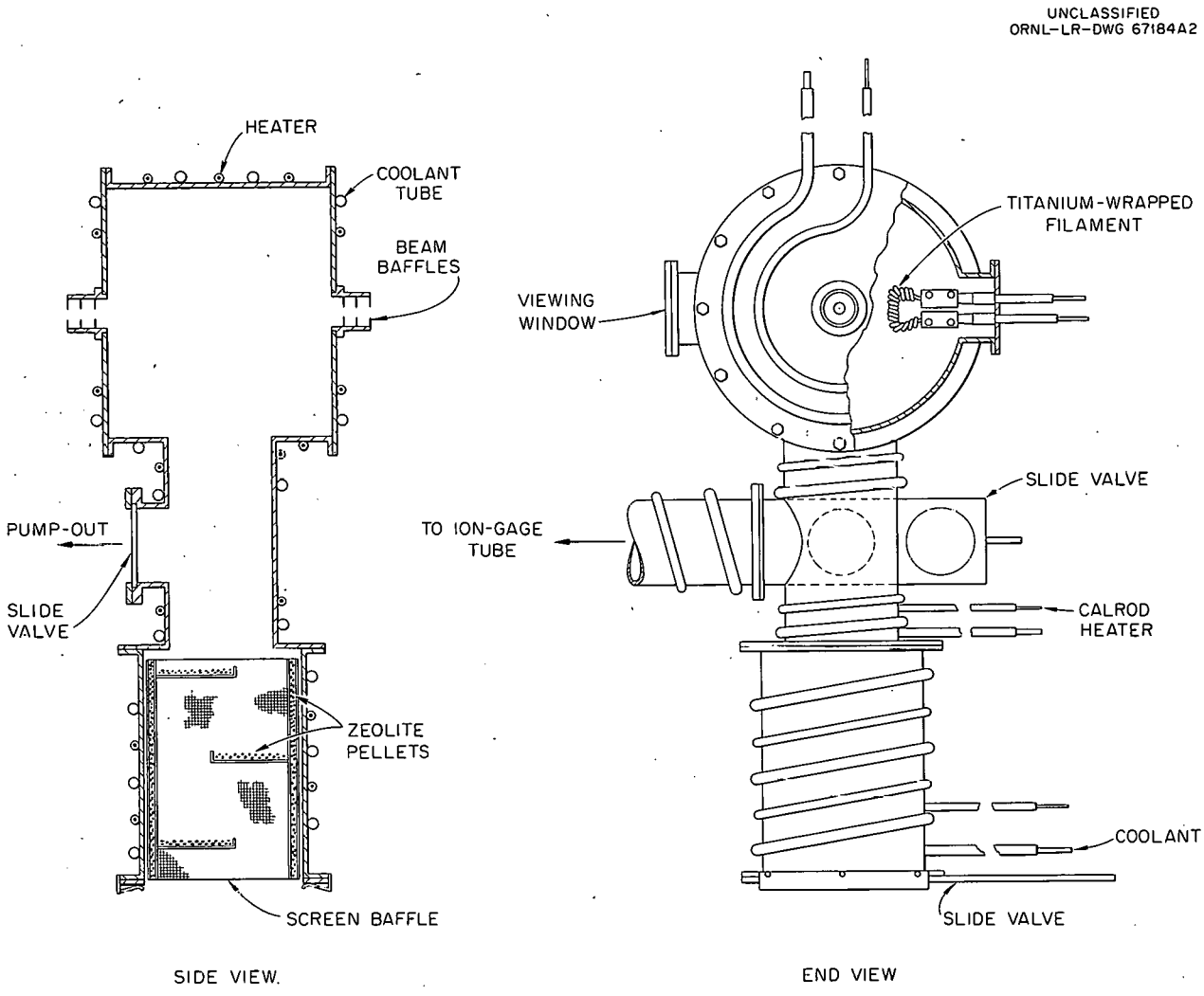

Fig. 4.7. Inner Vacuum Region (Liner).

filament emission were adjusted in order to maximize electron current to the target collector at zero bias voltage. The bias was then increased negatively until the current meter read zero. This ensured no steady-state voltage drop across the resistor. Upon shorting the arc electrodes (in about 3 msec) the bias voltage drew the ions from the system. The current pulse thus produced passed through the 50-ohm resistance, and the resulting voltage trace was photographically recorded with the aid of an oscilloscope. The value of the resistance and the area under this trace thus yielded an experimental value for the total charge collected. This value, according to ref 15, should then be multiplied by a factor of 2, since ions drift with equal probability in either direction along the field, only half of them arriving at the collector. The plasma density is the total charge collected divided by the volume of the plasma column. Figure 4.9 shows typical oscilloscope traces taken with two operating modes of the gun, using a hydrogen gas feed.

With the first mode, as shown in the upper trace, a total of 3×10^{11} charges were recorded. The calculated volume of the plasma column is 50 cm^3. Therefore, the ion density in this case was about 1.2×10^{10} cm^{-3}, taking into account the factor 2 mentioned above.

A check of the density measurement was made with a Langmuir probe positioned in the intermediate region next to the entrance baffle of the inner liner. Though the probe was not reliable

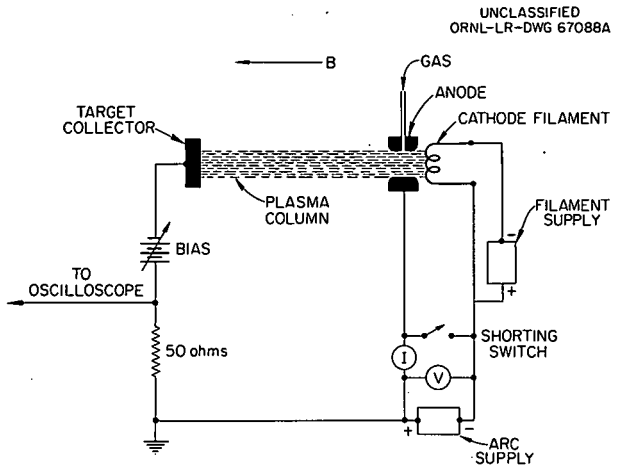

Fig. 4.8. Plasma Sweeper Circuit.

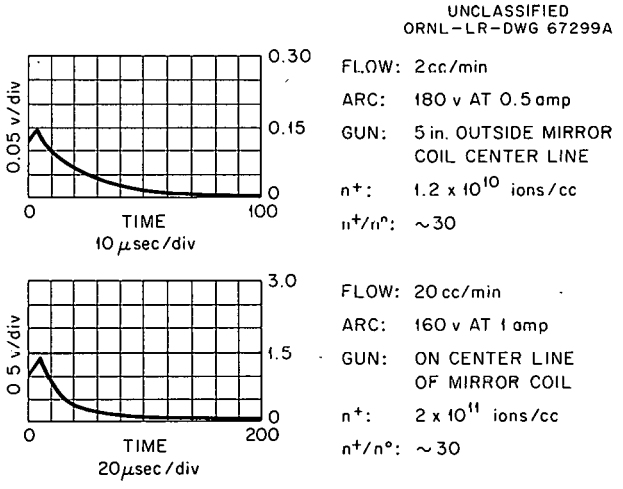

Fig. 4.9. Plasma Sweeper Oscilloscope Traces.

when biased positively, reproducible results could be made at negative voltages. The data indicated the temperature of the electrons in the arc column was about 7 ev. This yields an electron density of about 3×10^{10} cm^{-3}.

The upper trace in Fig. 4.9 was taken at an inner-liner gage pressure of 3×10^{-9} torr. To convert this to neutral density, the reading must be multiplied by 2, since the background gas was predominantly hydrogen. In addition, there is another factor-of-two correction because the temperature of the vacuum gage was about 4 times that of the liquid-nitrogen-cooled inner liner. Thus the corrected pressure was about 1.2×10^{-8} torr, which yields a neutral density of about 4×10^{9} particles cm^{-3}. The ion density was 1.2×10^{10} cm^{-3}; therefore, the ratio of ions to neutrals was about 30.

An effort was made to find out whether the required plasma could be produced with the gun removed to the weaker field of an auxiliary coil so that more efficient pumping of the neutral gas escaping from the anode could be gained. Because of alignment difficulties, the system would not operate properly if the gun were withdrawn more than 5 in. from the mirror coil center line. At this point, the magnetic field is 11,900 gauss or 88% of the value on the center line. Oscilloscope traces at the 5-in. location were identical to those obtained on the mirror coil center line.

The mode of operation depicted by the lower trace in Fig. 4.9 was sensitive to gas flow and magnetic field. With bias voltage at zero, the collector current peaked sharply with gas flow or magnetic field, indicating a second mode of operation. With the gun on the mirror coil center line (13,500 gauss), either an increase or a decrease in the flow would lower the collector current. The inner-liner pressure was 5×10^{-8} torr during the second mode of operation. Corrected by the factor of 4, the neutral density was 6×10^{9} particles cm^{-3}. Since the ion density was 2×10^{11} cm^{-3}, the ratio of ion to neutral density was again about 30.

Operation of the arc in either mode was very stable. At gas feeds of 2 cm^3/min with the arc assembly on the mirror coil center line, the inner liner vacuum rose from 2×10^{-9} torr to 3×10^{-9} in an hour and a half. The carbon anode should last indefinitely; the tantalum filament should operate at least 50 hr in magnetic fields no greater than 10 kilogauss. At fields between 10 and 12 kilogauss, it becomes necessary to reverse the filament current leads periodically. A thoriated tungsten filament has been developed for use in fields higher than 12 kilogauss.

4.2.2 An Arc Plasma of Adjustable Density for H_2^+ Dissociation in DCX-2

R. A. Gibbons R. J. Mackin, Jr.
T. F. Rayburn

Introduction. – This section describes the design and preliminary experiments with a steady-

state plasma column of adjustable density. The ion density range extends up to 5×10^{11} cm^{-3} under current operating conditions.

The primary purpose of this device is to serve as a trapping plasma in DCX-2. Calculations[16,17] show that the high-density energetic deuterium arc initially developed by this group[18] would cause intolerable energy losses for the trapped protons in DCX-2. This would be true unless the electron temperature could be raised to the vicinity of a kiloelectron volt, which seems an unlikely prospect. The desirable ion density for a trapping plasma appears to be about 10^{11} to 10^{12} cm^{-3}, and our efforts are now directed toward the generation of such a plasma. If the development is successful, there are other possible applications which may be more important than the initial one.

In order to be useful as a trapping plasma this device must meet the following requirements:

1. Be able to increase significantly the dissociation efficiency for molecular ions.
2. Not add significantly to the energy loss rate of trapped protons over the loss rate to the electrons in the remainder of the plasma.
3. Not add significantly to the charge-exchange losses of the trapped protons to either extra neutral gas or molecular ions.
4. Not constitute a localized potential anomaly which would produce drifts or instabilities of the hot plasma.

These requirements may be expressed as:

1. $n_a \sigma_{Ba} L_a \geqq (n_0 \sigma_{B0} + n_+ \sigma_{B+}) L$,

2. $n_a \epsilon_a V_a \leqq (n_+ \epsilon_F + n_0 \epsilon_B) V_+$,

3. $Q_a \leqq \Gamma I$, $\quad n_a' \sigma_{xa} V_a \leqq n_0 \sigma_x V_+$,

4. $\Phi_a \approx \Phi_{sp}(r_a)$.

The notations are defined as follows:

n's are densities (a, +, 0 ≡ arc, ion, neutral),

σ_B's are dissociation cross sections,

L's are molecular-ion path lengths in the respective media,

ϵ's are stopping powers (rate of energy loss per electron – F, B = free, bound),

V's are volumes,

σ_x's are charge-exchange cross sections,

n_a' is the density of partially stripped ions in the arc,

Q_a is the rate of gas influx associated with the arc,

ΓI is the rate of gas influx associated with the beam,

Φ's are potentials.

Defining $\sigma_{Ba} = Z^2 \sigma_B$; taking $L/L_a = 0.4\pi d_2/d_a$, where d_2 is the molecular ion orbit diameter, and 0.4 is the fraction of an orbit in the plasma region; $V_+/V_a \approx d_2^2/d_a^2$ (which follows from the approximate equality of d_2 and the plasma diameter), $\epsilon_F \doteq \epsilon_B = \epsilon$, and $\sigma_{xa} \doteq \sigma_x$, we get

$$\frac{n_a}{n_0 + n_+} \geqq \frac{0.4\pi d_2}{d_a Z^2} ,$$

$$\frac{\epsilon_a}{\epsilon} \leqq \frac{d_2 Z^2}{0.4\pi d_a} ,$$

$$\frac{n_a'}{n_0} \leqq \frac{d_2^2}{d_a^2} .$$

For $d_a = 2$ cm, $d_2 = 25$ cm,

$$\frac{n_a}{n_0 + n_+} \geqq \frac{16}{Z^2} ,$$

$$\frac{\epsilon_a}{\epsilon} \leqq 10 Z^2 ,$$

$$\frac{n_a'}{n_0} \leqq 150 .$$

These parameters, taken in conjunction with DCX-2 plasma estimates, suggest that desirable hydrogen parameters are $n_a \sim 10^{12}$ ions cm^{-3},

---

[16] D. J. Rose, *Ion Energy Distribution, Energy Degradation, and Exponentiation Criteria in a Plasma Formed by Beam Trapping and Charge Transfer*, ORNL CF-60-9-112 (September 1960).

[17] N. H. Lazar and G. G. Kelley, private communication, 1960.

[18] C. L. Cocke, Jr., *et al.*, *Thermonuclear Div. Progr. Rept. Oct. 31, 1961*, ORNL-3239, pp 58–61.

$T_{ea} > 100$ ev, and $n_a' < 5 \times 10^{10}$ molecular ions cm^{-3}. The present development, begun before the energy-loss problem was fully appreciated, has been aimed only at $n_a \sim 10^{11}$ ions cm^{-3}, with no explicit requirements on the other parameters. The experiments to be reported, however, suggest that the more stringent conditions can be met.

Concept and Preliminary Estimates. – Just as the energetic carbon arc was used as a model in the initial design of the energetic deuterium arc,[19,20] the deuterium arc was used as a model for the design of the present plasma. The minimum deuterium-arc density was fairly well established by the requirement of maintaining the cathode hot by ion bombardment. In order to drop the density by three decades, we went to a non-self-sustained discharge and used a resistance-heated cathode. As before, gas is introduced at the base of a deep tubular anode. The ions produced there drift along field lines to the cathode and provide space charge neutralization.

The preliminary estimates of the plasma performance rested on two fundamental assumptions: (1) The electrons become at least randomized if not thermalized fairly near the cathode by collective interactions. (2) The ion drift velocity is comparable to that observed in the high-density deuterium arc: 10^6 cm/sec.

Because the ion current (nv_d) is thus reduced by three orders of magnitude, the gas input at the anode is reduced accordingly, and the requirement of high ionization efficiency in the anode is relaxed. As before, we rule out the temptation to "make more efficient use of the electrons" by using a reflex geometry, because of the intense plasma oscillations always associated with such devices.

Assuming the same plasma cross section as in previous work (1 cm^2) we expect an ion current of about 15 ma. For the cathode we assume an electron gun which puts out 150 ma. Thus the anode chamber pressure must be such that the efficiency for producing an emergent ion is 10% per electron.

Space neutralization limits the electron drift velocity to 10 times the ion drift velocity. Thus the path length traced out by an electron per unit axial distance drifted is given by the ratio of the thermal to drift velocities – for 100-v electrons a factor of about 60. Assuming an ionization cross section of 4×10^{-17} cm^2, the efficiency per unit length per unit pressure of an anode tube then is about 8% per centimeter-micron. This figure leads to a readily accessible range of anode dimensions and pressures.

The ionizing efficiency actually required is uncertain by the ratio of ions produced to ions actually emergent.

Note that, in contrast to the high-density deuterium arc, this arc has an expected gas feed small enough to be handled easily by titanium pumps.

The fraction of the emerging ions which will be H_2^+ (and thus possible charge-exchange centers) might be high. However, in the 3-m drift distance between an anode in DCX-2 and the plasma region we estimate this fraction to be reduced by a factor of 3. The estimated time constant for a proton to charge exchange in passing through the arc in the plasma region is then about 10 sec, and this is not expected to be a noticeable phenomenon.

The estimated cathode sheath which comes out of these parameters has a thickness of 0.02 cm and a corresponding voltage of about 200 v. This is reasonably consistent with the above set of assumptions.

Apparatus and Experiments. – The apparatus is shown schematically in Fig. 4.10. The differential pumping system permitted lower pressures in the central region than would have been possible with straight pumping on the whole volume. Operating pressures were in the 10^{-3}- to 10^{-4}-mm range in the anode region and 10^{-5} to 10^{-6} in the central and cathode regions. As a result of the low ionization efficiency for anode gas there was negligible gas transfer along the arc.

The electron gun employed a negatively biased, resistively heated, straight-filament cathode and a slotted accelerator plate at tank potential. The gun furnished up to 150 ma of electrons at 300 to 500 v. The electron beam was constrained by the applied magnetic field (3.5 to 9 kilogauss in the central region and twice that at the coil centers) to flow through the vacuum baffles to the anode. In the center, the beam cross section was approximately 1 cm by 3 mm.

The initial anode was an 80-cm-long, 2.5-cm-diam, cylindrical copper tube which confined the

[19] P. R. Bell and J. S. Luce, pp 166–68 in *The ORNL Thermonuclear Program*, ORNL-2457 (1958).

[20] R. A. Gibbons *et al.*, *Thermonuclear Project Semiann. Rept. Jan. 31, 1960*, ORNL-2926, pp 47–51.

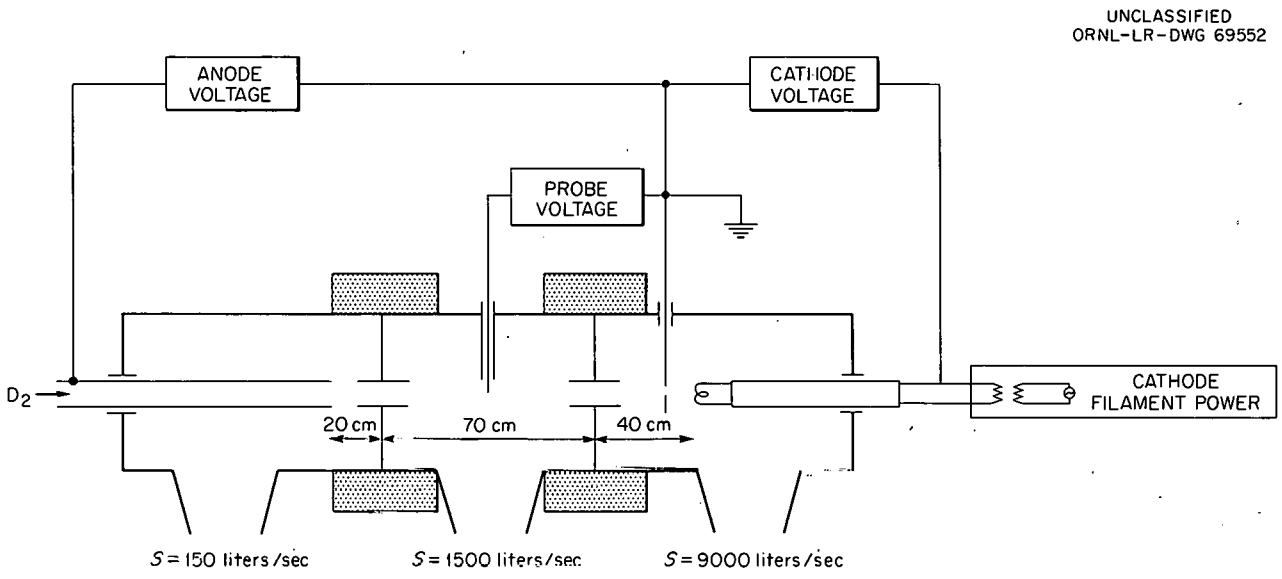

Fig. 4.10. Low-Density Deuterium Arc in the Gas Arc Facility.

neutral gas in order to yield maximum ionization probability. Between 10^{-3} and 10^{-1} atm cm^3/sec of deuterium was introduced at the end of the anode as shown. Deuterium was used instead of hydrogen in order to take advantage of the expected increased ionization efficiency.

The plasma was studied with a single electrostatic probe located in the center as shown. The probe data were used for the estimation of ion density, electron temperature, and space potential.

Probes are expected to give reasonably good accuracy even in intense magnetic fields (10 kilogauss). The major objection to their use comes from disturbance of the plasma. However, cylindrical tungsten probes about 0.125 in. long with 1.0- to 10-mil diameters gave generally identical results. For the lower-density cases, perturbation of the electron energy distribution and arc characteristics were found, but the indicated density seemed unaffected.

Experimental Results. – Most of the experiments were performed with a 50- to 100-ma electron beam at 300-v acceleration. The plasma density fell in the desired range during the initial experiments with the elementary electron gun and anode designs; so, most of the experimental effort was directed toward the investigation of parameters controlling the density, in order to predict arc operation in DCX-2. Because many parameters affected the density, the results are sketchy and should be regarded as preliminary.

Figure 4.11 shows a plot of indicated density vs deuterium gas input. The difference between circles and points indicates the correction for the central-region pressure contribution to the ion input (and thus to the density). The curve thus represents the expected density at zero background pressure.

Probe characteristics in this regime of operation gave no indication of streaming electrons beamed

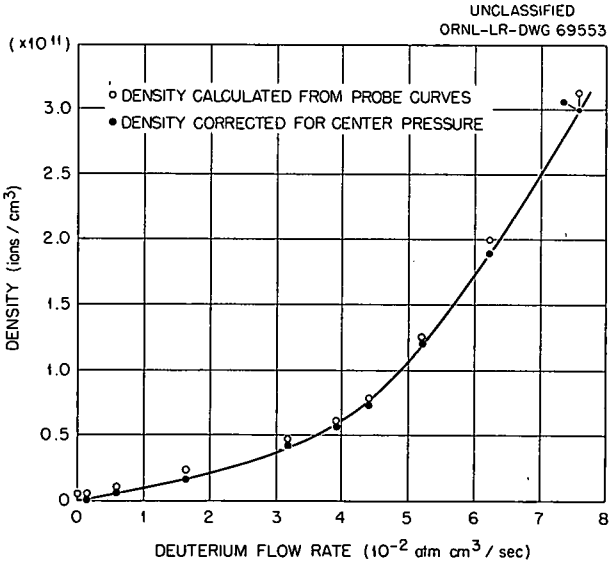

Fig. 4.11. Plasma Density vs Deuterium Flow Rate.

from the cathode, tending to bear out the randomization hypothesis.

It is of interest to estimate the efficiency with which deuterium fed into the anode is converted into emergent ions. Assuming a drift velocity of 10^6 cm/sec and all molecular ions, the ion flow for $n = 10^{11}$ cm^{-3} corresponds to 1×10^{-3} atm cm^3/sec. The actual input was 50 times greater.

The effective anode depth, because of diverging magnetic field lines, was about 12 in. However; the magnetic mirror effect acted to discourage ions from emerging from the anode, and only an estimated 3% were able to do so. (Two tacit assumptions underlie this estimate: that the anode sheath voltage is negative, as would be expected for this plasma regime, and that the scattering lengths are great enough that the ion motions are essentially those of individual particles.)

The calculated mean deuterium pressure inside the anode was 1 μ for a gas input of 5×10^{-2} cm^3/sec. Thus, the estimate made in "Concept and Preliminary Estimates" would indicate an ionizing efficiency per electron of almost 100% and, correspondingly, repeated ionization and recombination of the deuterium. If the ion current to the anode end is thus 50 times that through the hole leading to the column, the assumption of the same drift velocity leads to an ion density of 5×10^{12} cm^{-3} inside the anode, and we may properly expect the existence of more plasma phenomena between anode end and hole than were dreamed of in one philosophy. The numbers in fact indicate that sufficient ions are produced in the first 2 or 3 cm of the anode to provide the observed flow along the arc.

The next experiments employed inside the anode a movable plunger, insulated from the anode wall, which could be used for varying the anode depth and for attempting to influence the internal potential distribution.

Figures 4.12 and 4.13 show the effects on plasma density of varying these parameters. Some features of the voltage effects may be understood qualitatively, but the anode depth effects are not at all understood.

The probe characteristics did not generally yield linear logarithmic plots of electron current, implying a non-Maxwellian electron-velocity distribution. However, a mean slope was identified as $\frac{2}{3}$ of the electron energy and defined as electron temperature for comparison purposes. The variation of T_e with anode conditions is shown in Fig. 4.14.

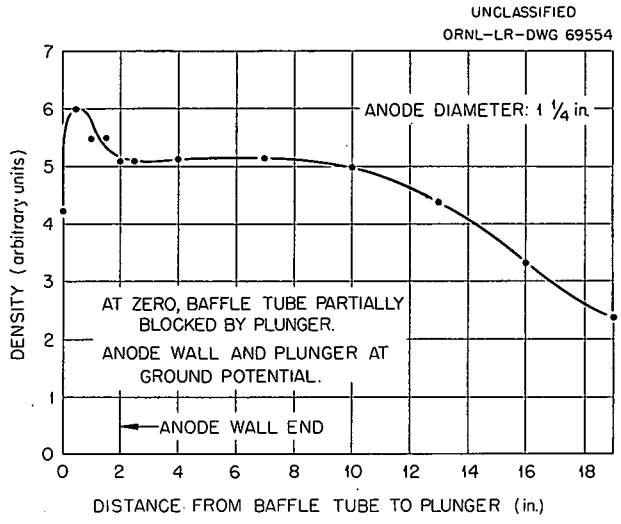

Fig. 4.12. Plasma Density vs Anode Plunger Position.

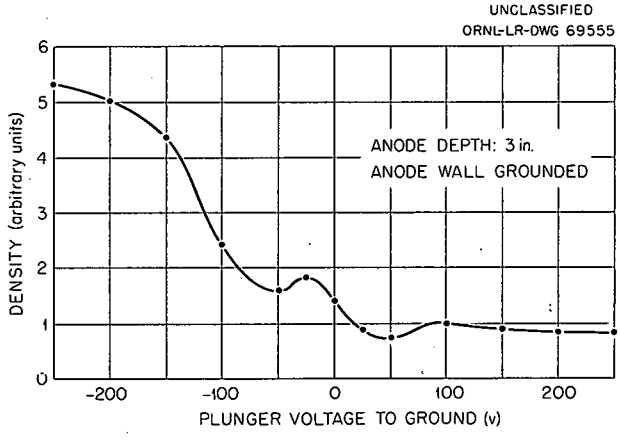

Fig. 4.13. Plasma Density vs Anode Plunger Voltage.

Other parameters observed to affect density are as follows:

1. Anode current: the relationship was not linear.
2. Cathode heating power: a maximum density was observed well below the power limit.
3. Magnetic field: proportional between 6 and 9 kilogaus, steeper below 6 kilogauss.
4. Anode voltage (plunger and wall varied together): a density maximum was observed at -25 v.

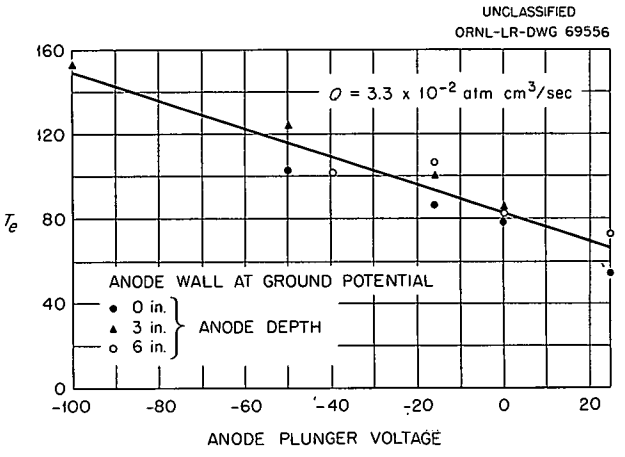

Fig. 4.14. Electron Temperature vs Anode Plunger Voltage.

The extreme ion density limits observed were 3×10^8 and 3×10^{11} cm^{-3}. The density was approximately uniform over the plasma's cross section; however, the electron temperature peaked sharply at the center. Streaming electrons became noticeable at the lower plasma densities.

Examination of the electron patterns produced at the base of the anode (by using fluorescent materials or thin tantalum foils) showed that the expected line image of the gun appeared only at currents of the order of microamperes. For higher currents, space-charge and/or collective effects gave quite distorted patterns even with substantial amounts of gas feed. Supplying gas in sufficient quantity to the enclosed electron-gun box gave a sharp source image, presumably as the result of sheath formation at the cathode. The resultant plasma density was about 10^{11}, but the electron temperature was only 45 ev, lower than desirable in a dissociating plasma. The arc in this instance was essentially the same as that in the "Ioffe experiment" arc of Yushmanov[21] or its variation, more recently studied by Stirling.[22] It does not appear to have available the same extended density range, and the electron temperature seems fairly well tied to a low value. Even the use of a "gas-conservation tube" on the cathode[21] did not make it possible to avoid space-charge effects in a discharge supported by gas fed only into the anode.

A conical anode was designed such that the electron column extended a full 80 cm to its base. With this anode, however, it was impossible to produce enough plasma at the cathode to generate there a beam-plasma instability and attendant randomization. Instead, when gas feed was raised, the electrons beamed from the cathode produced a large ion current to the wall. The plasma density between the mirrors was never made to exceed 10^9 ions cm^{-3}.

Conclusions. – A highly-ionized, steady-state plasma with density adjustable up to 3×10^{11} has been developed and studied. The factors affecting plasma density have not yet been accurately delineated, but operating experience suggests that application to DCX-2 is readily feasible.

---

[21] E. E. Yushmanov, pp 284–85 in *Plasma Physics and the Problem of Controlled Thermonuclear Reactions*, vol IV, Pergamon Press, 1960.

[22] C. W. Blue *et al.*, *Thermonuclear Div. Progr. Rept. Oct. 31, 1961*, ORNL-3239, pp 61–63; this report, sec 4.2.1.

5. Ion Production, Acceleration, and Injection

5.1 DEVELOPMENTS IN THE HIGH-BEAM ACCELERATOR

R. C. Davis
R. R. Hall
G. G. Kelley
C. E. Moore
O. B. Morgan
R. F. Stratton

Since the last report most of the effort of this group was applied to the details of getting a beam into DCX-2. Information concerning the performance of this injector is given elsewhere in this report.[1] No major difficulties were encountered. The leakage magnetic field, in spite of shielding, is slightly more than had been hoped (see Fig. 2.2 of Sec 2.3). Two outboard pairs of bending coils were added in the injector pumping chamber to compensate for this field and for small misalignment.

The Freon-nitrogen bag around the accelerator tube (to prevent external voltage breakdown) is still a nuisance. Tests were made on cast epoxy skirts (42 in. in outer diameter) between electrodes. One section held 300 kv. A stack of four insulator sections and Lucite plates, intended to simulate the tube, held over 600 kv for several hours with no breakdown when the top section was provided with a Freon-nitrogen atmosphere. It may be that sharp corners in the Lucite, which are not present in the epoxy skirts, caused the need for the bag. In any event, the arrangement should be a considerable improvement. A small bag in this position can be sealed and left inflated.

A new tube, using skirts, is being assembled for use at the high-intensity-beam facility.[2,3] It will be used to test electrode arrangements, to study the effect on beam quality of changes in extraction geometry, and to find out more about the anomalous spreading of a beam beyond a crossover reported before.[2,4]

For these studies, an aperture plate, water-cooled probe, and target are being made. The probe can be positioned accurately under the hole in the plate, as may be seen in Fig. 5.1. All measurements on these components will be calorimetric. Electric probes also will be used to determine space potentials in the vicinity of the beam.

Additional information will be derived from use of a copper funnel now being built to simulate the duct leading into DCX-2. It will be possible to mass-analyze the beam by using the mass-dependent focal length of the magnetic solenoid lens to pass preferentially only one component through the funnel.

5.2 100-KEV NEUTRALIZED-BEAM ACCELERATOR

C. W. Blue
H. C. Hoy
R. L. Knight
O. D. Matlock
V. J. Meece
W. L. Stirling

Both the electron gun and the ion-source arc of the 100-kev accelerator (Fig. 5.2) have undergone successful individual operation. The accelerator easily holds the 100 kev (no arcs on) for which it was designed. However, it was discovered that the upper, high-voltage insulator shield becomes quite hot in a ring pattern over a 1-in. section of its surface. Since there is no such heating in the lower section, the insulator shields have

[1] This report, sec 2.6.

[2] G. G. Kelley *et al.*, *Thermonuclear Div. Semiann. Progr. Rept. Jan. 31, 1961*, ORNL-3104, p 19.

[3] G. G. Kelley *et al.*, *Thermonuclear Div. Progr. Rept. Oct. 31, 1961*, ORNL-3239, p 64.

[4] G. G. Kelley and O. B. Morgan, "Space-Charge Neutralized Ion Beams," *Phys. Fluids* 4(11), 1446–47 (1961).

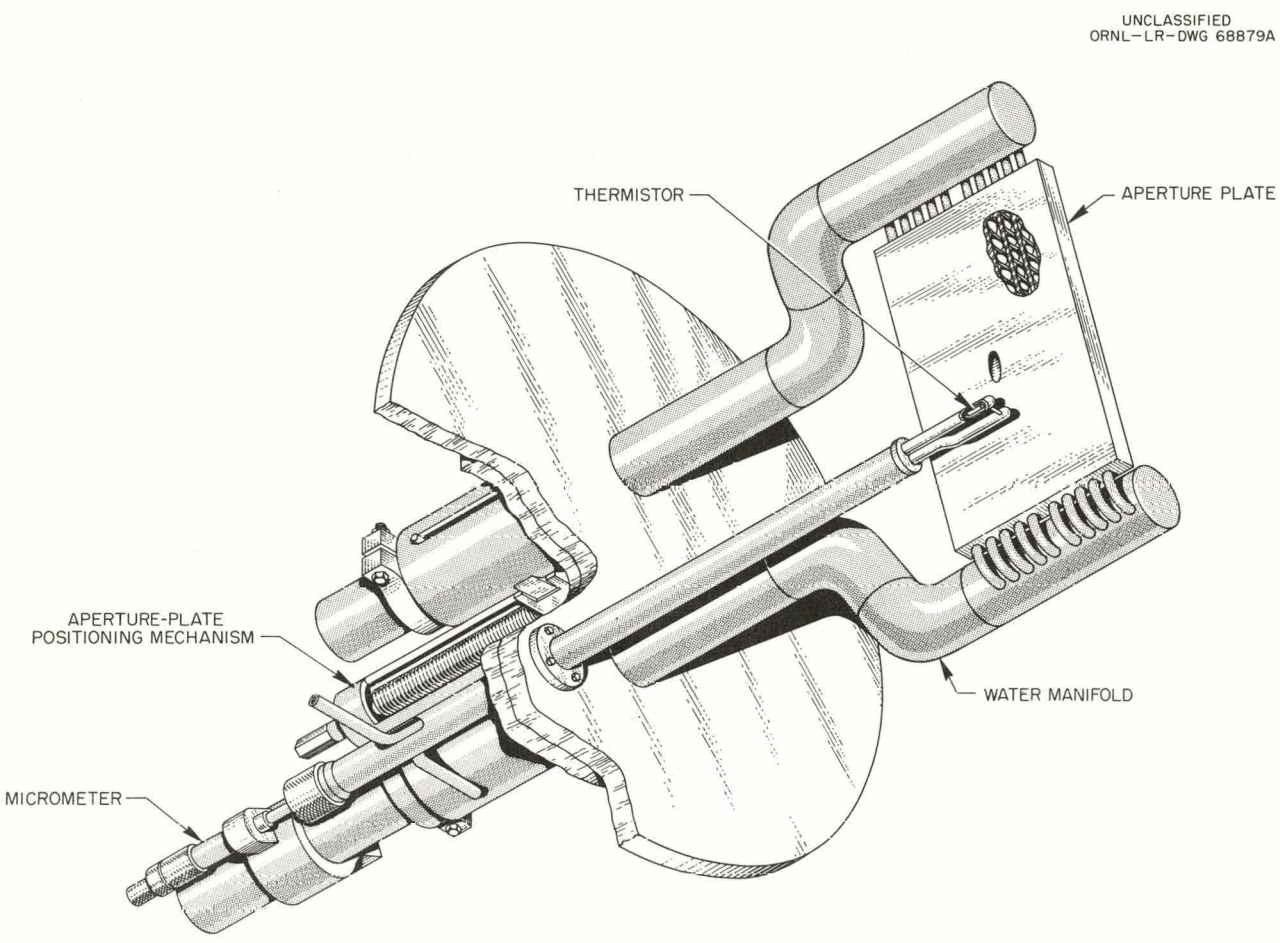

Fig. 5.1. Apparatus for Beam-Emittance Measurements.

been modified to make them identical to those on the bottom.

Tests of electron injection into the ion source of the accelerator have not been made as yet because the center coil failed. While waiting for a new one to be wound, the accelerator was installed on a vacuum test stand in order to achieve independent operation from DCX-EPA. Reassembly of the accelerator with the new center coil is complete, and tests should get under way again between May 15 and June 1, 1962.

5.3 HOLLOW-CATHODE ARC ION SOURCE

O. D. Matlock V. J. Meece
W. L. Stirling

A hollow-cathode arc discharge (Fig. 5.3) was developed for use as an ion source in the 100-kev neutralized-beam accelerator.[5] However, full exploration of the properties of this ion source has only recently been started.

Figure 5.4 shows typical curves of the accelerating electrode current and the target current at low accelerating voltages. The currents are the total hydrogen-ion output; analysis of the beam is not possible in the present apparatus. At an accelerating voltage of 16 kev over an accelerating gap of $\frac{3}{16}$ in., the target current reached 250 ma, while the current to the accelerating electrode peaked at about 8 to 9 kev and fell to a value of 430 ma at 16 kev. Upon reducing the arc current to 10 amp, keeping the gas flow constant and the accelerating potential constant at 16 kev (not shown on curve), the target current rose to 300 ma

[5] *Thermonuclear Div. Progr. Rept. Oct. 31, 1961*, ORNL-3239, p 67.

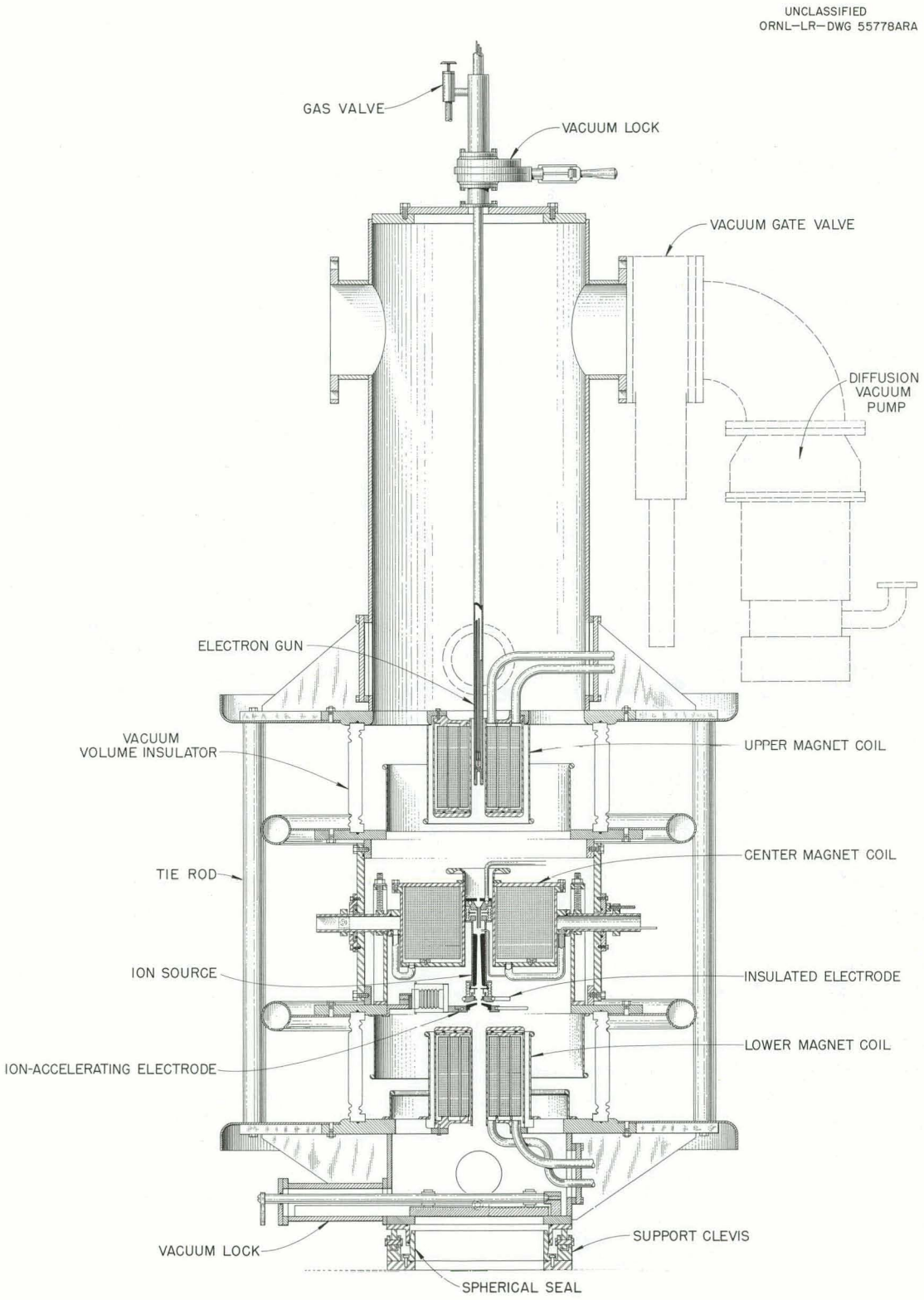

Fig. 5.2. 100-kev High-Energy Plasma Accelerator.

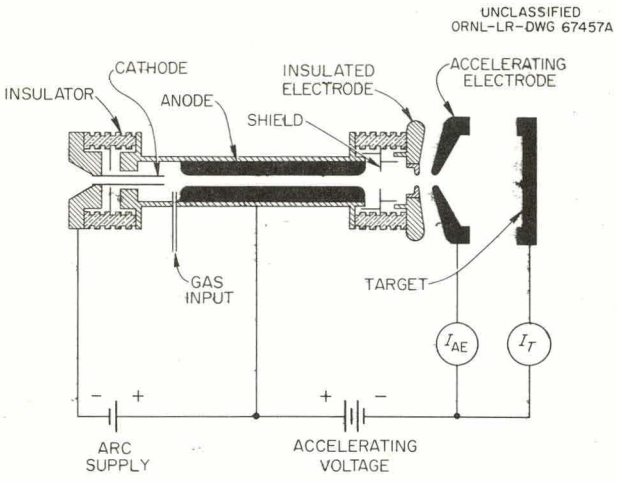

Fig. 5.3. Hollow-Cathode Arc Ion Source.

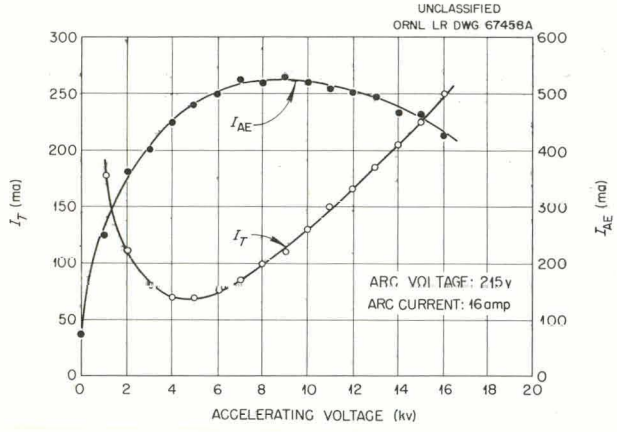

Fig. 5.4. Ion-Source Output vs Accelerating Voltage.

and the accelerating electrode current fell to 140 ma.

In order to extend the range of the applied accelerating voltage, a new shielded enclosure (electron dump) was designed for the source. Voltages up to 37 kev have been held during tests with no arc. However, output-current limitations with the present high-voltage supply temporarily stalled further operational tests with the arc on. These tests will cover a comprehensive study of the ion-source performance with variation of the arc parameters.

5.4 NEUTRAL SOURCE DEVELOPMENT

R. L. Knight
H. C. Hoy
O. D. Matlock
W. L. Stirling

The experimental apparatus is being assembled in order to utilize the hollow-cathode arc discharge in a neutral-beam source.[6] Figure 5.5 is an assembly drawing of this source. Both the ion-source arc and the neutralizing or converter arc are hollow-cathode discharges mounted coaxially in a solenoidal field of 3000 gauss.

Below about 40-kev ion energy, the neutrals will be produced (1) by charge transfer to the neutral gas background in the converter arc chamber and (2) by dissociation of molecular ions in the converter arc. Above 40 kev, the principal neutral production will be by dissociation. In either case, the neutral population produced will be subjected to losses because of reionization of the neutrals. There is then an optimum length for the converter arc, which is dependent upon the cross sections for the production and loss of the neutrals. Considering these cross sections as dissociation and ionization, respectively, the length X may be shown to be

$$X = [n_e (\sigma_d - \sigma_i)]^{-1} \ln (\sigma_d/\sigma_i) ,$$

where

n_e = electron density in converter arc,

σ_d = dissociation cross section,

σ_i = ionization cross section.

In the ion energy range up to 50 kev, the converter arc length is in the magnitude of inches, a condition very easily satisfied.

A number of desirable features are inherent in a neutral-beam source of this kind: (1) The type of converter arc discharge (all gases and carbon equally practicable) as well as the interaction distance X may be easily varied with no adverse

[6] This report, sec 5.3.

effect on other systems to which the neutral-beam source is connected. (2) Neutral-beam collimation should be very good. Collimation is achieved by the confinement of the undissociated ion beam along the magnetic field. In addition, collimation of the neutrals is aided by the converter-arc geometry. (3) The longitudinal magnetic field will simplify pumping any ions coming through the converter-arc exit. These ions follow the field lines and may be readily removed.

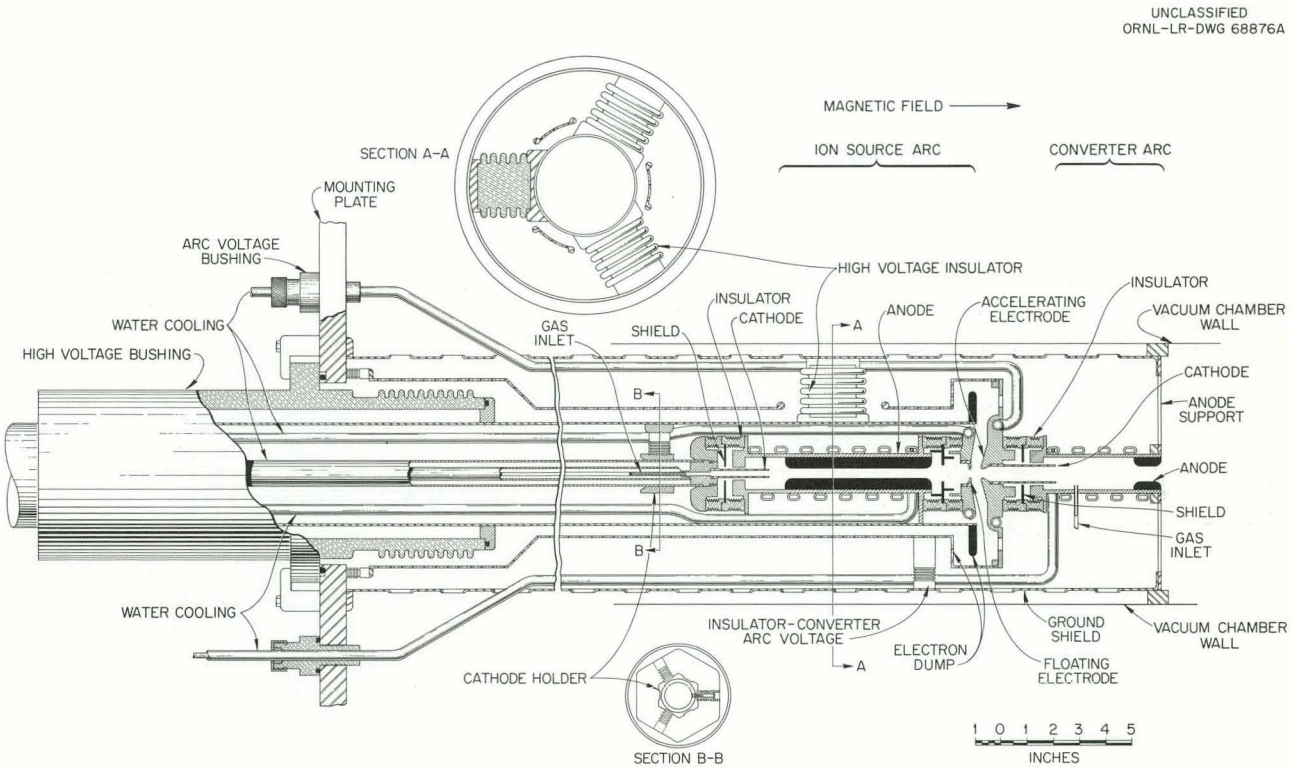

Fig. 5.5. Neutral-Beam Source.

6. Theory and Computation

6.1 ON A MINIMUM PRINCIPLE FOR STABILITY

T. K. Fowler

Three new features have emerged from continued study of the well-known criterion, a kind of minimum principle, that it is sufficient for stability that there exist a positive constant of motion quadratic in perturbations. Put differently, it is sufficient that there exist a time-independent, positive definite Hermitian operator whose expectation values over solutions of the linearized Vlasov equation are constant in time. It has been noted previously[1] that an operator H_+ is such a constant if, for example, multiplying the Vlasov equation by some operator yields the form

$$H_+(\partial f/\partial t) + Af = 0 , \qquad (1)$$

where A is anti-Hermitian. Using Eq. (1), stability was proved for all equilibrium distributions of the form

$$\frac{\partial f_0(\epsilon)}{\partial \epsilon} < 0 , \qquad \epsilon = \frac{1}{2} m v^2 + V(x) . \qquad (2)$$

Here, ϵ is the single-particle energy, $V(x)$ being a static potential representing gravitation and/or an equilibrium electric field. Inasmuch as the instantaneous particle phase-space distribution alone was assumed to represent the plasma, effects of retardation in the propagation of fields derived from the distribution had to be neglected in the proof.[1]

New results are:

1. Retardation need not be neglected in proving the stability of f_0 satisfying Eq. (2) if the instantaneous description of the plasma includes not only the distribution but also, separately, the electric and magnetic fields. Then the system composed of the linearized Vlasov equation together with the two curl equations of Maxwell takes the form

$$\frac{\partial \psi}{\partial t} = M\psi . \qquad (3)$$

Here ψ is a column vector whose components are distribution and field perturbations. The term M is a matrix of linear integro-differential operators. Maxwell's divergence equations may be included merely as initial conditions, since solutions of Eq. (3) satisfying them initially do so for all time. Now, as a sufficient condition for stability one may seek a multiplier of Eq. (3) yielding the form [Eq. (1)] above.

2. If f is the distribution perturbation and $\vec{E}$ and $\vec{B}$ are the field perturbations, the constant H_+ corresponding to equilibria satisfying Eq. (2) has expectation values

$$(\psi, H_+\psi) = \int d\vec{x}\, d\vec{v}\, f^2 \left(\frac{-\partial f_0}{\partial \epsilon} \right)^{-1} + \int d\vec{x} (E^2 + B^2) . \qquad (4)$$

For a Maxwell distribution, $f_0 = \exp(-\epsilon/T)$, the term in addition to the field-energy term turns out to be the quadratic term of an expansion of $-TS = T \int f \ln f \, d\vec{x}\, d\vec{v}$ about f_0. The term H_+ is the free energy, a sum of internal energy, U, and $-TS$ with terms higher than second order neglected, consistent with linearizing the Vlasov equation. The linear terms in $U - TS$ have cancelled, leaving a quadratic form, as in the derivation of this constant in the small m/e limit by Kruskal and

[1] T. K. Fowler, *Phys. Fluids* 4, 1393 (1961); 5, 249 (1962); and *Thermonuclear Div. Progr. Rept. Oct. 31, 1961*, ORNL-3239, p 75.

Oberman,[2] and by Trubnikov.[3] If a linearized collision term is added to the Vlasov equation, H_+ in Eq. (4) becomes monotonically damping in time, and its positive definiteness still ensures stability. With or without collisions, the fact that for a Maxwellian f_0, perturbations in free energy, given by Eq. (4), are always positive implies that the total plasma free energy is minimal at equilibrium, thus satisfying a thermodynamic stability requirement. Note that the perturbation in free energy may be identified with what Buneman has called "rf energy."[4]

3. A method for seeking quadratic constants of motion, whether or not they be positive definite, derives from the following theorem: Given any convenient scalar product defining a representation, a time-independent operator, H, which is Hermitian in that product, has constant expectation values over solutions of Eq. (3) if and only if HM is anti-Hermitian in the same product. In quantum mechanics, where $M = i\mathcal{H}$, $\mathcal{H}$ being the Hamiltonian which is always taken Hermitian in the products employed, this rule reduces to the familiar requirement that constants of motion must commute with $\mathcal{H}$. To prove the above theorem, take

$$\frac{\partial}{\partial t}(\psi, H\psi) = (\psi, [HM + M^{\dagger}H]\psi) , \qquad (5)$$

$M^{\dagger}$ being the Hermitian conjugate. If HM is anti-Hermitian, the right side vanishes, and $(\psi, H\psi)$ is constant. If H is a constant of motion so that the right side vanishes for all ψ, the operator in brackets is identically zero, and HM is anti-Hermitian.

6.2 SECONDARY PLASMA PHENOMENA

T. K. Fowler

A simple mechanism implying enhanced energy transfer to electrons in DCX-1 is offered as at least a partial explanation for the following qualitatively similar experimental observations. In the electron cyclotron heating experiment (PTF), the plasma density generally increases abruptly when the neutral pressure exceeds a critical value, P_0, around 10^{-5} mm Hg.[5] In DCX-1 and calutron beams, the emerging slow ion current reflecting the rate of ionization of neutrals tends to increase abruptly when the pressure exceeds a critical value comparable to P_0 above. A possible explanation in both cases is the accumulation of slow ions if $P > P_0$.

We make two assumptions: First, let the electron temperature exceed the ionization threshold. Second, assume that slow ions resulting from ionization events escape only by drifting out of the plasma at thermal speed. That is, ions receive negligible energy by collisions (satisfied in the above experiments), and electric fields which might accelerate the ions are confined to the plasma surface. Then, the slow-ion lifetime, τ_s, is determined by the plasma dimensions, about the same in all the experiments (a few centimeters). With these assumptions, it follows that slow ions accumulate when the mean free time between ionizations, τ_i, is less than τ_s, and their density grows until the accompanying electrons (hot, by assumption) burn out the neutral population sufficiently to increase τ_i to equal τ_s. Once a critical pressure is reached, the average neutral density inside the plasma remains fixed as the pressure outside is increased further, and the slow-ion density makes up the difference. The term τ_i corresponding to P_0 agrees pretty well with τ_s equal to the 100-μsec drift times for thermal ions across the plasmas.

One interesting prediction for PTF, not yet verified experimentally, is that the plasma potential changes sign at P_0, going from a modest negative value at lower pressures, where the cyclotron-heated electrons govern the density, to a large positive value at higher pressures, where slow ions accumulate and hold in hot electrons electrostatically. No such sign change would occur in the other experiments, since a primary beam of fast ions dominates the low-pressure situation.

The fact that it has been necessary to assume the electrons to be hot enough to ionize neutrals has interesting implications for DCX-1 and

[2] M. D. Kruskal and C. R. Oberman, *Phys. Fluids* 1, 275 (1958).

[3] B. A. Trubnikov, *Phys. Fluids* 5, 184 (1962).

[4] See O. Buneman's article in *Radiation and Waves in Plasmas*, M. Mitchener, ed., Stanford University Press, 1961.

[5] *Thermonuclear Div. Progr. Rept. Oct. 31, 1961*, ORNL-3239, p 18.

calutrons. In neither case does it seem possible for sufficiently high electron temperatures to be achieved merely by collisions with the fast ion beams. Presumably, collective phenomena, possibly associated with previously observed rf noise, is responsible. A high electron temperature is consistent with plasma potential measurements in DCX-1.[6]

6.3 ION DENSITY VS INJECTION CURRENT IN DCX-2

T. K. Fowler Mozelle Rankin

The "*S*-curve" relation between DCX-2 molecular ion injection current and the trapped atomic ion density achieved has been recalculated, still along the lines of the work of Simon,[7] but with charge-exchange and ionization cross sections properly averaged over ion and electron energy distributions. It had been feared that, because of the rapid increase in the charge-exchange cross section with decreasing ion energy, energy loss from ions to cold electrons would markedly increase the upper critical current, I_{UC}, required to reach burnout in OGRA-type operation. However, as can be seen from the new result, taking ion energy losses into account (Fig. 6.1), I_{UC} is little affected. This can probably be attributed to a somewhat smaller energy transfer rate to the actual electron distribution than to a Maxwellian and to the fact that electrons are heated sufficiently to help ionize neutrals. Sample ion and electron distributions near burnout are given in Fig. 6.2.

The principal consequence of the refinements in the calculation of the *S* curve is that the lower critical current I_{LC} marking the lower bend in the *S* curve now almost coincides with I_{UC}. Thus initial, supplemental dissociation of molecular ions by an arc, useful only between I_{UC} and I_{LC} to provide a better "initial condition" once the arc is turned off, would seem to be of limited importance.

The energy distributions are obtained from the code, discussed previously,[8] which solves coupled Fokker-Planck equations for ions and electrons.

[6] *Ibid.*, pp 6–8.

[7] A. Simon, *J. Nuclear Energy: Part C, Plasma Physics* 3, 235 (1961).

[8] T. K. Fowler and M. Rankin, submitted to the *Journal of Nuclear Energy: Part C, Plasma Physics*, also, *Energy Distribution of Ions and Electrons in DCX After Burnout: ORACLE Code EDDIE*, ORNL-3161 (Aug. 29, 1961).

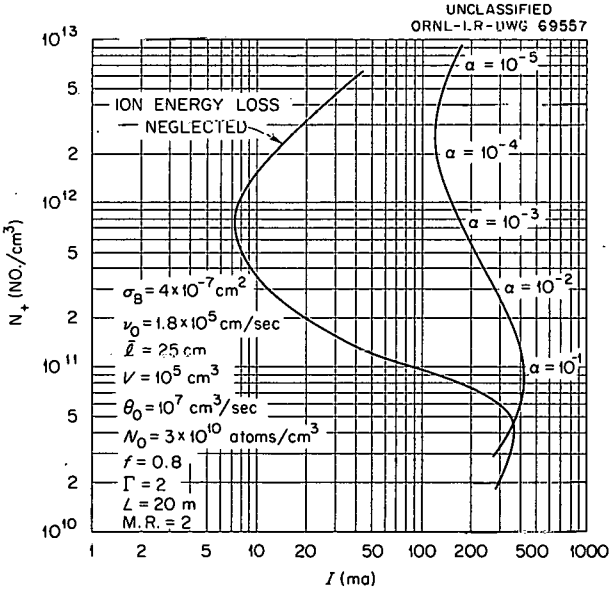

Fig. 6.1. DCX-2 Performance Curve Relating Trapped Ion Density N_+ to Molecular Ion Injection Current *I*. A curve neglecting ion energy loss is given for comparison.

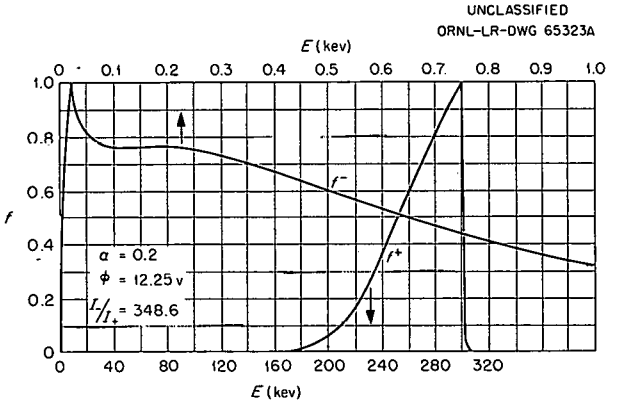

Fig. 6.2. Ion and Electron Energy Distributions in the Vicinity of the Critical Injection Current, $\alpha = 0.1$. Normalization is arbitrary. Upper energy scale is for electrons and lower is for ions.

Both equations contain loss terms and monoenergetic source terms, representing the injection of hot ions and the release of cold electrons in the ionization of neutrals. The ion-loss term includes loss by charge exchange with neutrals. Both ion- and electron-loss terms include scattering out of mirrors. We take an energy-dependent effective mirror ratio that depends on the average electrostatic potential drop through the plasma. This potential drop is a consequence of difference in rates of ion and electron escape when ion-scattering losses begin to dominate. The potential drop is determined along with the energy distributions. At present, the scattering-loss terms have the form $PE^{-3/2}$, where P, always <1, contains the effective mirror ratio. The loss term is being revised as suggested by Rosenbluth *et al.*[9]

6.4 CROSSED-STREAM INSTABILITY

E. G. Harris[10]

The following is the abstract of a paper that has been sent for publication in the *Bulletin of the American Physical Society*.

We consider a beam of energetic ions moving perpendicular to a magnetic field through a background plasma. We show that an instability exists which is similar to the familiar two-stream instability. It differs from it in that the electron motion is essentially parallel to the magnetic field and, hence, perpendicular to the direction of ion streaming. When the ion paths close on themselves and the electrons are cold, we recover previous results.[11] Our present work includes the effect of electron temperature. A nonzero electron temperature increases the instability.

6.5 ELECTRON CAPTURE IN FAST COLLISIONS

6.5.1 Capture by Fast Protons from Positive Ions

M. R. C. McDowell[12]

The following is the abstract of a paper that has been submitted for publication in the *Proceedings of the Royal Society of London* (Section A).

The formal theory of scattering is employed in order to derive an expression for the matrix element for electron capture by positive ions from positive ions. The first-order solution (Coulomb-Born approximation) is examined in detail for capture to the ground state of ions of charge Z_2, mass M_2 from the ground state of hydrogen-like positive ions of charge Z_1, mass M_1. It is shown that, except at very low impact energies, this approximation reduces to the well-known Brinkmann-Kramers result. Cross sections for proton impact on ions of some representative light elements are tabulated.

6.6 DCX-1 POTENTIAL-DISTRIBUTION CODE

Mozelle Rankin

An IBM 7090 code for solving Poisson's equation in cylindrical coordinates was written and is being used in collaboration with G. R. Haste's experimental studies of plasma potential. The code now uses a toroidal charge of uniform density; however, the density may be given as any function of r and z. Boundary values of the potential Φ on the radial surface and ends are left free as input parameters.

Poisson's equation,

$$\frac{\partial^2\Phi}{\partial z^2}+\frac{\partial^2\Phi}{\partial r^2}+\frac{1}{r}\frac{\partial\Phi}{\partial r}=-\rho(r,z)\,, \qquad (1)$$

is written as the difference equation:

$$\frac{\dfrac{\Phi_{i,j+1}-\Phi_{i,j}}{(k_{j+1}-k_j)}-\dfrac{\Phi_{i,j}-\Phi_{i,j-1}}{k_j-k_{j-1}}}{\tfrac{1}{2}(k_{j+1}-k_{j-1})} + \frac{\dfrac{\Phi_{i+1,j}-\Phi_{i,j}}{h_{i+1}-h_i}-\dfrac{\Phi_{i,j}-\Phi_{i-1,j}}{h_i-h_{i-1}}}{\tfrac{1}{2}(h_{i+1}-h_{i-1})} + \frac{1}{h_i}\frac{(\Phi_{i+1,j}-\Phi_{i-1,j})}{(h_{i+1}-h_{i-1})}=-\rho_{i,j}\,, \qquad (2)$$

---

[9] See G. Bing and J. E. Roberts, *Phys. Fluids* 4, 1039 (1961).

[10] Consultant, University of Tennessee.

[11] P. Burt and E. G. Harris, *Phys. Fluids* 4, 1412 (1961).

[12] Consultant from Royal Holloway College, University College of London, London, England.

where k_j ($j = 1, \ldots n$) and h_i ($i = 1, \ldots m$) are the selected grid points in the z and r directions, respectively. Unequal spacing of grid points is allowed and, in fact, is usually necessary in order that the arbitrary boundary of the charge density and the grid lines coincide.

With the boundary values of Φ and the additional conditions $\left.\frac{\partial\Phi}{\partial z}\right|_{z=0} = 0$ and $\left.\frac{\partial\Phi}{\partial r}\right|_{r=0} = 0$, Eq. (2) specifies a system of $n \times m$ linear equations in $n \times m$ unknowns. From a practical viewpoint, a grid sufficiently fine to obtain reliable solutions could not often be found in a machine with 32,000 storage capacity if the entire $(n \times m)^2$ matrix had to be stored. Fortunately, each equation contains only five unknowns, and we have a band matrix of width $(2n + 1)$. A SHARE subroutine, Le4F, has been used to solve this band matrix equation. With grids of 23 × 24 ($r \times z$) points, solutions which appear to be independent of the grid choice have been found.

In all cases thus far, Φ has been set at zero all along the boundary, and ρ has been set equal to 10^7 particles/cm^3. (The potential scales linearly with ρ.) Cases have been run with both the charge dimensions and the liner dimensions as parameters. Typical results are shown in Figs. 6.3 and 6.4.

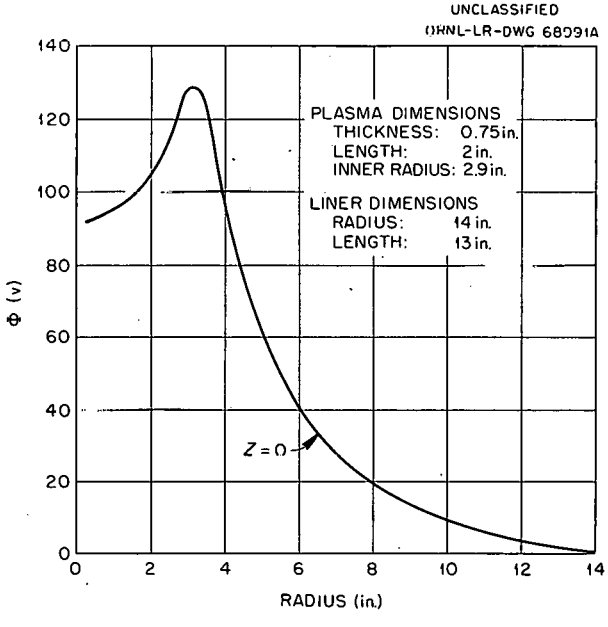

Fig. 6.3. Radial Variation of Potential.

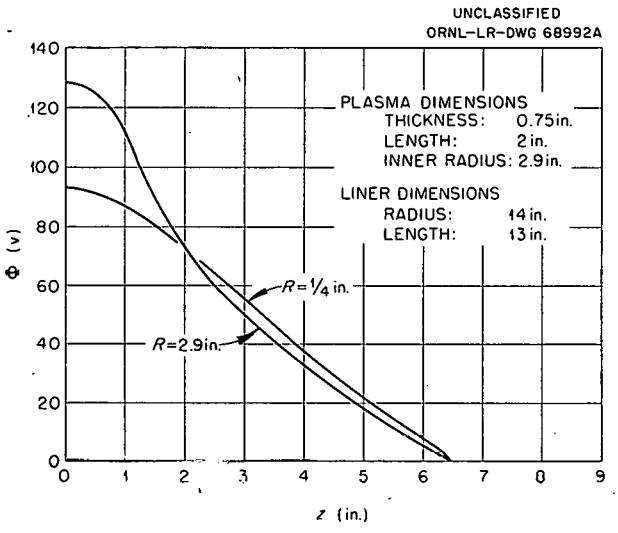

Fig. 6.4. Axial Variation of Potential.

6.7 CODE FOR STUDYING STABILITY OF PLASMA COLUMNS IN A MAGNETIC FIELD

Y. Shima R. G. Alsmiller[13]

A method for investigating the stability of inhomogeneous plasmas has been developed[14] which consists of reducing the Vlasov equation to an integral equation of the form

$$\rho(\vec{x}) = \int K(\vec{x}, \vec{x}\,''; p)\, \rho(\vec{x}\,'')\, d\vec{x}\,'' ,$$

where ρ is the charge-density perturbation.

The kernel $K(\vec{x}, \vec{x}\,''; p)$ contains the distribution function f_0 describing the equilibrium plasma and depends also on a parameter p arising from the Laplace transform in time. The condition for instability is that solutions to the above equation exist for parameters p whose real part is positive.

The distribution function f_0 can be written as a function of the constants of motion in equilibrium. For plasmas in a uniform magnetic field, a considerable simplification occurs if f_0 depends only on the following three constants:

$$v_\perp, v_z, p_\theta = rv_\perp \sin(\phi - \theta) + \tfrac{1}{2}r^2\omega .$$

[13] Neutron Physics Division.

[14] T. K. Fowler, *Plasma Stability Analysis Employing Equilibrium Constants of Motion*, ORNL-3123. (1961).

The constant magnetic field is in the z-direction, and $r, \theta,$ and $v_\perp, \phi$ are the polar coordinates in the $x, y,$ and v_x, v_y planes, respectively. The cyclotron frequency is denoted by ω. Such distributions have r dependence but no dependence on z and θ. Then eigenfunctions of K_p have as z and θ dependence just $e^{ik_z z} e^{il\theta}$, and the integral equation can be reduced to the following one-dimensional equation:

$$\rho(r) = \int_0^\infty K(r, r''; p; k_z, l)\, \rho(r'') r'' dr'' .$$

The evaluation of the kernel K involves four quadratures and is in general very difficult. It can be written in the form:

$$K_p = \Sigma \int d\vec{v} \int_{-\infty}^{0} dt\, e^{(p - il\omega + ik_z v_z)t}$$

$$\times \{F\}\, I_l(k_z r', k_z r'') \left[\frac{x - y e^{i(\omega t - \psi)}}{r'}\right]^l (-i)^l e^{il\phi} ,$$

$$d\vec{v} = v_\perp\, dv_\perp\, d\phi\, dv_z ,$$

$$\{F\} = il \frac{\partial f_0}{\partial p_\theta} - \frac{p + ik_z v_z}{v_\perp} \frac{\partial f_0}{\partial v_\perp} + ik_z \frac{\partial f_0}{\partial v_z} ,$$

$$x = -\frac{v_\perp}{\omega},$$

$$y = \sqrt{x^2 + r^2 - 2xr \sin\phi}$$

$$\cos\psi = \frac{x - r\sin\phi}{y}$$

$$\sin\psi = \frac{r\cos\phi}{y}$$

$$r' = \sqrt{x^2 + y^2 - 2xy\cos(\omega t - \psi)}$$

$$I_l(k_z r, k_z r'') = \begin{cases} K_l(k_z r) I_l(k_z r'') , & r > r'' , \\ K_l(k_z r'') I_l(k_z r) , & r'' > r , \end{cases}$$

where $K_l(x)$ and $I_l(x)$ are the usual modified Bessel functions. The summation is over the two species of the plasma.

A code was written for the IBM 7090 computer that calculates the kernel K and then finds the eigenvalues p of the integral equation above.[15] As a particular example distribution, we consider:

$$f_0 \propto e^{-ap\theta - bv_\perp^2 - \frac{v_z^2}{\sigma}} .$$

The corresponding charge density is $\propto e^{-\alpha r^2}$ where $\alpha = (a\omega/2)(1 - a/2b)$.

6.8 CALCULATION OF ELECTRON TRAJECTORIES IN THE DOUBLE-FOLDED-CUSP "ELMO"

Mozelle Rankin R. J. Kerr

A calculation of electron trajectories in the double-folded-cusp magnetic field (Fig. 6.5) is being made. The purpose is to delineate the adiabatic and nonadiabatic regions of this field and to study the effects of the impressed radio-frequency electromagnetic field on the particle transit times. Solid lines in Fig. 6.5 are field lines, and dotted lines are field-strength contours. The line at 850 gauss is the resonance surface for the present "Elmo" radio-frequency heating field of 2.4 kMc. Therefore, an electron must spend some time in this region in order to be greatly affected by the oscillating field.

Figure 6.6 is an R, Z plot of a portion of the trajectory of particle No. 1, whose initial conditions of motion are given by Table 6.1. Though only two reflections are shown, this particle has been followed through five reflections thus far, with no apparent increase in energy parallel to the field lines. The integration step is necessarily of the order of 0.01 nanosecond, and thus orbits cannot be followed for a very long time. The maximum cyclotron radius for this particle is 4.6 mm, and the minimum radius of curvature for the field line it is on is about 4.5 cm. Therefore, the particle and field interaction is expected to be adiabiatic, according to a criterion due to H. Grad.[16]

Particle No. 2, whose initial conditions appear in Table 6.1, is shown by Fig. 6.7. This particle is scattered by the field, is reflected twice, and

[15] Written by R. Edwards of the Central Data Processing Group of ORGDP.

[16] H. Grad, *Containment in Cusped Plasma Systems*, NYO-9496 (Mar. 30, 1961).

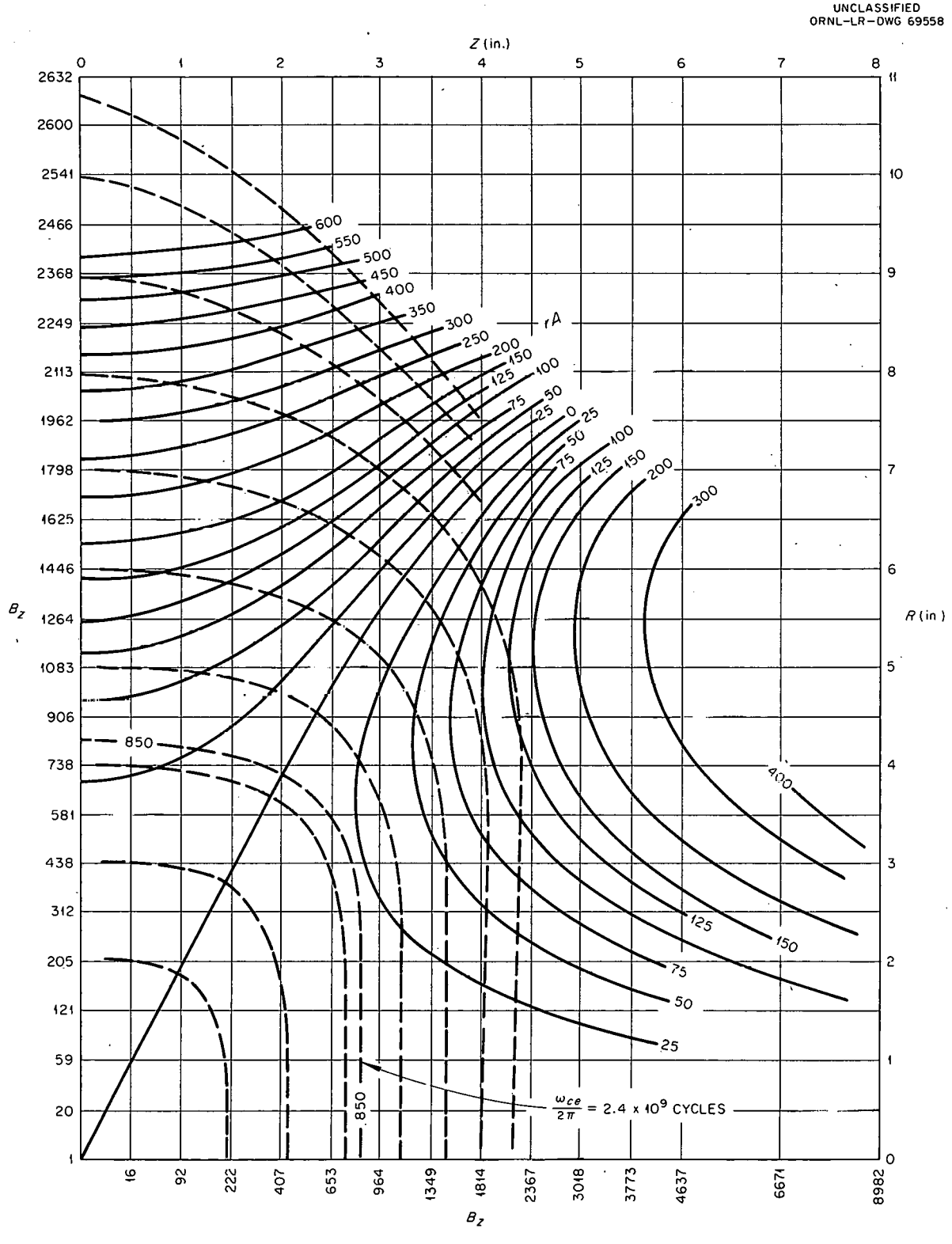

Fig. 6.5. Double-Folded Cusp in Elmo, Showing Field Lines (Solid) and Field-Strength Contours (Dotted).

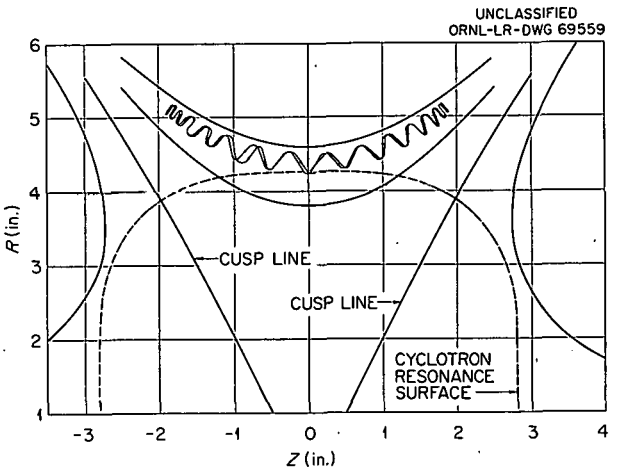

Fig. 6.6. Particle Orbits in the "Elmo" Cusp. Particle 1.

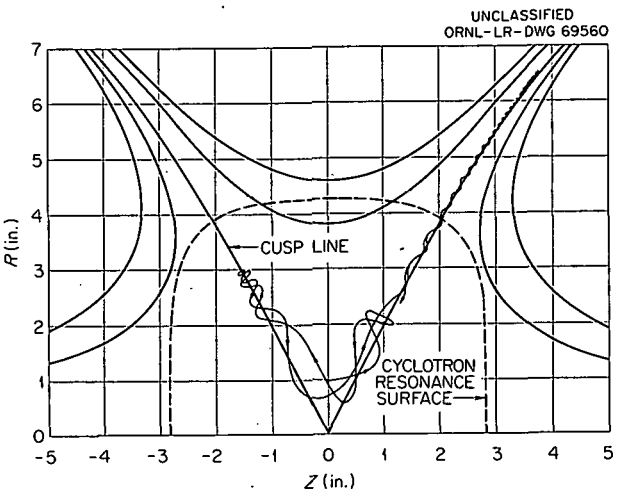

Fig. 6.7. Particle Orbits in the "Elmo" Cusp. Particle 2.

Table 6.1. Initial Conditions of Motion of Particles in Elmo Field

$E/r = 1\ \nu/\text{cm}$

Resonance frequency = 2.4×10^9 cps

No.	R (in.)	θ (radians)	Z (in.)	$\dot{R}$ (in./νsec)	$\dot{\theta}$ (radians/νsec)	$\dot{Z}$ (in./νsec)	E (kev)	Time (sec)
1	4.25	0	0	0	0.476	1.17	10	30
2	1	0.5	0	0	0.476	1.17	2.8	20

then appears to be escaping along a cusp line, but is finally reflected again near R = 3.5 in., Z = 3.8 in., and returns toward field center. Further studies on this particle will be made. No effect of the radio-frequency field is discernable on these two particles, since they are near the resonance zones for an extremely short time.

These orbit calculations were made with IBM 7090 computer code TILDA,[17] modified to include electric field forces in the equations of motion. The use of this code is limited to circles of convergence which exclude any coil of the system; hence, it is not suited for calculations near the cusp lines between coils. At present, provisions are being made in the code for other less restrictive though perhaps slower methods of magnetic field calculation. When this has been completed, other particles will be studied in order to determine the effect of initial conditions of position and velocity on particle-field interaction.

[17] G. R. North and C. E. Parker, *Thermonuclear Div. Progr. Rept. Oct. 31, 1961*, ORNL-3239, pp 77–78.

7. Magnetics

7.1 AUXILIARY CURVES FOR RAPID DESIGN OF MAGNET COILS

C. E. Parker J. E. Simpkins

The following short report is based on well-known properties of magnet coils. It seems, however, that practical design work – especially when approximate parameters are needed quickly – can be somewhat simplified by the use of the normalized curves described below.

The attached graph (Fig. 7.1) can be used to easily find the maximum field strength in the center of a magnet coil having a rectangular cross section and a homogeneous current density, when the following data are known: (1) inside radius, a_1, in centimeters; (2) wire length, l, in centimeters; (3) turn density, n, in turns per square centimeter; and (4) when different values are assumed for α, the ratio of outside to inside diameter.

These curves are based on the following relations:[1] For any assumed α, the ratio of coil length $2b$ to coil inside diameter $2a_1$ is:

$$\beta = \frac{l}{2\pi n a_1^3(\alpha^2 - 1)} = \frac{K_1}{\alpha^2 - 1}, \tag{1}$$

with

$$K_1 = \frac{l}{2\pi n a_1^3}. \tag{2}$$

Then the flux density at the coil center is:

$$B_c = \frac{2\pi}{5} nla_1\beta \ln\frac{\alpha + \sqrt{\alpha^2 + \beta^2}}{1 + \sqrt{1 + \beta^2}},$$

or,

$$B_c = K_2\beta \ln\frac{\alpha + \sqrt{\alpha^2 + \beta^2}}{1 + \sqrt{1 + \beta^2}}, \tag{3}$$

with

$$K_2 = \frac{2\pi}{5} nla_1. \tag{4}$$

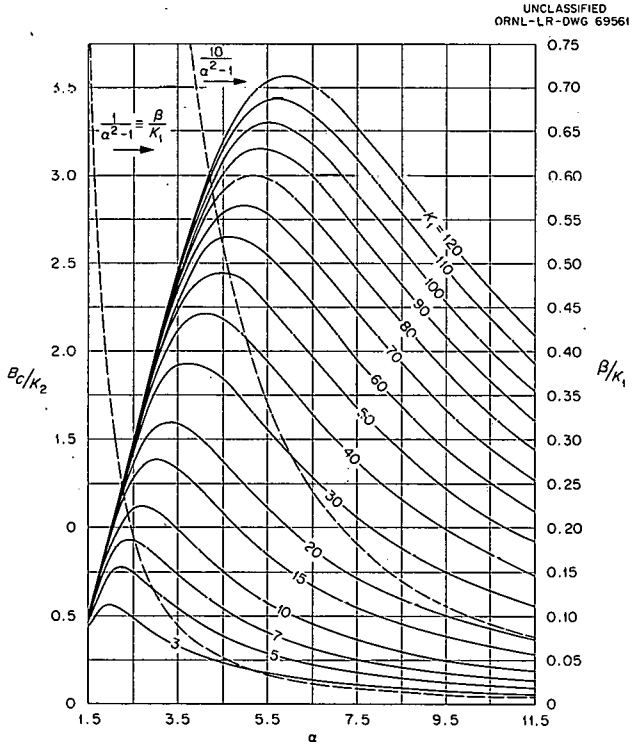

Fig. 7.1. Normalized Curves for Finding Coil Parameters.

[1] W. F. Gauster and C. E. Parker, "Some Concepts for the Design of Superconducting Solenoids," pp 3–13 in *Proceedings of the International Conference on High Magnetic Fields, Cambridge, Mass., Nov. 1–4, 1961*, MIT Press and Wiley, New York, 1962.

The family of curves shows the dependence of B_c/K_2 on α for different values of K_1. Optimum values of B_c/K_2 can be seen. Under certain conditions it is advisable to use nonoptimum values of α in order to satisfy special conditions, for instance, to restrict the outside radius of a superconducting coil because of limitations of the Dewar dimensions. By means of these curves, the variation of B_c for different parameter values can be judged easily.

The value of B_M (maximum flux density, occurring in the coil midplane at a distance a_1) can be found by:

$$B_M = kB_c \,. \tag{5}$$

This flux density is necessary for finding the "quenching characteristic" of a superconducting coil. The parameter k is a function of α and β, and a useful graph of k is shown elsewhere.[2]

On the graph, the two dotted lines show the functions $1/(\alpha^2 - 1)$ and $10/(\alpha^2 - 1)$, respectively, which permit the calculation of β by multiplying by K_1, and $K_1/10$, respectively.

The auxiliary curves are useful for the design of conventional and superconducting magnet coils, as shown in examples 1 and 2.

Example 1. – To calculate a water-cooled coil with $a_1 = 3.75$ in. (9.53 cm), powered by a 9860-amp, 679-v motor-generator set, using a hollow tubular copper conductor 0.565 in. square and having a 0.3-in.-diam hole:

For proper resistance to match the power supply, the conductor length must be 1800 ft (5.5×10^4 cm). Allowing for insulation, the turn density n is 0.436 turn/cm^2.

$$K_1 = \frac{5.5 \times 10^4}{2\pi(0.436)\,(9.53)^3} = 23.2 \,,$$

and

$$K_2 = 4\pi(0.436)\,(9860)\,(9.53) = 5.15 \times 10^4 \,.$$

From the solid curves, the greatest field obtainable is $B_c/K_2 = 1.7$, occurring at $\alpha = 3.48$. From this α, the lower dotted curve gives $\beta/K_1 = 0.091$. Thus the ideal characteristics of the coil are:

$\alpha = 3.48$,
$\beta = 0.091(23.2) = 2.11$,
$B_c = 1.7(5.15 \times 10^4) = 87{,}500$ gauss.

The actual coil would be somewhat different, due to the fact that the dimensions of the coil cross section cannot be varied smoothly, but only in steps corresponding to integral numbers of turns. Another condition for water-cooled coils is the necessity for using appropriate numbers of parallel water paths.

Example 2. – For a superconducting coil, you are given the following parameters: $a_1 = 2$ cm; $n = 800$ turns/cm^2; $l = 3 \times 10^5$ cm; $I = 15$ amp. The problem is to find the maximum allowable field. This can be done as follows:

$$K_1 = \frac{3 \times 10^5}{2\pi \times 800 \times 8} = 7.46 \,,$$

$$K_2 = \frac{2\pi}{5}\, 800 \times 15 \times 2 = 3.02 \times 10^4 \,,$$

$$\alpha_{opt} = 2.4 \,, \qquad \beta_{opt} = \frac{7.46}{[(2.42)^2 - 1]} = 1.57 \,,$$

$$B_{c\ opt} = 3.02 \times 10^4 \times 0.95 = 28{,}700 \text{ gauss} \,,$$

$$a_{opt} = 4.8 \text{ cm} \,, \qquad b = 3.14 \text{ cm} \,,$$

$$K = 1.07 \,, \qquad B_M = 30{,}700 \text{ gauss} \,.$$

If α is assumed to be 2.0 ($a_2 = 4$ cm), then

$$\beta = \frac{7.46}{2^2 - 1} = 2.49 \,,$$

$$b = 4.97 \text{ cm} \,,$$

$$B_c = 3.02 \times 10^4 \times 0.85 = 25{,}700 \text{ gauss} \,,$$

$$K = 1.021 \,.$$

It should be well understood that the optimum flux density at the coil center is calculated for an assumed value of I. If a "short-sample experiment" would be decisive for the actual coil performance, then Eq. (5) and the short-sample quenching characteristic together would be sufficient to determine the value of the critical coil current I_c.

[2] R. W. Boom and R. S. Livingston, "Superconducting Solenoids," to be published in the *Proceedings of the Institute of Radio Engineers*.

7.2 RECENT DEVELOPMENTAL WORK ON DIRECT-CURRENT MAGNET COILS

R. L. Brown J. N. Luton, Jr.

7.2.1 An 80-kilogauss Magnet Facility

A design of magnet coils consisting of "pancakes" with multiple water paths (described previously)[3] has been extensively used in this laboratory. It seems, however, to be desirable to improve the reliability of these solenoids; therefore, carefully planned engineering tests will be made with a new 80-kilogauss magnet facility which can be easily adapted to this purpose.

This facility consists of a two-coil vertical-axis magnet about 22 in. long, with a 7-in. bore and a 24-in. outer diameter. The axial gap between the coils may be varied, giving with 6.8 Mw a central field of 86 kilogauss at zero gap to 78 kilogauss with a spacing of 1.3 in. With a gap of 0.6 in., the homogeneity of the field (82.5 kilogauss) is good – at a distance of 2 in. from the center the field strength decreases by 0.1% in the midplane and by 0.2% on the axis. Sight ports can be provided at any desired locations around the gap-spacer plate. Current and cooling water are being supplied through the floor, leaving the top platform and all sides free for easy access and auxiliary apparatus. This magnet will be a flexible device for research in superconductivity and for other experimental work.

Initially the 80-kilogauss coil assembly will be used for engineering studies aimed at obtaining reliable data for designs for water-cooled coils. Besides mechanical and electrical routine tests, the following unique test procedure can be carried out here: Since the two coils exert an axial force of 250 tons on the gap spacer, and since there is a strong magnetic field at this place, there is an exceptionally good opportunity to simultaneously expose any new type of pancake coil to mechanical forces and magnetic fields. Furthermore, such a test can be made with current and water flow through the test coils. These test conditions are far superior to stressing a nonenergized pancake coil in a hydraulic press. Some goals of these tests will be: (1) to develop more reliable "crossovers" (connections between the two halves of a pancake); (2) to investigate the elastic and nonelastic deformation of pancake coils under stress and therewith the performance of the electrical insulation material; finally, (3) to judge the merits of "breathing" coils vs rigidly potted coils.

Special care was taken to ensure reliability of the coil assembly. The conductors were machined at the crossovers in an effort to eliminate shearing action on the insulation, and all interior joints were eliminated. The conductors were completely wrapped with Dacron-Fiberglas "stage B" polyester impregnated tape, and in addition a Mylar–fish paper sandwich was inserted between all adjacent conductors. The individual pancakes were vacuum impregnated and baked, but they were not rigidly joined together. If a fault occurs in one pancake, the entire coil will not be lost, since the damaged pancake may be easily replaced. The outer surface of the coils will be covered with a strippable cocooning material in order to prevent the entrance of foreign particles, which might cause shorts.

7.2.2 Flexible-Cable Solenoid

For a neutral-beam experiment[4] a magnetic field is required with a shape that can be produced only by a coil that has nonuniform current density (partially negative). Cost and time estimates based on the use of pancakes of hollow copper tubing showed that a conventional solution was not feasible in this case. Therefore a method for a fast and relatively cheap construction of magnet coils was required. Accordingly, tests were made with a conductor consisting of a bare, stranded welding cable inside a water hose, which not only contains the cooling water but also provides electrical insulation. When this conductor is bent, its cross section changes from circular to elliptical, but water flow is still maintained. Radial forces can be held by banded slats at the outer surface of the coil. With this kind of flexible cable a coil was designed which provides the desired field shape mentioned above. The coil cross section and axial field shape are shown in Fig. 7.2.

[3] *Thermonuclear Project Semiann. Progr. Rept. July 31, 1960*, ORNL-3011, p 23.

[4] This report, sec 5.4.

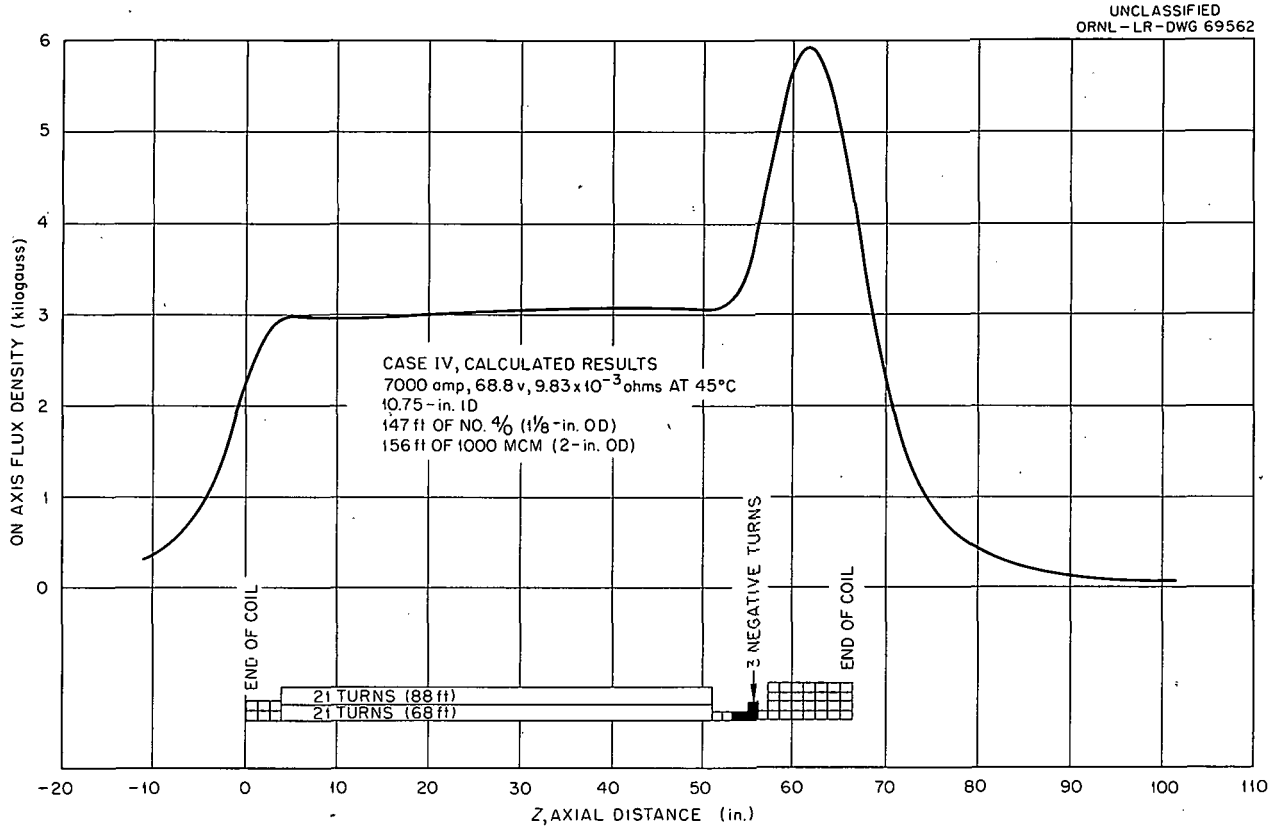

Fig. 7.2. Cable Coil for Neutral-Beam Experiment.

The construction described above has severe limitations compared with the construction of conventional coils – neither a high current density nor a good packing factor is obtainable. If only fields below about 6 kilogauss are required, and if inefficient use of power can be tolerated, however, this design offers several advantages. Both the water hose and the welding cable are standard items, quickly available in many sizes. This, combined with the fact that a very flexible conductor is easy to work with, means that such a coil can be provided in a much shorter time than a conventional one. Further, the conductor can be easily wound into coils that have nonuniform current densities and irregular cross sections, and, finally, the flexible cable can be salvaged and reused.

7.3 CALCULATION OF AXIAL FORCES IN MAGNETIC COIL SYSTEMS

J. N. Luton, Jr. P. A. Thompson

The method for calculating the axial electromagnetic forces between a pair of rotationally symmetrical coaxial coils previously discussed[5] has since then been subjected to extended computer studies. The essence of this approximate method is the replacement of one of the coils by a certain number of discrete loops, each carrying a current such that NI remains the same as for

[5]P. A. Thompson, *Thermonuclear Semiann. Progr. Rept. Jan. 31, 1961*, ORNL-3104, p 113.

the original coil, then summing $I \times B$ forces on the loops, the radial component of B from the other coil at the position of each loop being obtained in any convenient manner. As a consequence of the rotational symmetry of the system, the problem reduces itself to one of determining the shape and size of the areas in the coil cross section to be replaced by the loops.

Order-of-magnitude results or better can be obtained in almost all cases by simply replacing one of the coils by a single loop located at the centroid of its cross section. The studies carried out on the IBM 7090 computer indicate that rapid convergence to the proper force is obtained when the replacement area is as nearly square as possible and that very good accuracy always results when the dimension of these squares is less than a tenth of the inside radius of the coil in question. The value of the proper force was recently verified[6] by the completely independent method involving the derivative of mutual inductance, which is being included in Garrett's comprehensive magnetic field code based on zonal harmonics.[7]

Following these studies, the IBM 7090 codes were modified for practical application, calculating B_r of the second coil according to an early version of the zonal harmonics code if the coil separation were sufficient,[7] otherwise by the elliptical integral code.[8] Subsequently, this force code was used for Elmo and the Zero Gradient Facility, both of which contain a sufficiently small number of coils that the resultant forces were obtained by desk-calculator summation. However, when an investigation of forces in the Long Solenoid (which consists of 17 coils) was requested, it became obvious that a computer summation was needed.

Using this force code, the forces F^*_{ij} between every pair of coils of the Long Solenoid were calculated for an arbitrary current I_0. The axial force between coils i and j for any current I_i and I_j then is given by

$$F_{ij} = I^*_i \, I^*_j \, F^*_{ij}, \qquad (1)$$

where $I^*_i = I_i/I_0$, and $I^*_j = I_j/I_0$.

If a plane between two coils is considered to divide the coil system into two sections, then the force which must be held by the structural members cut by this plane is just the total magnetic force between the two sections, being the sum of the individual forces between each coil of one section and every coil of the other. Thus, the force across the gap between coils m and $m + 1$ is:

$$f_{m,\,m+1} = \sum_{j=1}^{m} \left(\sum_{j=m+1}^{N} I^*_i \, I^*_j \, F^*_{ij} \right), \qquad (2)$$

where the coils in the system are consecutively labeled 1 through N. Attractive forces result when the I^*'s are of the same sign (i.e., currents are in the same direction), and repulsive forces when they are of opposite sign. Positive values of $f_{m,\,m+1}$ then indicate net compression of the gap structural members and negative values tension.

A computer code was written to evaluate Eq. (2) and, in addition, since most of the coils of the Long Solenoid are identical, to calculate the complete F^*_{ij} matrix from the minimum number of different values. The code was then employed to calculate all the gap forces for the original system as designed[9] and for many possible cases in which currents in some coils are reversed. These latter cases were requested in order to study the feasibility for certain arc experiments of producing a magnetic field which reverses its axial direction. As a safeguard, since the Long Solenoid does not include mechanical members for restraining large, expansive axial forces, the main restriction on possible solutions was that any repulsive forces between coils be small. A summary[10] of the cases considered and the results obtained are given in Table 7.1 and Fig. 7.3, respectively.

---

[6] Private communication from M. W. Garrett.

[7] M. W. Garrett, *Computer Program Using Zonal Harmonics*, to appear as an ORNL report.

[8] M. Rankin, *Thermonuclear Project Semiann. Rept. Jan. 31, 1959*, ORNL-2693, p 11. Incidentally, these studies indicate that the same rule-of-thumb of loops replacing squares no larger than a tenth the inside radius is applicable to the elliptical integral code.

[9] J. N. Luton, Jr., *Long Solenoid Technical Memo No. 1*, p 7 (July 7, 1960).

[10] For details, see *Long Solenoid Technical Memo No. 3*, (Feb. 26, 1962).

Table 7.1. Summary of Cases Considered

Case Number	Coil Connections			Positive Current (amp)	Reversed Current (amp)	B_{center} (kilogauss)	B_{max} (kilogauss)	Force in Critical Gap;[a] Negative Numbers Represent Tension (tons)	Distance from Field-Reversal Point to Center Line of Nearest Sight Port (in.)
	No. of Reversed Coils	No. of Buffer Coils	No. of Positive Coils						
A	3	0	14	4840	505	2.1	14	0	No field reversal
A_2	3	0	14	4840	2290	−2.0	14	−4.58	+3.1
C	1	0	16	4275	2630	4.3	12	0	No field reversal
C_2	1	0	16	4275	8050	−2.0	12	−8.38	−0.8
D	2	0	15	4550	980	2.9	13	0	No field reversal
D_2	2	0	15	4550	3550	−1.9	13		−3.0
E	2	0	10	7360	1390	4.8	19	0	No field reversal
F	1	0	10	7360	4160	7.5	20	0	No field reversal
G	1	0	8	9190[b]	4940	9.3	23	0	No field reversal
H	2	0	8	9190[b]	2625	4.1	23	0	No field reversal
I	3	0	8	9190[b]	750	4.2	28	0	No field reversal
J_2	2	4 (2 pairs)	11	6050	1758	−2.0	17	−0.29	+1.3
L_2	2	2	13	5190	2315	−2.06	15	−2.10	−0.7
L_5	2	2	13	4840[c]	3800	−5.0	14	−2.34	+1.9
Accidental	9	0	8	3000	3000	−8.1	7.6	−5.18	0.0

[a] Gap between the positive and negative sections of the solenoid.
[b] Generator overloaded 7%.
[c] Not matched to generator.

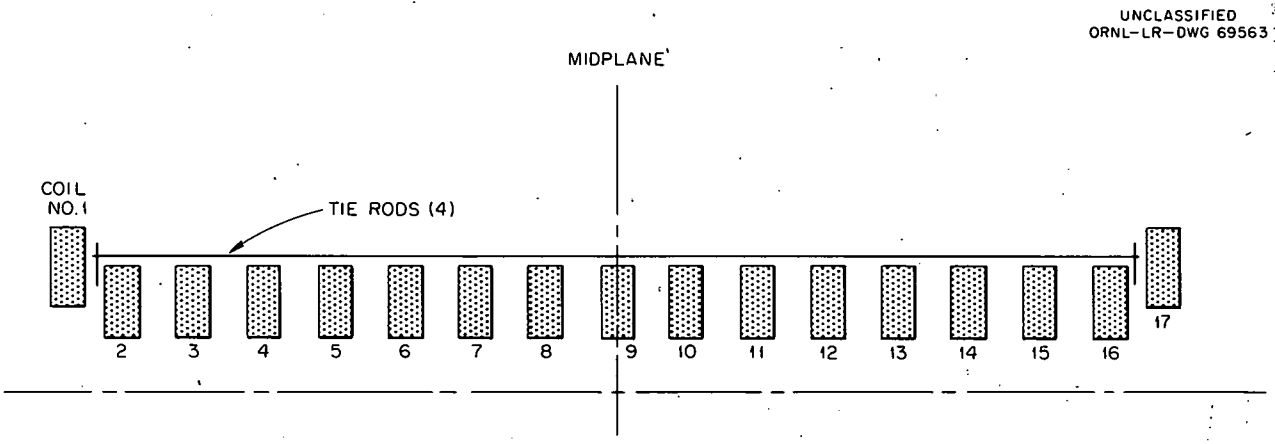

GAP NUMBER (TIE RODS)	I GAP AND STRUCTURAL FORCES (TONS)	GAP FORCES (TONS)	II STRUCTURAL FORCES (TONS)
	0		5.18
1-2	44.1	4.50	4.50
2-3	43.9	3.60	8.78
3-4	43.1	1.36	6.54
4-5	43	−5.18	0
5-6	43	1.32	6.50
6-7	43	3.42	8.60
7-8	43	4.21	9.40
8-9	43	4.50	9.68

Fig. 7.3. Long Solenoid Coil Outline with Gap and Structure Forces for Two Cases. I. Rated operation – all currents in same direction, 8570 amp. II. Coils 4 through 12 reversed, 3000 amp in all coils (case accidental). Note: Numbers for structural forces are based on the assumption that all forces are zero when the system is not energized. Present tie rods are rated at 8.25 tons, total.

8. Vacuum Systems, Techniques, and Material Studies

R. E. Clausing[1] R. A. Strehlow[2]
J. D. Redman[2] O. C. Yonts

8.1 METAL-FILM PUMPING

Data from the large-scale getter pump test[3] were obtained without the advantage to be derived from baking the deposition surfaces. The apparatus in its present modification includes a bakable inner liner and additional ion gages, as shown in Fig. 8.1. Ion gage G is used to determine the flux of particles n_g (as defined in ref 3) rebounding from the walls. Ion gage T is used to determine the total flux of particles n_t onto the wall. (The quantity n_t includes both gas molecules coming directly from the gas source and those rebounding from the inside wall of the liner.) These two flux measurements can be used by themselves or together with the measured gas admission rate to determine accurately the sticking fraction for selected gaseous species incident on the films previously deposited on the liner wall.

The new inner liner can be baked to 400°C or cooled to liquid-nitrogen temperatures. The liner can be separated from the outer vacuum by either a liquid-nitrogen-cooled baffle or a Zeolite-filled trap. The conductance of the trap or baffle is less than 100 liters/sec. During evaporation the pressure is commonly in the high 10^{-10} to middle 10^{-9} torr ranges, with the base pressure after film preparation only slightly lower (2×10^{-10} to 5×10^{-9} torr), depending upon the liner temperature, the nature of the film, and other factors. The size of the system, general characteristics, and performance are similar to those of the inner liner of DCX-1.

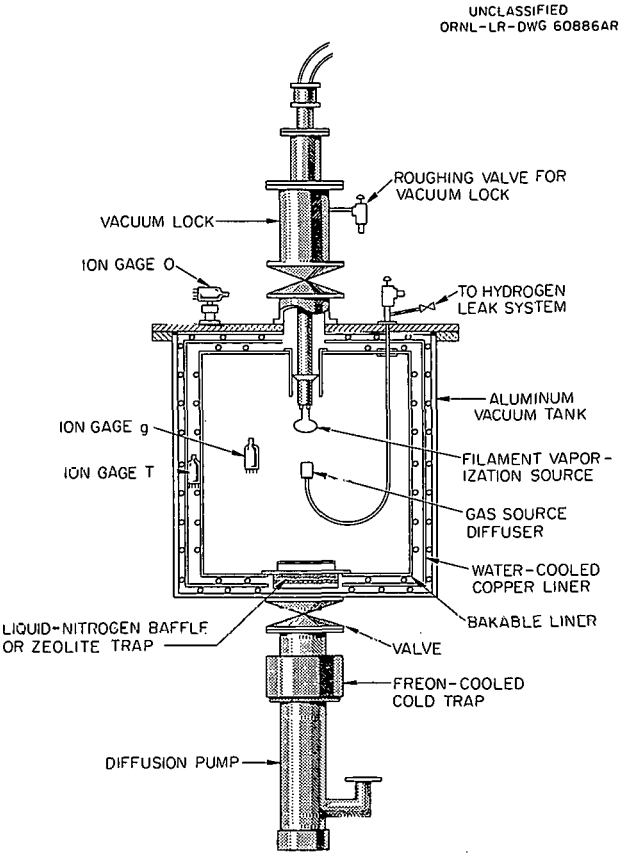

Fig. 8.1. Large-Scale Getter Pump Test with Bakable Liner.

Titanium films deposited on the baked inner liner in high vacuum (5×10^{-9} torr) while holding the liner at liquid-nitrogen temperature have considerably greater sorption rates for hydrogen than those deposited onto an unbaked surface at 5×10^{-8} torr. Figure 8.2 compares previous data

[1]Metals and Ceramics Division.

[2]Reactor Chemistry Division.

[3]C. E. Normand *et al., Thermonuclear Div. Progr. Rept. Oct. 31, 1961,* ORNL-3239, pp 85 *et seq.*

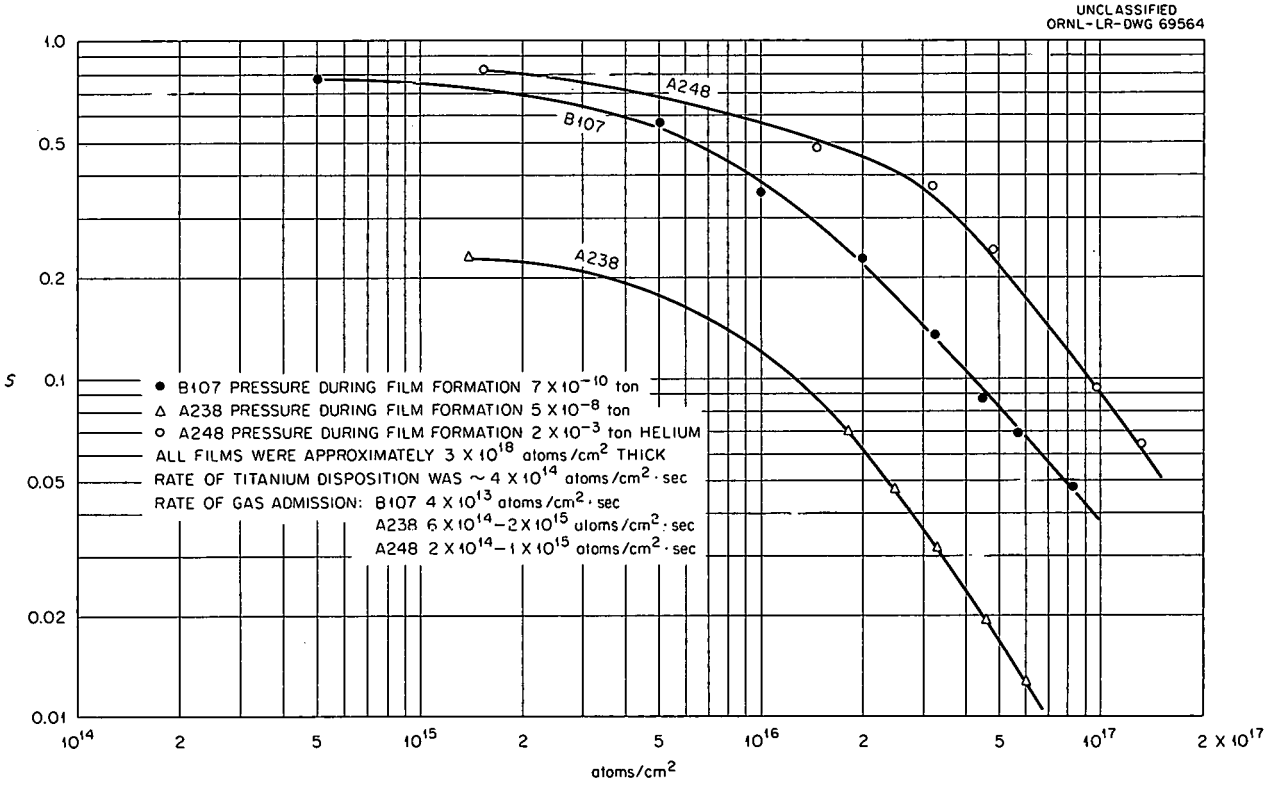

Fig. 8.2. Sorption of Hydrogen on Films Formed and Used at −195°C.

with data obtained under the present conditions. No explanation is offered for the improved results at this time.

The lower base pressures now attained permit measurements to be made with smaller gas-admission rates and allow careful measurement of the changes in the sticking fraction during the formation of the first layers of adsorbed gas. Preliminary analysis of the data indicates that the sticking fraction decreases only slightly until a monolayer of hydrogen is formed. The sorption rate for hydrogen on these deposits decreases linearly as increasing amounts of gas are adsorbed beyond about 5×10^{15} atoms/cm^2 when the deposit is at liquid-nitrogen temperature.

It appears that accurate values for the sticking fraction can be obtained from the equation

$$\alpha = \frac{n_t - n_g}{n_t}$$

[which is based on Eq. (4) in ref 3], where n_t and n_g are determined from ion gage measurements. The gages are calibrated against each other, and the difference $(n_t - n_g)$ is standardized by being set equal to n_a (calculated from the measured leak). Values of α may also be calculated satisfactorily from the formula used previously. The new method, however, compensates for changing ion-gage calibration and maintains the important advantage of providing increasing accuracy as α approaches unity.

A recheck of the data for the sorption of nitrogen onto titanium films formed during the measurement by continuous deposition onto a substrate at liquid-nitrogen temperature revealed that the limiting ratio of gas leak rate to titanium evaporation rate is 0.5 instead of 1.0 as reported previously.[3] Since the shape of the curve remains the same, the data given in Fig. 8.7, p 91 of ORNL-3239 can be corrected by multiplying the nitrogen-to-titanium ratio by 0.5.

The topography of vapor-deposited titanium films is shown in the electron-photomicrographs of Fig. 8.3. There appears to be a qualitative correlation

UNCLASSIFIED
PHOTO 57576

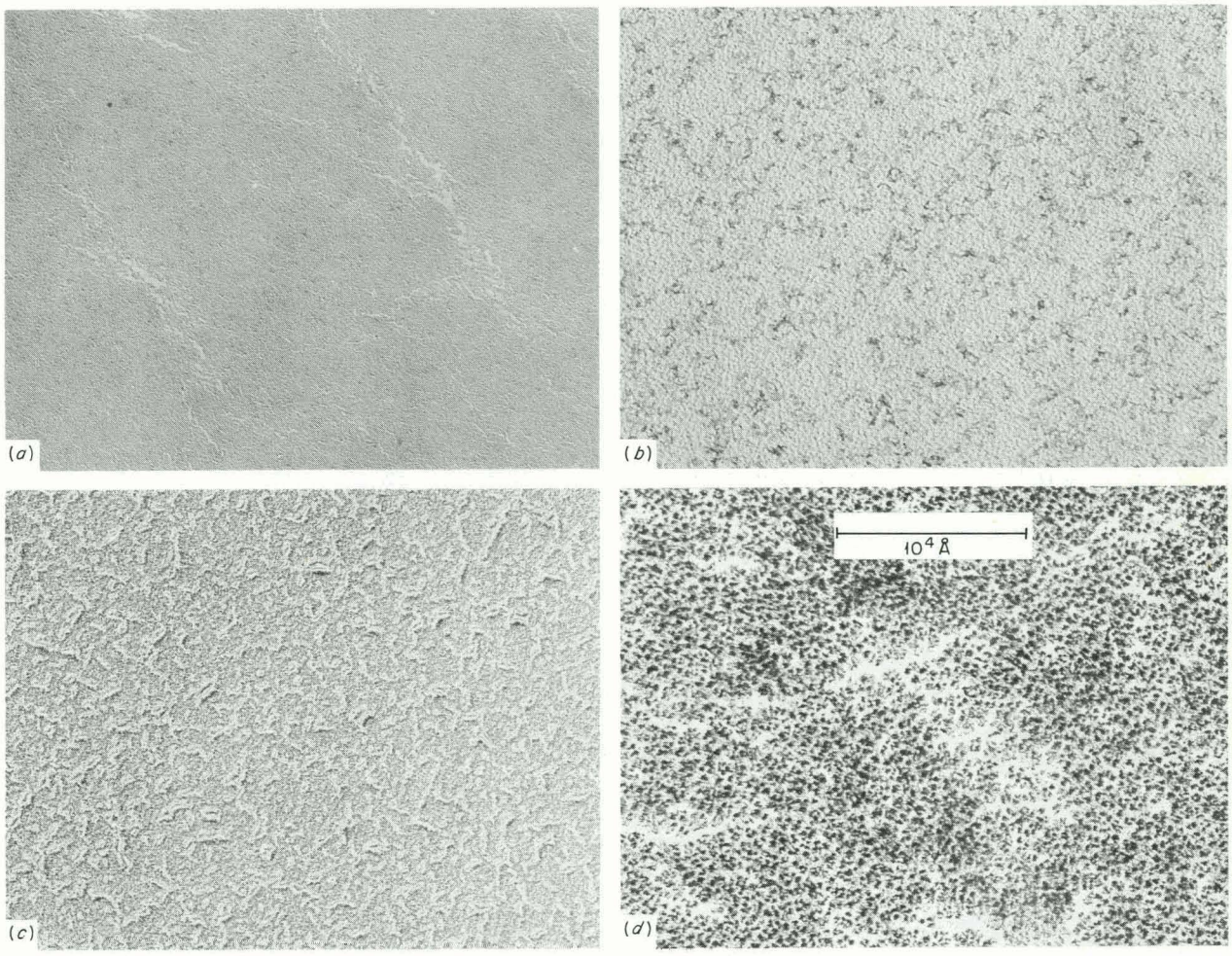

Fig. 8.3. Electron Photomicrographs Showing the Topography of Titanium Films Prepared at Various Temperatures and Pressures. (*a*) 10°C, 5×10^{-8} torr; (*b*) 10°C, 2×10^{-3} torr of helium; (*c*) −195°C, 5×10^{-8} torr; (*d*) −195°C, 2×10^{-3} torr of helium. The substrates were NaCl; the titanium deposition rates were 5×10^{14} atoms sec^{-1} cm^{-2}; the films were shadowed with palladium before exposure to high pressure and are shown at 35,000X. (*a*) and (*b*) were 10-min titanium evaporations; (*c*) and (*d*) are 1-hr titanium evaporations.

between the surface area of these films and their pumping capabilities. The initial sticking fractions for hydrogen on these types of films are: (*a*), 0.05; (*b*), 0.19; (*c*) 0.24; and (*d*), 0.85. Electron diffraction studies of the crystallite sizes indicate that in the deposits made in the presence of helium, either the crystal lattice is very badly distorted or each of the particles shown in the photomicrographs is made of many smaller ones. That is to say, the size of the particles shown in the photomicrographs is too large to cause the observed broadening of the diffraction lines.

8.2 VACUUM INSTRUMENTATION

8.2.1 Nude Ionization Gage Calibration

Work on the calibration of nude or envelopeless ion gages continued, using a relatively oil-free vacuum system. These studies are described in a recent report.[4] A Veeco RG-75 gage tube was

[4] J. D. Redman and R. A. Strehlow, ORNL TM-115, Feb. 15, 1962.

modified so that operating characteristics for several modes of assembly could be determined. The nude gage was tested with and without a screen surrounding the gage elements and, in some cases, with a shield around the screen to ensure that the wall potential was at ground.

Figure 8.4 shows the collector current vs collector voltage for the nude gage with and without a screen. The presence of a screen reduces the sensitivity of the gage to changes in collector voltage. The effect of screen voltage on collector current was examined for two potentials: floating (25 v positive, with respect to ground) and at ground. There was a small difference between the two modes of operation shown in Fig. 8.5 – in the direction which indicates that at less positive screen potentials the electron path length resulting in ionization may be larger.

8.2.2 Low-Emission Calibration Results

Studies of ion gage sensitivity as a function of emission current show that the sensitivity for an enveloped gage (in $\mu a\,\mu a^{-1}\mu^{-1}$) is constant down to 7.5×10^{-3} μa emission current and is equal to 10.0 ± 0.7, with somewhat more experimental scatter in the range of emission currents less than 50 μa. At emissions of 6.5 and 6.0 μa the sensitivities are 5.1 and 3.5 respectively. Nude gages

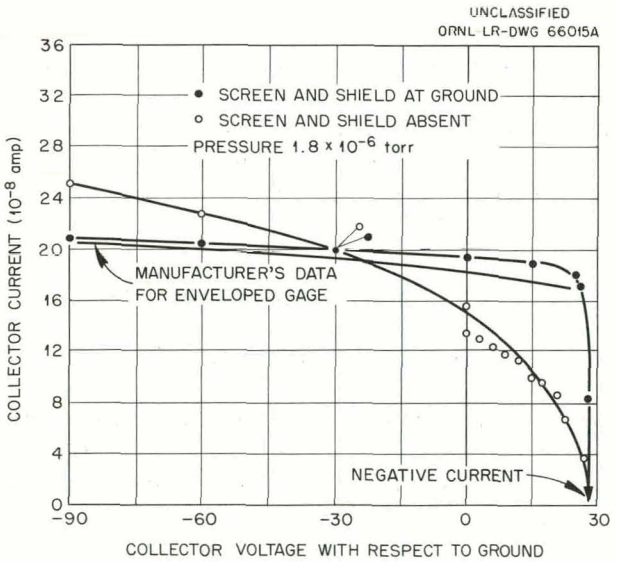

Fig. 8.4. Collector Current vs Collector Voltage for Nude Gage with Screen and Shield.

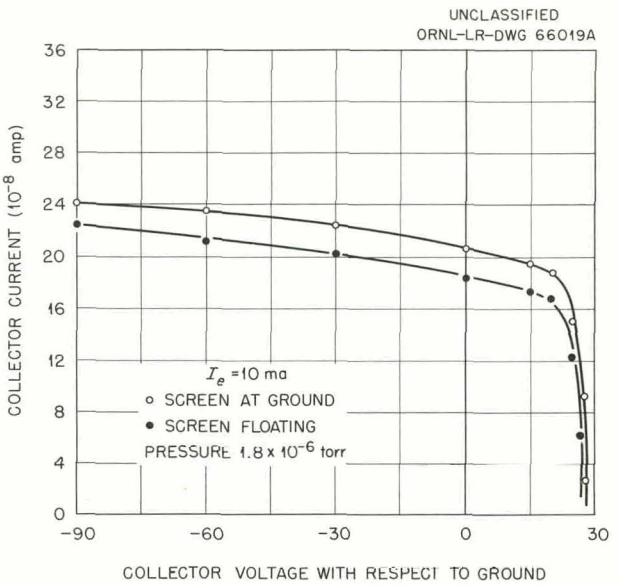

Fig. 8.5. Collector Current vs Collector Voltage.

operated with a shielding screen at 0 v and at +30 v with respect to ground have high sensitivities in this low-emission range identical to those for a tubulated gage. When the screen is allowed to float (at above filament potential), the sensitivity in the low-emission range slowly drops and reaches 10 only below 10-μa emission. A grounded screen appears necessary in order to maintain reasonable constancy of gage sensitivity with emission for nude gages.

8.2.3 Current Mapping in a Bayard Gage

With the use of a mobile collector probe $\frac{1}{2}$ in. long (as shown in Fig. 8.6), the ion current in a nude gage was monitored as a function of position of the collector. The nude gage was operated with and without a screen surrounding the gage elements. The presence of the screen (at a floating potential of about +30 v with respect to ground) had the effect of making the ion current much less sensitive to collector location and orientation and also appeared to minimize oscillations which were observed for some modes of operation. The differences in current readings in the grid region for the normal collector position are shown in Fig. 8.7 and approximately indicate that for a screen at a potential of +30 v, the lack of a screen resulted in pressure readings which

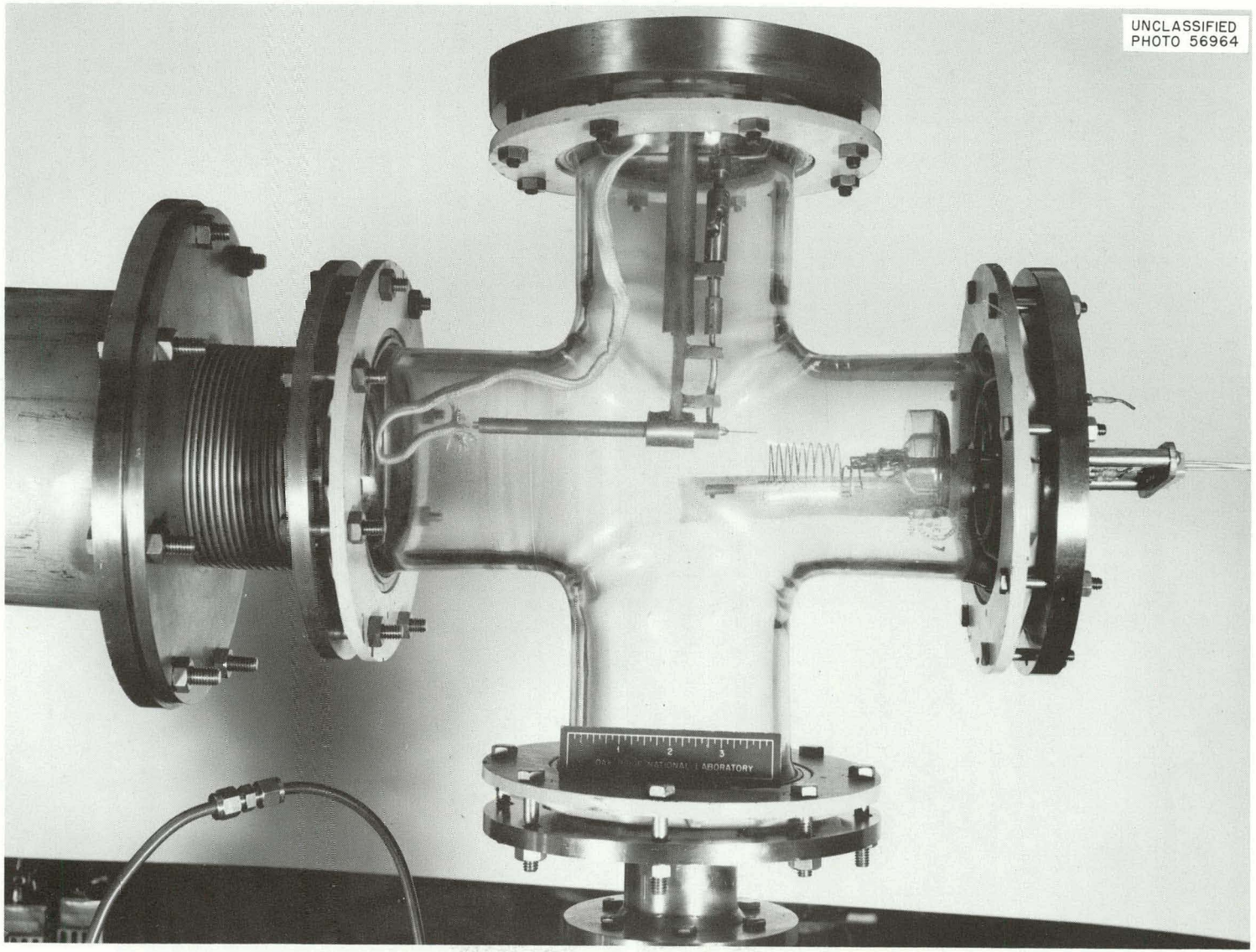

Fig. 8.6. Ion Current Mapping Apparatus with Bayard Type Nude Gage.

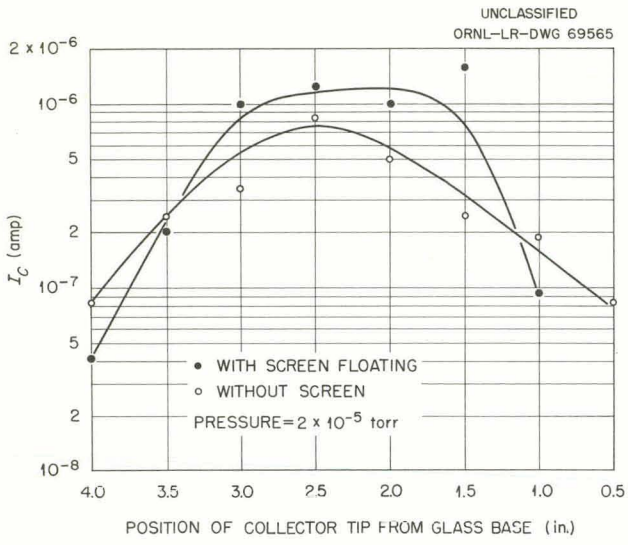

Fig. 8.7. Ion Current for Normal Collector Position for Zero Collector Potential.

were too low by about a factor of 3. Some other collector positions inside the grid differed from each other by factors of 10 in the absence of a screen, but by no more than a factor of 2 with a screen.

8.3 DIFFUSION PUMPS

8.3.1 Decomposition of Diffusion-Pump Oils

Operational tests of thermal decomposition were made for three diffusion-pump oils: Octoil (di-2-ethylhexylphthalate), Convoil-20 (a mixed hydrocarbon), and OS-124 (a mixed pentaphenylpolyether). The equilibrium gases over an operating fractionating diffusion pump containing these oils were allowed to enter a test dome monitored by a CEC residual-gas analyzer which was operating with a sensitivity of about 2×10^{-9} torr.

Octoil and Convoil introduced methane, ethane, and ethylene in distinctly observable amounts. For a system at a pressure of 2×10^{-8} torr, the partial pressure of the methane above the pump was about 3 to 4 $\times$ 10^{-9} torr. For Octoil there was a noticeably greater amount of mass 28 than for Convoil, presumably due to CO derived from the thermal decomposition of the ester linkage. The same test with OS-124 yielded no detectable introduction of any mass monitored. This finding is in agreement with work reported earlier.[3,5]

8.4 MATERIALS STUDIES

8.4.1 Bombardment of Titanium by Energetic Particles

The work reported in the previous progress report[3] on the uptake of deuterium by titanium bombarded by energetic deuterons left unanswered the question of the fraction of deuterium which the titanium absorbed from the background gas. A bombardment of titanium by energetic He^+ ions was carried out with the target exposed to an atmosphere of deuterium. No increase in target weight was found. Indeed, the normal sputtering ratio for titanium bombarded by helium was observed ($R = 0.014$).

---

[5] *Reactor Chem. Div. Ann. Progr. Rept. May 4, 1962*, ORNL-3262, pp 199–205.

9. Design and Engineering: Notes

9.1 CONSIDERATIONS OF BLANKETS FOR THERMONUCLEAR REACTORS

C. J. Barton[1] R. A. Strehlow[1]

A survey has been made of proposed blanket assemblies for thermonuclear reactors.[2] Although many uncertainties exist regarding the design of a successful thermonuclear reactor, the fact remains that some fraction of the energy of thermonuclear neutrons must be removed or recovered as heat. This consideration alone makes necessary the presence of a heat recovery or removal blanket surrounding the reactor, but the reproduction of tritium is an equally necessary function of the blanket for a deuterium-tritium fueled (D-T) reactor.

Since design details of a power device are not now delineable, it seemed advisable to consider in some detail only the two principal functions which a blanket assembly will probably be called upon to perform (heat transfer and tritium breeding) and to discuss factors which are pertinent to the fulfillment of these objectives. Included among the factors which pertain to the choice of a suitable breeding and heat removal blanket are the following:

1. Provision for neutron multiplication.
2. Moderation of neutrons to low energy and their absorption in $_3Li^6$.
3. Small parasitic neutron capture.
4. Absorption of secondary gamma rays.
5. Extraction of heat at useful temperatures.
6. Recovery of tritium.
7. Stability and chemical compatibility.
8. Compatibility of the blanket with magnetic requirements; small electrical loss.
9. Vapor pressure of the chemicals used in the blanket (should be low at the operating temperature).
10. Minimum induced radioactivity.
11. Minimum thickness.

Of the blanket materials considered in the report,[2] $LiF\text{-}BeF_2$ mixtures appear most readily capable of satisfying the requirements currently considered.

9.2 "LIFE" TESTS ON WATER-COOLED COPPER CONDUCTORS

J. Lewin

Tests have been run to determine whether there are any time limitations on the use of water-cooled copper conductors operating at high current densities, heat fluxes, and temperatures. Oxidation of the copper, with consequent formation of a surface layer having poor thermal conductivity, was thought likely to occur. The resulting effect, anticipated in the tests, was a gradual rise in copper temperature at constant heat flux. No such rise occurred in a conductor that was tested for periods up to 420 hr, so long as demineralized water was used as coolant. This effect was independent of the concentration of dissolved oxygen in the water.

In addition, resistance to water flow through the conductor was surveyed, as was the difference in heat-transfer performance between demineralized water and process water. Finally, the validity of a burnout heat flux[3] was verified at one operating point for the conductor used in the tests.

---

[1]Reactor Chemistry Division.

[2]C. J. Barton and R. A. Strehlow, *Blankets for Thermonuclear Reactors*, ORNL-3258 (May 1962).

[3]F. C. Gunther, "Photographic Study of Surface Boiling Heat Transfer to Water With Forced Convection," *Trans. ASME*, p 115 (February 1951).

A length of $\frac{3}{16}$-in.-square "OFHC" copper tubing, 0.12 in. in inner diameter, was used to transmit direct current at densities of over 200,000 amp/in.^{2}, under various cooling-water flow rates (see Figs. 9.1 and 9.2). The tube was insulated from ambient temperature, and iron-constantan thermocouples were used to measure temperature at several points along the outside surface. The difference between copper temperature at the entrance and at the hottest point downstream, divided by the square of the current, was plotted against running time in hours, as shown in Fig. 9.2.

All the tests except 2D (see Table 9.1) were run in the nucleate boiling region of heat transfer, with copper temperatures exceeding saturation by an amount designated as "ΔT wall boil." The subcooling of the bulk water at the exit is designated by "ΔT bulk s.c."

At the end of test 4C the flow was decreased to a point that corresponded to burnout by Gunther's correlation: (q/A) burnout = $0.0135\ V^{0.5}\ \Delta T$ bulk s.c. (ref 3). After about 1 hr of operation the tube burned out, and the test was shut down by the automatic pressure-monitoring system.

Tests B, 1C, and 2C were made with demineralized water that had an oxygen content of about 8 ppm and a pH of 7.3. Tests 3C and 4C were made with water having a dissolved oxygen content of 1.1 ppm and pH's of 7.0 and 6.2 respectively.

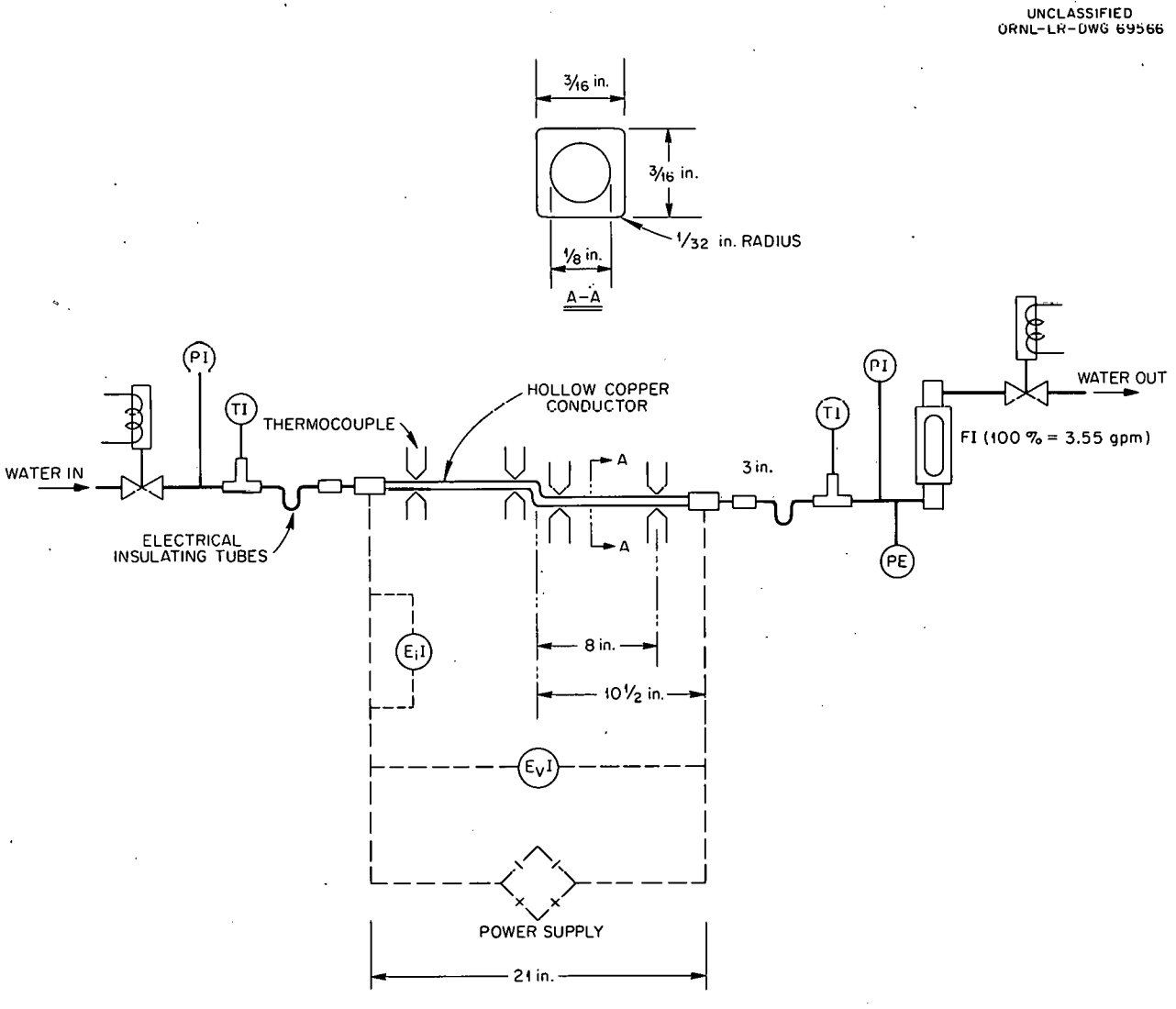

Fig. 9.1. Cross Section of Copper Conductor and Test Setup.

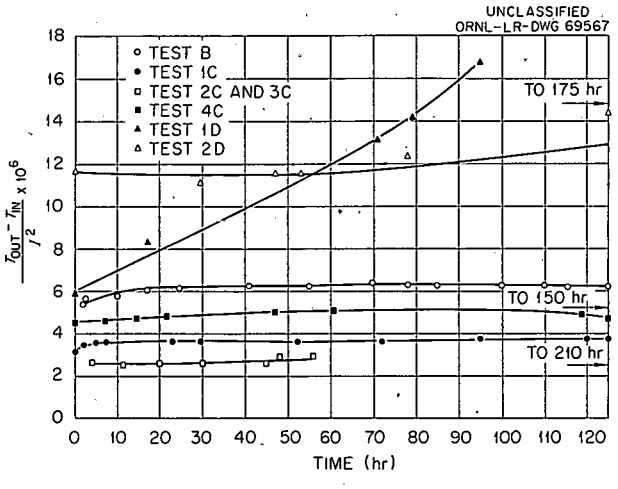

Fig. 9.2. Copper Temperature Rise per Unit I^2 vs Time.

Test D was made with "process water" (potable water) which had an oxygen content of 10.8 ppm and a pH of 7.53.

Other conditions for each test are shown in Table 9.1.

It was possible to create a steady "disastrous" rise of copper temperature only in the case of test D, using process water, and this occurred only in the nucleate boiling region and not under subcooled wall conditions as in test 2D.

It appears that it is entirely feasible, from the heat transfer standpoint, to operate water-cooled copper conductors in the nucleate boiling region using demineralized water at pH 7 without incurring the gradual temperature rises predicted by Griess

Table 9.1. Test Conditions for Heat-Transfer Studies of Hollow Copper Conductors

	Test Number						
	B	1C	2C	3C	4C	1D	2D
Current, amp	4500	6250	7100	6850	5550	4400	3070
Current density, amp/in.^{2}	209,200	290,560	330,080	318,456	258,020	204,556	142,800
Heat flux, Btu hr^{-1} ft^{-2}	1.08×10^6	1.86×10^6	2.51×10^6	2.09×10^6	1.68×10^6	1.01×10^6	0.42×10^6
Flow velocity, fps	27.5	55	75	61	35	28	27.5
Maximum copper temperature, °F	284	302	302	320	330	644	302
Bulk water outlet temperature, °F	160	160	155	170	220	187	105
Bulk outlet subcooling, °F	90	91	133	83	51	87	171
Wall-temperature superheat, °F	34	51	14	67	59	370	−19 to 0
Duration of test, hr	126	207	49	11	153	95	175
Total time on tube, hr	126	207	256	267	420	95	270
Dissolved oxygen content, ppm	5.5 to 8.4	8.0	8.0	1.1?	1.1	10.8	10.8
Total solids content, ppm	~2	~2	~2	1.9	1.9	80	80
Total hardness, ppm	<1	<1	<1	<1	<1	87.5	87.5
Specific resistivity, ohm-cm	8.9×10^6	4.2×10^6	4.2×10^6	7.5×10^6	7.5×10^6	6×10^3	6×10^3
pH	7.3	7.3	7.1	7.0	6.2	7.5	7.5

et al. for aluminum (ref 4). The burnout predictions of Gunther,[3] also appear to be applicable for the tubing used here.

The inner surfaces of as-received tubing and the tubes of tests B and C were inspected metallographically, and the formation of copper oxide was about 0.0005 in. thick, maximum, but was evident only in spots. The oxidation was overshadowed by the effects of erosion. This was manifested through the appearance of characteristic craters along the entire half of the tube examined. The craters were fairly uniform in depth – 0.00075 to 0.0018 in. At the maximum depth, this indicates an erosion rate of about 4.5×10^{-6} in./hr for the rather high velocities used in test C.

The arrangement and installation of the test equipment, as well as other assistance and guidance, were provided by members of the Engineering Science Group.

[4] J. C. Griess *et al.*, *Effect of Heat Flux on the Corrosion of Aluminum by Water*, ORNL-3230 (Dec. 5, 1961).

10. Design and Engineering: Service Report

J. F. Potts, Jr.

The activities of the Engineering Services Group are generally reported incidentally with the research efforts of other groups of the Thermonuclear Division. The group executes or coordinates engineering design, shop fabrication, building operations, and maintenance. In addition, during the current interval, the group engaged in a number of testing activities in order to reinforce choices of materials and methods in design.

Design activities are summarized as follows:

Jobs on hand 11-1-61 on which work had not started	22
New jobs received	179
Total jobs	201
Jobs completed	166
Jobs in progress	15
Backlog of jobs, 4-30-62	20
Total drawings completed for period (does not include report and slide drawings)	236
Overtime (draftsmen, man-days)	11

During this interval the design activity was largely concentrated on support for field changes and additions to DCX-1, DCX-2, and Cyclotron Heating Projects, as well as on new diagnostic apparatus for these and basic research efforts. Since a peak of major construction activity has passed, a smaller amount of engineering was done by outside agents.

Shop fabrication for the period is summarized as follows:

Jobs requiring 16 man-hours or less	376
Jobs requiring 16 to 1200 man-hours	369
Jobs over 1200 man-hours	1
Jobs of miscellaneous character in plating, carpenter, electrical, and millwright shops	209
Shop manpower (averaged weekly)	26.4

Under a continuing program, improvements in the quality and reliability of the demineralized cooling water system were realized. Water conductivity is routinely in the range 5 to 8×10^6 ohm-cm, solids less than 2 ppm, dissolved oxygen less than 2 ppm. A method of safely interlocking and monitoring the high-current dc distribution system is nearing completion. In addition to other advantages, this will help us maintain flexibility of operation in the face of scheduled plant-load demands.

Publications, Papers, and Traveling Lecture Program

PUBLICATIONS

OPEN LITERATURE

Author(s)	Title of Article	Journal
T. K. Fowler	Stability of Plasmas Against Electrostatic Perturbations	*Phys. Fluids* 4(11), 1393 (1961)
T. K. Fowler	Theoretically Stable and Confined Plasma	*Phys. Fluids* 5(2), 249 (1962)
G. G. Kelley, N. H. Lazar, and E. C. Moore	A Source for the Production of Large DC Ion Currents	*Nuclear Instr. and Methods* 10, 263 (1961)
J. E. Francis, Jr., C. C. Harris, and P. R. Bell	A Focusing Collimator for Research in Scanning	*J. Nuclear Med.* 3, 10 (1962)
R. J. Mackin, Jr.	Recent Aspects of Controlled Fusion Research	*Our Nuclear Future* (ed. by James E. Noblin, Jr.), p 29, Mississippi Industrial and Technological Research Commission, Jackson, Miss., 1961
G. R. Haste and C. F. Barnett	Plasma Potential Measurements Using an Ion Beam Probe	*J. Appl. Phys.* 33(4), 1397 (1962)
W. F. Gauster and C. E. Parker	Some Concepts for the Design of Superconducting Solenoids	*Proc. Intern. Conf. High Magnetic Fields, MIT, Nov. 1–4, 1961* (ed. by H. Kolm, B. Lax, F. Bitter, and R. Mills), p 3, publ. jointly by MIT Press and Wiley, 1962
F. T. May and R. A. Dandl	A Sub-Millimicroampere Current Amplifier Utilizing an Unusual Transistor Effect	*IRE Trans. Nuclear Sci.*, NS-8(4), 16–20 (1961)
Herman Postma	DCX-1 Instrumentation	*IRE Trans. Nuclear Sci.* NS-8(4), 77–80 (1961)
J. R. McNally, Jr.	Hollow Cathode Discharge Tube	*Encyclopaedic Dictionary of Physics* 2 (ed. by J. Thewlis), p 454, Pergamon, 1961

P. M. Griffin	Echelle Grating	*Encyclopaedic Dictionary of Physics* 2 (ed. by J. Thewlis), p 602, Pergamon, 1961

ORNL REPORTS

Author(s)	Title	Number	Date
I. Alexeff and R. V. Neidigh	The Plasma Eater: A Device to Measure the Rate of Flow of a Plasma	ORNL-3246	2-5-62
T. K. Fowler and E. G. Harris	The Cyclotron Resonance Instability with Negative Mass Ions	ORNL TM-25	10-17-61

PAPERS PRESENTED AT SCIENTIFIC AND TECHNICAL MEETINGS

American Physical Society, Division of Plasma Physics, Colorado Springs, Colo., Nov. 15–18, 1961

W. L. Stirling, C. W. Blue, and H. C. Hoy, "Experimental Investigation of Ion Beam Neutralization by Coaxially Injected Electrons."

O. C. Yonts, A. M. Veach,[1] E. D. Shipley, and R. N. Goslin,[2] "Preliminary Studies of Ion Beam and Secondary Plasma Interactions."

R. A. Dandl and R. J. Kerr, "Molecular Beam Transmission of a Microwave Heated Electron Plasma."

M. C. Becker, R. A. Dandl, H. O. Eason, Jr., A. C. England, R. J. Kerr, and W. B. Ard,[3] "Further Investigations of a Plasma Formed by Electron Cyclotron Heating."

I. Alexeff, R. V. Neidigh, and E. D. Shipley, "A Study of the Plasma Associated with an Electron Stream."

American Physical Society, Washington, D.C., Apr. 23–26, 1962

E. G. Harris,[4] "The Crossed Stream Instability."

A. C. England, R. A. Dandl, and R. J. Kerr, "Determination of Plasma Configuration from Diamagnetic Measurements."

W. B. Ard,[3] R. A. Dandl, A. C. England, and R. J. Kerr, "Equilibrium Between a Continuously Heated Plasma and the Surrounding Neutral Gas."

R. J. Kerr, R. A. Dandl, H. O. Eason, Jr., A. C. England, M. C. Becker, and W. B. Ard,[3] "Recent Experiments with the Electron Cyclotron Plasma."

I. Alexeff and R. V. Neidigh, "The Plasma Eater: A Device to Measure the Rate of Flow of a Plasma."

Third Symposium on Engineering Aspects of Magnetohydrodynamics, University of Rochester, Rochester, New York, Mar. 28–29, 1962

I. Alexeff and R. V. Neidigh, "A Way to Measure Plasma Density – 'The Plasma Sweeper.'"

R. J. Mackin, Jr., "Status of the DCX-2 Program."

---

[1]Isotopes Division.

[2]Consultant, Oglethorpe University.

[3]Consultant, University of Florida.

[4]Consultant, University of Tennessee.

American Physical Society, Southeastern Section, Florida State University, Tallahassee, Apr. 5–7, 1962

W. L. Stirling, H. C. Hoy, O. D. Matlock, and R. L. Knight, "A Low-Density Arc Plasma for Dissociation."

Fourth Symposium on Engineering Problems in Controlled Thermonuclear Research, Fontenay-aux-Roses, France, Apr. 17–20, 1962

J. F. Potts and W. F. Gauster, "Current Engineering Status of the ORNL Experimental Devices for CTR."

TRAVELING LECTURE PROGRAM

The Traveling Lecture Program is conducted in cooperation with the Oak Ridge Institute of Nuclear Studies as a part of the AEC's program of disseminating scientific and technical information to universities, particularly those in the South. Lectures delivered by ORNL personnel present unclassified information to university undergraduate and graduate students and members of the faculty. The lectures serve to stimulate interest in research in the university departments and also to assist the teaching staff in expanding the scope of instruction offered under their regular curricula. Through such personal contacts, ORNL staff members are also able to observe departmental activities at the universities. Listed below are members of the Thermonuclear Division who participated in the Traveling Lecture Program during the academic year 1961–1962.

P. R. Bell	Vanderbilt University, Apr. 13, 1962 "Thermonuclear Status at Oak Ridge National Laboratory"
R. J. Mackin, Jr.	Fisk University, Jan. 17, 1962 "Present Status of Controlled Fusion"
	Hampton-Sydney College, Feb. 15, 1962 "Present Status of Controlled Fusion"
	University of Virginia, Apr. 9, 1962 "Present Status of Controlled Fusion"
A. H. Snell	University of Wisconsin, Oct. 24, 1961 "Current Status of Controlled Fusion Research at Oak Ridge National Laboratory"

ORNL-3315
UC-20 – Controlled Thermonuclear Processes
TID-4500 (17th ed., Rev.)

INTERNAL DISTRIBUTION

1. I. Alexeff
2. R. G. Alsmiller
3. W. B. Ard
4. C. F. Barnett
5. M. C. Becker
6-11. P. R. Bell
12. D. S. Billington
13. E. P. Blizard
14. C. W. Blue
15. G. E. Boyd
16. R. L. Brown
17. R. E. Clausing
18. D. L. Coffey
19. F. L. Culler
20. J. S. Culver
21. R. A. Dandl
22. R. C. Davis
23. S. M. DeCamp
24. J. L. Dunlap
25. H. O. Eason, Jr.
26. R. S. Edwards
27. A. C. England
28. J. C. Ezell
29. J. L. Fowler
30. T. K. Fowler
31. J. E. Francis, Jr.
32. J. H. Frye, Jr.
33. W. F. Gauster
34. R. A. Gibbons
35. P. M. Griffin
36. W. R. Grimes
37. E. Guth
38. C. C. Harris
39. G. R. Haste
40. R. E. Hill
41. A. S. Householder
42. H. C. Hoy
43. R. P. Jernigan, Jr.
44. R. G. Jordan (Y-12)
45. G. G. Kelley
46. M. T. Kelley
47. R. J. Kerr
48. R. L. Knight
49. J. A. Lane
50. C. E. Larson (K-25)
51. N. H. Lazar
52. G. F. Leichsenring
53. J. Lewin
54. R. S. Livingston
55. J. N. Luton, Jr.
56. J. R. McNally, Jr.
57. R. J. Mackin, Jr.
58. W. D. Manly
59. O. D. Matlock
60. K. Z. Morgan
61. O. B. Morgan
62. J. P. Murray (K-25)
63. R. V. Neidigh
64. M. L. Nelson
65. J. Neufeld
66. C. E. Parker
67. W. F. Peed
68. H. Postma
69. J. F. Potts
70. M. Rankin
71. J. A. Ray
72. R. G. Reinhardt
73. P. W. Rueff
74. W. K. Russell
75. H. E. Seagren
76. Y. Shima
77. E. D. Shipley
78. M. R. Skidmore
79. M. J. Skinner
80-89. A. H. Snell
90. W. L. Stirling
91. R. F. Stratton, Jr.
92. R. A. Strehlow
93. J. A. Swartout
94. E. H. Taylor
95. P. A. Thompson
96. R. M. Warner
97. H. L. Watts
98. A. M. Weinberg
99. E. R. Wells
100. T. A. Welton
101. G. K. Werner
102. W. L. Wright
103. O. C. Yonts
104. W. P. Allis (consultant)

105. W. H. Bostick (consultant)
106. F. E. Dunnam (consultant)
107. J. W. Flowers (consultant)
108. M. W. Garrett (consultant)
109. E. G. Harris (consultant)
110. D. E. Harrison (consultant)
111. R. Hefferlin (consultant)
112. G. W. Hoffman (consultant)
113. V. W. Hughes (consultant)
114. D. W. Kerst (consultant)
115. E. W. McDaniel (consultant)
116. M. R. C. McDowell (consultant)
117. D. R. Montgomery (consultant)
118. J. E. Mott (consultant)
119. C. E. Nielsen (consultant)
120. W. B. Pardo (consultant)
121. F. F. Rieke (consultant)
122. H. S. Robertson (consultant)
123. D. J. Rose (consultant)
124. L. P. Smith (consultant)
125. P. M. Stier (consultant)
126. C. H. Weaver (consultant)
127. J. D. Tillman (consultant)
128-137. Thermonuclear Division Library
138. Reactor Division Library
139. Biology Library
140-141. Central Research Library
142. Laboratory Shift Supervisor
143-167. Laboratory Records Department
168. Laboratory Records, ORNL RC
169-170. ORNL – Y-12 Technical Library Document Reference Section

EXTERNAL DISTRIBUTION

171. S. C. Brown, Massachusetts Institute of Technology
172. M. B. Gottlieb, Princeton University
173. H. Grad, New York University
174. J. M. B. Kellogg, Los Alamos Scientific Laboratory
175. A. C. Kolb, Naval Research Laboratory
176. J. A. Phillips, Los Alamos Scientific Laboratory
177. R. F. Post, University of California, Lawrence Radiation Laboratory
178. A. Simon, General Atomic, San Diego, California
179. L. Spitzer, Princeton University
180. M. Rosenbluth, General Atomic, San Diego, California
181. E. Teller, University of California, Lawrence Radiation Laboratory
182. C. M. Van Atta, University of California, Lawrence Radiation Laboratory
183. R. W. McNamee, Union Carbide Corporation
184-185. Research and Development Division, AEC, ORO (1 copy each to H. M. Roth and R. B. Martin)
186-187. Controlled Thermonuclear Branch, AEC, Washington (1 copy each to A. E. Ruark and H. S. Morton, Jr.)
188-791. Given distribution as shown in TID-4500 (17th ed. Rev.) under Controlled Thermonuclear Processes category (75 copies – OTS)